Centre Eau Terre Environnement

TECTONOMETAMORPHIC EVOLUTION OF THE MAURICIE AREA, CENTRAL GRENVILLE PROVINCE, QUEBEC CANADA

By

Muhammad Zahoor Iqbal

Thesis submitted for the degree of Master (M.Sc.) in Earth Sciences

Jury members

Chair of jury and internal examiner	Antoine Godet Commission géologique du Canada, Québec
External examiner	Aphrodite Indares Earth Sciences, Memorial University of Newfoundland
Research director	Renaud Soucy La Roche Centre Eau Terre Environnement, Institut national de la recherche scientifique

ACKNOWLEDGEMENTS

I am deeply grateful to my supervisor, Dr. Renaud Soucy La Roche, for introducing me to the geology of the Grenville Province exposed in Canada—a fascinating region for exploring protracted metamorphism and intricate tectonic evolution. His critical reviews and insightful guidance throughout my project have significantly shaped my results, interpretation and discussion, establishing a solid foundation in metamorphic geology and petrochronology.

I extend my sincere thanks to Dr. Kyle Larson at University of British Columbia (UBC), Okanagan, whose invaluable mentorship at the Fipke Laboratory for Trace Element Research (FiLTER) during my research exchange greatly enhanced my understanding of U—Th—Pb petrochronology. His expertise and discussions in petrochronology, data analysis and data filtering have been pivotal to this thesis. I am also indebted to Dr. Sudip Shrestha for his assistance with EPMA analysis at the FiLTER, UBC, Okanagan.

My heartfelt thanks go to Dr. Mark Button, who supported me through *in situ* U—Th—Pb and Lu–Hf analyses at FiLTER, providing consistent guidance and helping me filtering and analyzing the data. His remote support with Iolite software access was crucial for data processing.

I am equally thankful to Arnaud De Coninck, technical manager at INRS–ETE, for his dedication to SEM–EDS elemental mapping in identifying accessory phases in thin sections, and for his help with carbon coating. I am also grateful to Dr. Carl Guilmette at Université Laval for his assistance with micro—X—Ray fluorescence elemental mapping of thin sections.

My project was funded by my supervisor's INRS startup grant and Natural Sciences and Engineering Research Council of Canada (NSERC) Discovery Grant (2020–2025). I also gratefully acknowledge the funding I received from the Geological Society of America through a Graduate Student Research Grant, which partially supported my research project, and the Eric Mountjoy Exchange Award, from the Geological Association of Canada that allowed me to travel to FiLTER.

I would like to sincerely thank the members of my thesis jury, Dr. Antoine Godet at Commission Géologique du Canada, Québec, and Dr. Aphrodite Indares at the Department of Earth Sciences, Memorial University of Newfoundland, for their valuable editorial feedback and insightful comments.

On a personal note, I am deeply appreciative of my family—my mother, brothers, sisters, and especially my wife, who joined my journey in 2023. Their unwavering support has been my anchor throughout this process. I fondly remember my father (late), whose presence and pride I feel with me, and I wish he could celebrate this milestone by my side in Quebec.

RÉSUMÉ

Malgré des décennies de recherche sur l'orogénie de Grenville datant du Mésoprotérozoïque tardif au Néoprotérozoïque précoce, des aspects essentiels, tels que l'âge du début de la collision continentale et la durée du métamorphisme, restent mal établis. Dans cette étude, j'intègre la pétrochronologie U-Th-Pb sur monazite et sur xénotime et la pétrochronologie Lu—Hf sur grenat avec des observations microtexturales détaillées, afin de contraindre l'évolution métamorphique des gneiss alumineux des domaines de Mékinac-Taureau, de Shawinigan et de Portneuf-Saint-Maurice dans la région de la Mauricie, dans la partie centrale de la Province de Grenville au Québec. Trois stades métamorphiques distincts sont identifiés. Un stade prograde aux conditions métamorphiques du faciès des amphibolites liées au début de la collision continentale est enregistré dès 1137 ± 13 | 24 Ma, avant la phase Ottawan de l'orogénie du Grenville (environ 1090 Ma, tel que défini habituellement). Le pic métamorphique s'est produit pendant la phase Ottawan (vers 1100-1050 Ma) à des conditions suprasolidus au faciès des granulites dans les domaines de Mékinac-Taureau et de Shawinigan, les plus bas structuralement, et à des conditions subsolidus au faciès des amphibolites dans le domaine de Portneuf-Saint-Maurice, le plus haut structuralement. Le métamorphisme rétrograde et le refroidissement ont suivi à ≤1045 Ma et se sont poursuivis jusqu'à au moins ca. 980 Ma. Ces résultats témoignent d'une longue histoire métamorphique qui s'étend sur ~150 millions d'années, dont ~50 millions d'années de résidence au sein de la croûte moyenne à haute température. Cette évolution est compatible avec une orogenèse de collision continentale de longue durée. Mes nouvelles données ne s'intègrent pas facilement dans les modèles géodynamiques actuels. Les modèles futurs devront mieux prendre en compte l'évolution prolongée de l'orogenénie de Grenville-qui a débuté vers 1137 ± 13 | 24 Ma—et son chevauchement temporel avec le développement d'un système de rift majeur à l'intérieur de Laurentia.

Mots clés: Début de collision continentale, épaississement crustal, métamorphisme prolongé, pétrochronologie des monazites, géochronologie in situ des grenats.

ABSTRACT

Despite decades of research on the late Mesoproterozoic to early Neoproterozoic Grenville Orogeny, key aspects, such as the timing of initial continental collision and the duration of metamorphism, remain poorly resolved. In this study, I integrate *in situ* U–Th–Pb monazite and xenotime and *in situ* Lu–Hf garnet petrochronology with detailed microtextural observations to constrain the metamorphic evolution of aluminous gneiss from the Mékinac–Taureau, Shawinigan, and Portneuf–St. Maurice domains in the Mauricie region, Quebec, central Grenville Province. Three distinct metamorphic stages are recognized. Amphibolite facies prograde metamorphic conditions related to the onset of the continental collision are recorded as early as 1137 ± 13 | 24 Ma, predating the traditionally defined Ottawan phase (ca. 1090 Ma) of the Grenville Orogeny. Peak metamorphism occurred during the Ottawan phase (ca. 1100–1050 Ma) under suprasolidus granulite facies conditions in the structurally lowest Mékinac–Taureau and Shawinigan domains and under subsolidus amphibolite facies conditions in the structurally highest Portneuf–St. Maurice domain. Retrograde metamorphism and cooling followed at ≤1045 Ma and continued until at least ca. 980 Ma. These results document a protracted metamorphic history spanning ~150 Myr, including ~50 Myr of high-temperature mid-crustal residence, supporting a long-lived, continental collisional Grenville Orogeny. Our new data do not readily fit in current geodynamic models. Future models must address more effectively the protracted evolution of the Grenville Orogeny, which initiated as early as 1137 ± 13 | 24 Ma, and its temporal overlap with the development of a major rift system within Laurentia.

Keywords: Continental collision onset, crustal thickening, protracted metamorphism, monazite petrochronology, *in situ* garnet geochronology

SOMMAIRE RÉCAPITULATIF

La province de Grenville du centre et de l'ouest du Québec, est le résultat d'une longue série d'événements tectono-magmatiques qui ont eu lieu le long de la marge sud-est de Laurentia, depuis environ 1800 Ma jusqu'à la collision finale avec Amazonia lors de l'orogénie de Grenville, entre environ 1090 et 980 Ma (Rivers et al., 2012; Swanson-Hysell et al., 2023). L' orogénie grenvillienne (environ 1090—980 Ma) est marquée par une période prolongée (>100 Ma) d'épaississement crustal épisodique à l'échelle régionale, suivie de phases d'amincissement par extension, qui ont principalement affecté la croûte laurentienne partiellement remaniée (Corrigan et van Breemen, 1997; Hynes et Rivers, 2010; Rivers et al., 2012). La région de la Mauricie, située dans la province de Grenville, est composée des domaines lithotectoniques de Mékinac-Taureau, Shawinigan et Portneuf-Saint-Maurice. Elle offre un cadre idéal pour étudier la chronologie et les conditions du métamorphisme prograde, pic et rétrograde associés à l'orogénie de Grenville. La combinaison de la pétrochronologie U-Th-Pb sur monazite et xénotime avec la datation Lu—Hf sur grenat utilisées dans le cadre de mon mémoire offre de nouvelles contraintes sur le moment de l'épaississement de la croûte et du métamorphisme prograde, du pic métamorphique au faciès des granulites et du métamorphisme rétrograde subséquent. Six échantillons de gneiss alumineux ont été analysés, soit deux échantillons pour chacun des trois domaines. La pétrochronologie U-Th-Pb *in situ* sur monazite et xénotime et la pétrochronologie Lu—Hf *in situ* sur grenat ont été intégrées à des observations microtexturales afin de relier la cristallisation de la monazite, du xénotime et du grenat à des stades spécifiques de croissance ou de résorption de minéraux.

Dans l'échantillon RS11-058, qui provient du domaine Mékinac-Taureau, cent vingt datations sur 25 grains de monazite définissent une fourchette de dates comprise entre 1098 ± 54 Ma et 981 ± 42 Ma, tandis que onze datations provenant de six inclusions de monazite dans le grenat donnent une moyenne pondérée de 1024 ± 15 | 25 Ma (MSWD = 0.5). L'yttrium et le Yd/Gb dans la monazite ne varient pas systématiquement en fonction des dates ou de la position texturale, mais la position dans la lame mince influence la composition de la monazite. Dans l'échantillon ZI–2105, vingt datations sur huit grains de monazite couvrent une période allant de 1096 ± 78 Ma à 992 ± 74 Ma. Sept datations provenant de cinq inclusions de monazite dans le grenat donnent une moyenne pondérée de 1028 ± 26 | 36 Ma (MSWD = 0.4, n = 6), bien qu'une inclusion à environ 1076 ± 57 | 68 Ma se distingue par des valeurs élevées de Y, Yb/Gd et de Eu_N/Eu^*_N moins négative. Ces nouvelles données pétrochronologiques sur la monazite suggèrent donc que dans

le domaine Mékinac-Taureau, le métamorphisme prograde n'est que faiblement contraint par l'inclusion de monazite dans le grenat datant de 1076 ± 57 | 68 Ma, tandis que la majorité de la monazite s'est formée pendant un stade post-pic dans des conditions où la biotite, le feldspath potassique et la sillimanite étaient stables, et après la décomposition partielle du grenat.

Le domaine de Shawinigan couvre la plus grande fourchette de dates et de compositions chimiques. Dans l'échantillon ZI-2101A, soixante-huit datations sur 16 grains de monazite donnent des dates comprises entre 1115 ± 53 Ma et 1025 ± 98 Ma. Neuf datations provenant de trois inclusions de monazite dans des bordures de grenat donnent une moyenne pondérée de 1060 ± 19 | 30 Ma (MSWD = 0.41, n = 9). Les anomalies Y, Yb/Gd et Eu_N/Eu^*_N ne varient pas systématiquement avec les dates. En revanche, l'échantillon ZI-2102A présente un spectre d'âge et de compositions chimiques plus large, avec cent neuf dates sur 28 grains de monazite allant de 1190 ± 120 Ma à 987 ± 50 Ma. Dix-sept datations provenant de neuf inclusions de monazite dans des noyaux de grenat donnent une moyenne pondérée de 1137 ± 13 | 24 Ma (MSWD = 0.71, n = 17), tandis que neuf datations sur trois inclusions de monazite dans des bordures de grenat donnent une moyenne pondérée de 1071 ± 18 | 29 Ma (MSWD = 0.62, n = 9). La monazite dans les noyaux de grenat (environ 1190—1100 Ma) se caractérise par des teneurs élevées en Y, Yb/Gd et Eu_N/Eu^*_N faiblement négative. Les inclusions de monazite dans les bordures de grenat, dans la sillimanite et dans le feldspath potassique, ainsi que les grains de monazite dans la matrice datant d'environ 1100—1045 Ma, se caractérisent par de faibles teneurs en Y, Yb/Gd et Eu_N/Eu^*_N. Après environ 1045 Ma, les valeurs de Y et Yb/Gd montrent une légère augmentation, cohérente avec la résorption du grenat et la cristallisation du liquide de fusion partielle. Ensemble, ces deux échantillons du domaine de Shawinigan contraignent la croissance prograde du grenat en conditions sub-solidus à 1137 ± 13 | 24 Ma, les conditions suprasolidus dans le champ de stabilité du grenat, feldspath potassique, sillimanite à 1071 ± 18 | 29 Ma, et la rétrogression après environ 1045 Ma. Les données sur la monazite suggèrent une évolution métamorphique prolongée sur plus de 100 Ma, avec une résidence prolongée d'environ 50 Ma à des niveaux de croûte moyenne.

Dans le domaine de Portneuf-Saint-Maurice, la pétrochronologie sur monazite et xénotime combinée à la datation du grenat Lu—Hf ont permis de contraindre la chronologie du métamorphisme. L'échantillon ZI-2107 a donné vingt-cinq dates sur six grains de monazite et cinq grains de xénotime, allant de 1260 ± 140 Ma à 985 ± 54 Ma. Un grain de monazite partiellement enfermé dans un bord de grenat fournit une moyenne pondérée de 1060 ± 21 | 32 Ma (MSWD = 1, n = 5). L'échantillon ZI-2108 a donné six dates sur six grains de xénotime, allant de 1394 ± 43

Ma à 1012 ± 52 Ma. En excluant l'analyse la plus ancienne à 1394 ± 43 Ma qui a une composition chimique distincte, quatre inclusions de xénotime dans la cordiérite autour du grenat partiellement résorbé donnent une moyenne pondérée de 1039 ± 24 | 34 Ma (MSWD = 1.4, n = 4). Les compositions en éléments traces ne montrent aucune tendance temporelle systématique dans les deux échantillons.

La géochronologie Lu—Hf sur grenat dans le domaine de Portneuf-Saint-Maurice affine encore cette chronologie. Dans ZI-2107, le grenat présente des transitions nettes entre le centre et la périphérie, définies par une forte augmentation du Mn, une diminution du Ca et la disparition des inclusions d'ilménite. Deux cœurs de porphyroblastes de grenat présentent une zonation concentrique et des teneurs relativement faibles en Y, MREE et HREE qui diminuent vers l'extérieur, ce qui est typique de la zonation de croissance. La transition entre le cœur et la bordure est marquée par une augmentation de Y et Dy, un anneau riche en Lu et une diminution de Cr. Le bord extérieur résorbé du grenat se caractérise par des teneurs élevées en Y, Lu et Dy. Le bord extérieur riche en Lu est interprété comme résultant d'une rétrodiffusion de Lu à l'intérieur du grenat pendant la résorption du grenat, car il suit la forme irrégulière du bord résorbé et non les faces de croissance. Les datations Lu—Hf excluent donc les analyses situées sur le bord riche en Lu. Les analyses du coeur ont donné une date Lu—Hf de 1075 ± 169 Ma (Hf^0 = 0.287 ± 0.011 ; MSWD = 1.1, n = 49), statistiquement indiscernable de la date de 1091 ± 139 Ma obtenue à partir des analyses de la bordure (Hf^0 = 0.288 ± 0.033, MSWD = 0.73, n = 13). Les données isotopiques Lu—Hf provenant des cœurs et des bords définissent une régression avec une date Lu—Hf de 1089 ± 96 Ma (composition isotopique initiale $^{176}Hf/^{177}Hf$ (Hf^0) = 0.2865 ± 0.0091 ; MSWD = 0.98 ; n = 62/80) qui représente le meilleur estimé de l’âge de cristallisation du grenat. Dans l'échantillon ZI–2108, deux porphyroblastes de grenat présentent une zonation chimique différente. Les teneurs en Y et HREE diminuent légèrement du centre vers les bords et présentent une zonation concentrique, typique de la zonation de croissance (Baxter et al., 2017). Les MREE ne présentent pas de zonation significative. Toutes les analyses définissent une régression avec une date Lu—Hf de 1123 ± 35 Ma (Hf^0 = 0.2817 ± 0.0012, MSWD = 1, n = 78/80). Ces résultats suggèrent un métamorphisme prograde à pic dans des conditions de faciès amphibolite inférieur à moyen entre 1123 ± 35 Ma (date de grenat) et 1060 ± 21 Ma (dates sur inclusion partielle de monazite dans le grenat). La différence entre ces âges peut refléter un métamorphisme diachronique à travers le domaine ou une croissance prolongée du grenat. Les conditions du pic métamorphique ont été suivies d'une décompression dans le champ de stabilité de la cordiérite et ont à peine atteint les champs de stabilité de la sillimanite et du feldspath potassique (en raison de leur faible proportion) à 1039 ± 24 | 34 Ma (dates sur xenotime dans les couronnes de résorption du grenat).

La synthèse des résultats des trois domaines révèle d'importantes implications tectoniques régionales. Les datations d'inclusions de monazite dans les cœurs de grenat subsolidus dans le domaine de Shawinigan et une datation au Lu—Hf du grenat dans le domaine de Portneuf-St. Maurice définissent le début du métamorphisme prograde pendant l'enfouissement des séquences supracrustales et de l'épaississement crustal à 1137 ± 13 | 24 Ma et 1123 ± 35 Ma, respectivementLa phase métamorphique prograde d a transitionné vers un métamorphisme suprasolidus au faciès des granulites dans les domaines de Mékinac-Taureau et de Shawinigan au début et au milieu de la phase Ottawan (1100—1050 Ma), marquant l'apogée du pic thermique de l'Ottawan. Ces données sont compatibles avec un début précoce de l'orogénie Grenvillienne plutôt qu'avec du métamorphisme liée à l'orogénie Shawinigan, qui est légèrement plus ancienne. La fourchette de dates comprise entre 1100 et 1050 Ma implique la persistance de conditions suprasolidus dans les domaines de Mékinac-Taureau et Shawinigan pendant environ 50 millions d'années, ce qui indique une résidence prolongée dans la croûte moyenne. Dans le domaine de Portneuf-Saint-Maurice, le pic métamorphique aurait plutôt atteint des conditions subsolidus du faciès des amphibolites. Le métamorphisme rétrograde est bien contraint dans les trois domaines. Presque toutes les dates de monazite du domaine Mékinac-Taureau sont interprétées comme reflétant un métamorphisme post-pic pendant l'Ottawan moyen à Rigolet. Dans le domaine de Shawinigan, l'échantillon ZI-2102A contient de la monazite présentant une signature rétrograde après 1045 Ma.

Mes nouvelles données ne s'inscrivent pas facilement dans les modèles géodynamiques actuels. Notamment, elles impliquent le chevauchement temporel de la collilsion continentale de Grenville avec le développement d'un système de rift majeur à l'intérieur de Laurentia. Les futurs modèles révisés devront tenir compte de l'évolution prolongée de l'orogenèse de Grenville, qui a commencé dès 1137 ± 13 | 24 Ma plutôt que vers 1090 Ma.

TABLE OF CONTENTS

LIST OF FIGURES

LIST OF TABLES

LIST OF SYMBOLS AND ABBREIATIONS

AMCG	Anorthosite–mangerite–charnockite–granite
Ap	Apatite
BSE	Backscattered electron
Bt	Biotite
c.f.	Confer
ca.	Circa
cm	Centimeter
Crd	Cordierite
EPMA	Electron probe microanalyzer
FiLTER	Fipke Laboratory for Trace Element Research
Gr	Graphite
Grt	Garnet
HREE	Heavy rare earth elements
Hz	Hertz
ID–TIMS	Isotope-dilution thermal ionisation mass spectrometry
Ilm	Ilmenite
keV	Kiloelectronvolt
Kfs	K–feldspar
Km	Kilometer
kV	Kilovolt
LA–ICP–MS	Laser-ablation inductively coupled plasma mass spectrometry
Ma	Mega-annum
mA	Milliampere
mm	Millimeter
Mnz	Monazite
MPa	Megapascal
MREE	Medium rare earth elements
ms	Milliseconds
MSWD	Mean square of weighted deviates
Myr	Million years
nA	Nanoampere
OOL	Ottawan Orogenic Lid
Pl	Plagioclase
ppm	Parts per million
P—T—t	Pressure–temperature–time
Py	Pyrite
QQQ–ICP–MS	Triple Quadrupole Inductively Coupled Plasma Mass Spectrometer
Qz	Quartz
Rt	Rutile

SEM–EDS	Scanning electron microscopy with energy–dispersive spectroscopy
SHRIMP	Sensitive high-resolution ion microprobe
Sil	Sillimanite
WDS	Wavelength–dispersive spectrometers
Wm	White mica
Xtm	Xenotime
Zrn	Zircon
μm	Micrometre or micron
°C	Degrees Celsius
μ–XRF	Micro–X–ray fluorescence
2SE	Two times the standard error

1 INTRODUCTION

1.1 Background

The Grenville Orogen represents one of the Earth's most extensive mountain belts, spanning the present-day southeastern Laurentia and extending from the southwestern United States to Labrador in eastern Canada, with potential connections to Baltica in southern Scandinavia (Bingen et al., 2021; Rivers, 2021; Spencer et al., 2021). The prevailing geological model, primarily based on studies from the Grenville Province of eastern North America, suggests that the Grenville Orogen developed through a prolonged and complex evolutionary history. This evolution began with the formation of an extensive continental–margin arc due to northwest–directed subduction beneath Laurentia between ca. 1800 and 1300 Ma, followed by multiple phases of back–arc basin formation and closure, leading to periodic arc–continent accretionary orogenesis (Rivers and Corrigan, 2000). The culmination of this prolonged accretionary orogenesis, spanning over 600 Myr, occurred with the continental collision between Laurentia and Amazonia during the Grenville Orogeny (sensu stricto 1090—980 Ma; Hynes and Rivers, 2010; Jamieson et al., 2010; Rivers et al., 2012; Rivers, 2021).

The Grenville Province consists predominantly of high–grade metamorphic rocks that record multiple deformation and metamorphic episodes (Figure 1.1). The central and western parts of the Grenville Province preserve local evidence of metamorphism associated with the ca. 1250—1180 Ma Elzevirian Orogeny and the ca. 1190—1140 Ma Shawinigan Orogeny with spatially variable records of Grenville collisional Orogeny (Rivers, 2008; Rivers et al., 2012, Indares, 2025). The extent of these pre–Grenvillian orogenic events remains uncertain, largely due to the difficulty of distinguishing pre–Grenvillian metamorphism in regions that have been metamorphosed during the Grenville Orogeny. The Mauricie region, located in the central Grenville Province, provides an ideal setting to evaluate metamorphism associated with the Grenville Orogeny and to test if any pre-Grenvillian metamorphic events are preserved. The motivation behind this study was the limited and equivocal published geochronological constraints on the timing of metamorphism in the Mauricie region. The paucity of robust geochronological constraints emphasizes the need to refine the temporal framework of the Grenvillian metamorphism within the Mauricie region—an objective central to this study.

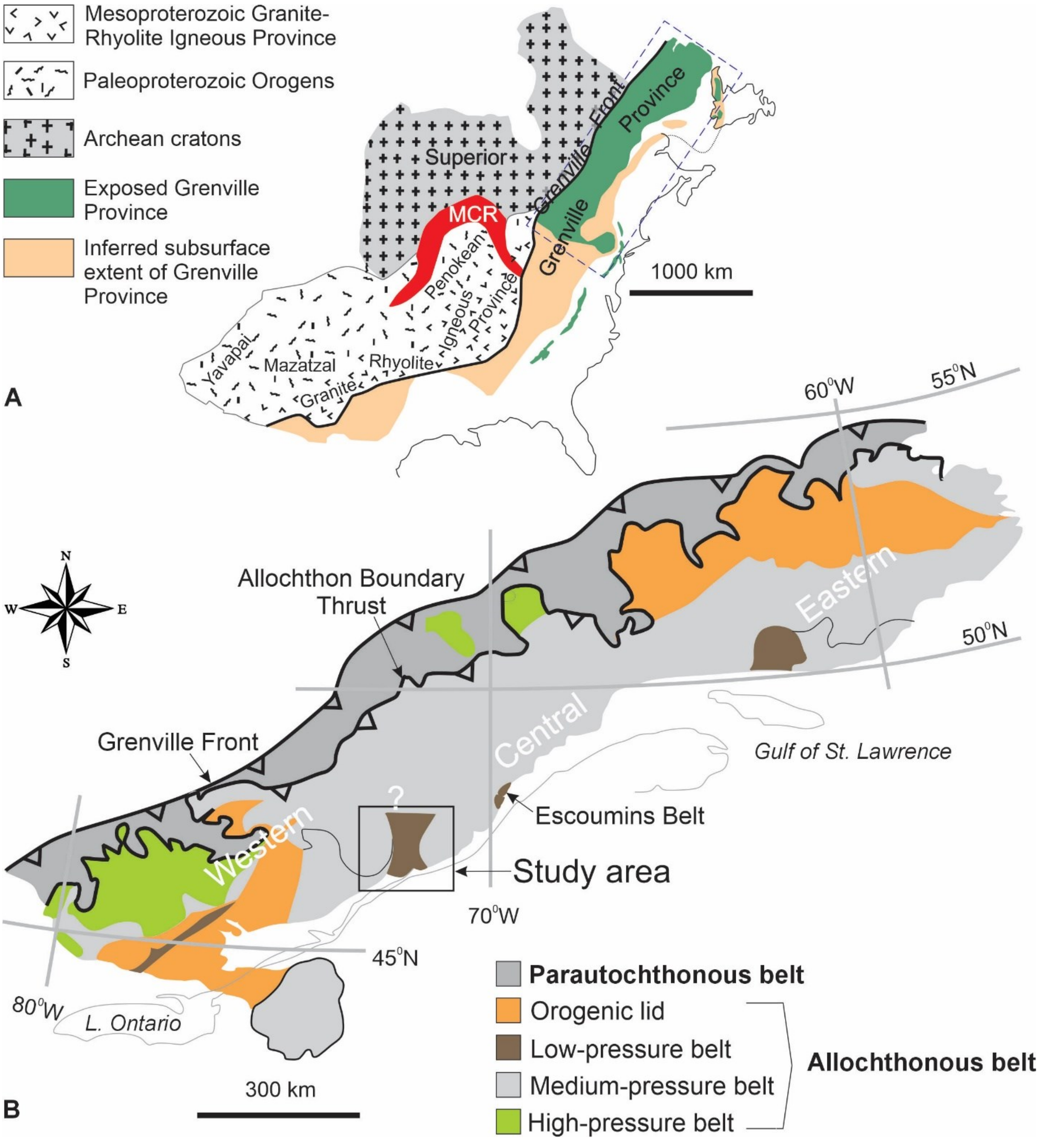

Figure 1.1: Precambrian tectonic framework of Laurentia and regional tectonic map of the Grenville Province.

(A) Tectonic framework of Laurentia during the Precambrian, illustrating major cratonic and orogenic domains. *From Rivers et al. (2012), modified from Hoffman (1989)*. (B) Enlarged view of the outlined area in (A), presenting a simplified geological map of the Grenville Province (modified from Rivers, 2008). The map delineates the distribution of Parautochthonous and Allochthonous belts. The study area is indicated by a black box.

To address this knowledge gap, I integrated multiple analytical techniques aimed at providing reliable metamorphic age constraints for the region. My methodology combines petrographic observations, thin section micro–X–ray fluorescence (μ–XRF) mapping, thin section electron probe microanalyzer (EPMA) geochemical mapping, scanning electron microscopy with energy–dispersive spectroscopy (SEM–EDS), *in situ* laser-ablation inductively coupled plasma mass spectrometry (LA–ICP–MS) U—Th—Pb on monazite and xenotime, and *in situ* LA–ICP–MS trace element mapping and Lu—Hf garnet petrochronology. The combination of isotopic and trace element analysis in petrochronometers along with detailed characterization of their textural relationship with metamorphic index minerals provides a powerful toolkit for linking petrochronometers crystallization to the growth of index minerals along the P—T path, which is useful to deduce the metamorphic evolution of a particular rock (Spear and Pyle, 2002; Pyle and Spear, 2003; Wing et al., 2003; Gibson et al., 2004; Rubatto et al., 2013; Mottram et al., 2014; Johnson et al., 2015; Engi, 2017; Weller et al., 2020). Aluminous gneisses are particularly well suited for this approach, as they commonly host petrochronometers such as monazite, xenotime, zircon, apatite and titanite, as well as a diverse suite of metamorphic index minerals that provide first–order constraints on the timing of metamorphism and pressure—temperature (P—T) conditions (Spear and Pyle, 2002; Engi, 2017; Weller et al., 2020). Furthermore, the integration of *in situ* U—Th—Pb isotopic dating on monazite and xenotime grains when interpreted in conjunction with Lu—Hf garnet petrochronology has been widely applied in metamorphic studies to establish precise temporal constraints on garnet growth and metamorphic evolution (Hagen-Peter et al., 2016; Godet et al., 2020; Larson et al., 2022; Tual et al., 2022; Battisti et al., 2024).

By applying this multi–method analytical approach, I present new petrochronological constraints on metamorphic evolution in the Mauricie region. The results demonstrate that all three lithotectonic domains within the study area—Shawinigan, Mékinac–Taureau, and Portneuf–St. Maurice—record Grenvillian metamorphism and there is no recorded evidence of upper amphibolite to granulite facies metamorphism during the Shawinigan Orogeny in the Mauricie region. Prograde metamorphism associated to the Grenville Orogeny, however, started at 1137 ± 13 | 24 Ma, illustrating that the commonly accepted date of the collision (ca. 1090 Ma; Hynes and Rivers, 2010; Rivers, 2012) does not take into account the early part of the metamorphic evolution.

1.2 The Grenville Province

The Grenville Province records evidence of multiple tectono–magmatic events along the long-lived southeastern margin of Laurentia starting at ca. 1800 Ma and followed by a collision with Amazonia during the ca. 1090 to 980 Ma Grenville Orogeny (Figure 1.1; Rivers et al., 2012;

Swanson–Hysell et al., 2023). The pre–Grenvillian development of the southeastern Laurentian margin (present-day coordinates) was separated into regional scale events or orogenies, including the Labradorian (ca. 1710—1600 Ma; Gower and Krogh, 2002), Pinwarian (ca. 1520—1460 Ma; Tucker and Gower, 1990), Elsonian (ca. 1460—1230 Ma; Gower and Krogh, 2002), Elzevirian (ca. 1250—1180 Ma; Carr et al., 2000) and Shawinigan (ca. 1190—1140 Ma; Rivers, 2012) orogenies.

The Labradorian Orogeny (ca. 1710—1600 Ma) involved the formation of an oceanic arc, outboard of Laurentia between ca. 1710 and 1655 Ma, and its accretion to the Laurentian margin at ca. 1665—1655 Ma, which resulted in granulite facies metamorphism (Gower and Krogh, 2002). This metamorphic event was followed by voluminous Trans–Labradorian magmatism that formed a linear belt over 600 km long at ca. 1654—1646 Ma concurrently to the deposition of felsic volcanic and sedimentary supracrustal sequences (Gower et al., 1992, 1996; Corrigan et al., 2000; Gower et al., 2008).

The Pinwarian Orogeny (ca. 1520—1460 Ma) is primarily characterized by felsic magmatism into Labradorian crust in Labrador, easternmost Quebec, and Newfoundland (Gower and Krogh 2002; Gower et al., 2008). Magmatism is likely the result of prolonged island–arc and continental–arc (and back–arc) processes, whereas associated metamorphism and deformation are related to accretion and active margin shortening (Gower, 1996; Rivers, 1997; Rivers and Corrigan, 2000; Gower and Krogh, 2002; Dickin and McNutt, 2007; Slagstad et al., 2009).

The concept of the “Elsonian Orogeny” was first proposed by Stockwell (1964) to describe a period marked by anorthosite–mangerite–charnockite–granite (AMCG) magmatism and reworked older gneiss units. However, Emslie (1978) noted that the Elsonian did not truly qualify as an orogenic event and should instead be viewed within a magmatic framework—a perspective that has since been widely adopted. Later, Gower and Krogh (2002) reintroduced the Elsonian Orogeny (ca. 1460—1230 Ma) in the eastern Grenville Province. There, magmatic activity is believed to be related to a continental arc and back–arc (Corrigan and van Breemen, 1997; Rivers and Corrigan, 2000; Gower and Krogh, 2002; Slagstad et al., 2009; Dunning and Indares, 2010). A tectonic event is recorded in the central Grenville Province during that period, involving the accretion of a peri–Laurentian arc system (Corrigan and van Breemen, 1997; Sappin et al., 2009; Groulier et al., 2018a). The Escoumins supracrustal belt (Figure 1.1) is composed of a ca. 1490—1460 Ma bimodal volcanic sequence and its ca. 1500 Ma calc–alkalic and high–K granitoid basement interpreted as having developed in a complex tectonic setting involving a peri–Laurentian island arc, a rifted–arc, and a back–arc system (Groulier et al., 2020). It was accreted to the Laurentian margin and metamorphosed during early Elsonian at ca. 1390 Ma. Southwest of the Escoumins belt, in the Mauricie area, the ca. 1450 Ma Montauban volcano–sedimentary belt records the accretion of an island arc at ca. 1400 Ma, contemporaneous with the development of an Andean–type continental margin (Hanmer and McEachern, 1992; McEachern and van Breemen, 1993; Corrigan and van Breemen, 1997; Sappin et al., 2009; Sappin et al., 2012).

The Elzevirian Orogeny occurred between ca. 1250 and 1180 Ma and represents an arc terrane accretion and amalgamation outboard of Laurentia (Carr et al., 2000). This tectonic event is marked by calc–alkaline magmatic activity and associated granulite–facies metamorphism (Corriveau and van Breemen, 2000; Boggs and Corriveau, 2004; Dickin and McNutt, 2007; Hynes and Rivers, 2010). Evidence for the Elzevirian accretionary Orogeny is predominantly documented in southwestern Grenville Province (Figure 1.2; Corfu and Easton, 1995; Davis and Bartlett, 1988; Carr et al., 2000; McLelland et al., 2010). Contemporaneous volcanic and plutonic rocks linked to extensional settings (rift or back–arc environments) have been identified in the central and eastern Grenville Province (Indares et al., 1998; Dunning and Indares, 2010; Indares and Moukhsil, 2013).

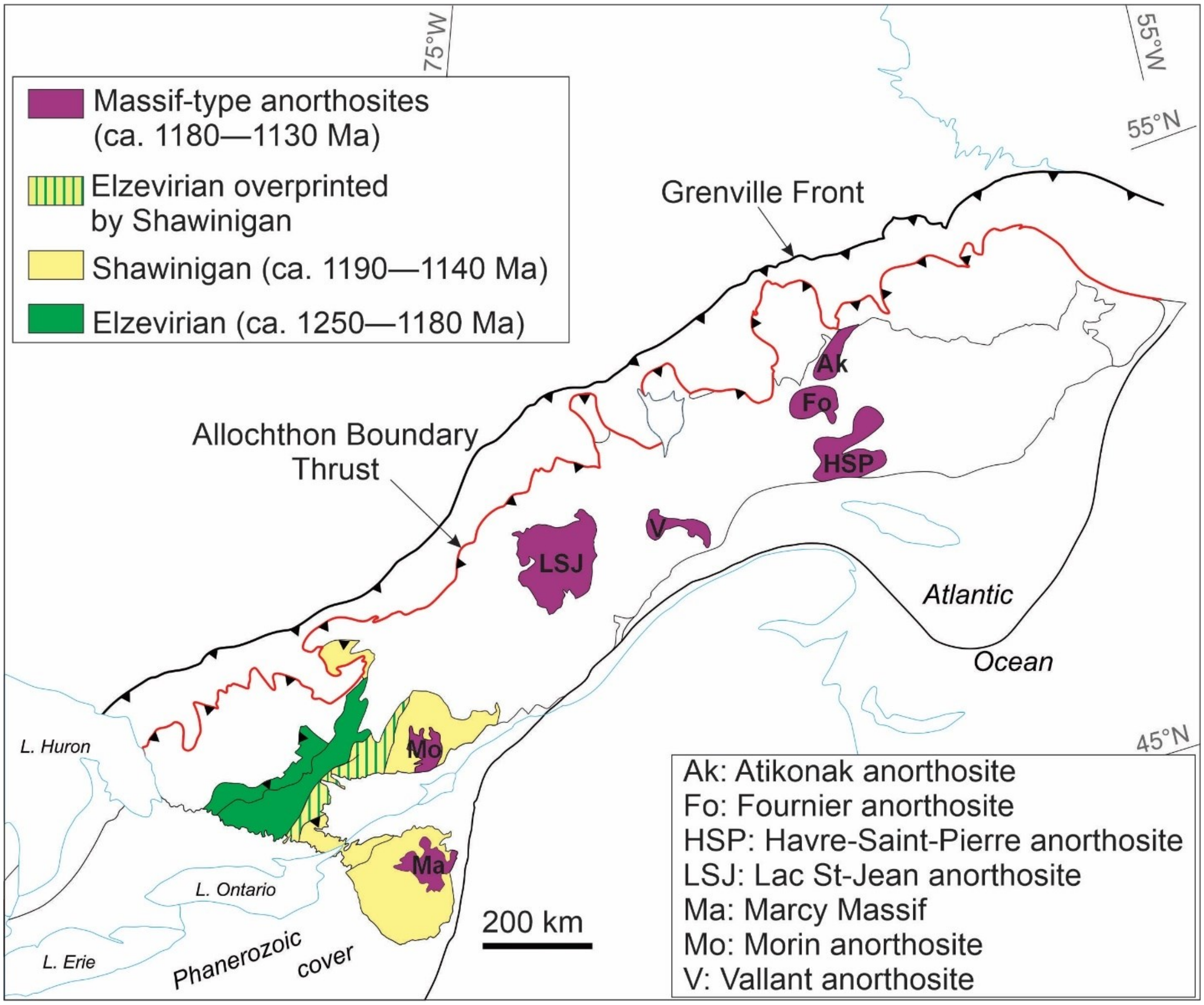

Figure 1.2 : Map of the Grenville Province.

Spatial extent of Elzevirian and Shawinigan metamorphism, and the distribution of ca. 1180—1130 Ma anorthosite bodies. Modified from Rivers et al. (2012), Corrigan (2024) and Indares (2024).

The Shawinigan Orogeny (ca. 1190—1140 Ma) is characterized by granulite facies metamorphism and deformation primarily identified in the southwestern Grenville Province (Adirondack Highlands, western Quebec and Ontario) that has been correlated with an accretionary episode (Figure 1.2; McLelland et al., 2010, 2013). Between ca. 1180 and 1120 Ma, magmatic activity was widespread in the Grenville Province (Gower and Krogh, 2002; Heumann et al., 2006; Hynes and Rivers, 2010; Rivers et al., 2012). This magmatic activity was predominantly characterized by anorthosite–mangerite–charnockite–granite (AMCG) suites, accompanied by a substantial presence of gabbroic to granitic plutons and mafic dyke and sill swarms (Doig, 1991; Higgins et al., 2002; Hébert and van Breemen, 2004). The formation of these igneous bodies is thought to be linked to late–to post–orogenic tectonic processes following significant crustal thickening associated with the accretionary Shawinigan Orogeny. Possible mechanisms include the delamination of overthickened lithospheric mantle in a compressional orogen, lithospheric convective thinning, flat–slab subduction, and slab breakoff (Corrigan and Hanmer, 1997; McLelland et al., 2010).

The Grenville Orogeny (sensu stricto. 1090—980 Ma) is marked by a prolonged (>100 Myr) period of episodic regional scale crustal thickening, followed by phases of extensional thinning, which mainly affected the partly reworked Laurentian crust (Corrigan and van Breemen, 1997; Hynes and Rivers, 2010; Rivers et al., 2012; Indares, 2025). It marks the continental collision between Laurentia and Amazonia (Rivers, 1997; Carr et al., 2000; Swanson–Hysell et al., 2023), although this final collision has also been interpreted to have started at ca. 1030 Ma (Gervais et al., 2023, 2024; cf. Slagstad et al., 2023). The Grenville Orogeny includes the Ottawan phase (ca. 1090—1020 Ma) and the Rigolet phase (ca. 1005—980 Ma). The Ottawan phase is characterized by widespread high–grade metamorphism and penetrative deformation, recorded in the Allochthonous belt in the orogenic hinterland (Figure 1.1). The Ottawan crustal thickening was followed by crustal extension, represented by mid-crustal shear zones such as, in the central Grenville Province, the 1064 ± 15 Ma eastern Taureau shear zone (Soucy La Roche et al., 2015), and the ca. 1065—1035 Ma Tawachiche shear zone (Corrigan and van Breemen, 1997). The ca. 1005—980 Ma Rigolet phase mainly affected the Parautochthonous belt in the NW part of the Grenville Orogen (Figure 1.1; Rivers et al., 2012; River, 2021). The Parautochthonous belt is separated from the Allochthonous belt by the Allochthon Boundary Thrust (Figure 1.1; Rivers et al., 1989; Rivers et al., 2012). In the Parautochthonous belt, the metamorphic grade increases from greenschist facies near the Grenville Front to the northwest to amphibolite, granulite, and locally eclogite–facies conditions in the footwall of the Allochthon Boundary Thrust to the southeast (Rivers, 2012; Lotout et al., 2023). Rigolet metamorphism overprints locally-preserved Archean metamorphic assemblages (Godet et al., 2024). The Rigolet phase has been interpreted as a relatively cold, large-scale orogenic thrust stack (Rivers, 2012), or as a major tectonometamorphic event that involved protracted melting and crustal flow (Jannin et al., 2018; Lambert et al., 2023).

The Allochthonous belt preserves signatures of Laurentian crust but is inferred to be more far travelled compared to the Parautochthonous belt (Rivers et al., 2012). Ottawan metamorphism persisted for at least ca. 30—40 Myr, though its exact timing varied across the Grenville Orogen (Jamieson et al., 2007; Rivers, 2012). The Allochthonous belt is subdivided into four distinct belts, based on their relative positions in the orogenic crust during the Ottawan phase (Rivers, 2008, 2012). The deepest part of the Ottawan orogenic infrastructure is represented by the allochthonous high–pressure belt, located structurally above the Allochthon Boundary Thrust (Figure 1.1). In western Grenville Province, mafic rock units are characterized by relict ca. 1090 Ma (early Ottawan) eclogite facies metamorphism overprinted by ca. 1080—1040 Ma granulite–facies metamorphism (Marsh and Culshaw, 2014). In the central Grenville Province, high–pressure granulite and locally eclogite facies metamorphism occurred during the late Ottawan to Rigolet phases, as reported from the western Manicouagan Imbricate zone (1033 ± 6 Ma, 1020 ± 20 Ma and 1013 ± 6 Ma Lu-Hf garnet crystallization ages; Lotout et al., 2023).

The allochthonous medium–pressure belt represents the mid–crustal level of the Ottawan orogenic infrastructure and is the most widely exposed belt, stretching along the entire length of the Grenville Province (Figure 1.1; Rivers, 2008, 2012; Indares, 2020). This belt is characterized by medium–pressure granulite facies metamorphism that occurred between ca. 1080 and 1040 Ma (e.g., central Grenville Province: Dunning and Indares, 2010; western Grenville Province: Slagstad et al., 2004).

The allochthonous low-pressure belt represents the highest structural level of the Ottawan orogenic infrastructure and is sparsely distributed along the southern, central and western portions of the Grenville Province (Figure 1.1; Rivers, 2008, 2012; Groulier et al., 2018a). Rock units in the allochthonous low-pressure belt are reported from the Escoumins supracrustal belt and the Mazinaw, Portneuf–St. Maurice, and Natashquan domains (Rivers, 2008; Groulier et al., 2018a; Groulier et al., 2018b). The allochthonous low-pressure belt is juxtaposed with the allochthonous medium–pressure belt along late–Ottawan extensional shear zones (Figure 1.1; Corrigan and van Breemen, 1997; Rivers, 2008, 2012; Soucy La Roche et al., 2015). The allochthonous low-pressure belt records metamorphic conditions ranging from greenschist metamorphic facies (e.g., Natashquan and Mazinaw domains; Wodicka et al. 2004) to amphibolite facies (e.g., Escoumins supracrustal belt; Groulier et al., 2018a) and low-pressure granulite facies (e.g., Portneuf–St. Maurice domain, although the age of granulite facies metamorphism in the latter has also been interpreted to be ca. 1400 Ma; Corrigan, 1995; Corrigan and van Breemen, 1997). Finally, the Ottawan Orogenic Lid forms the Ottawan orogenic suprastructure in the orogenic hinterland (Figure 1.1; Rivers, 2008, 2012). The rock units of the Ottawan Orogenic Lid, largely exposed in the SW and NE parts of the Grenville Province, escaped Ottawan penetrative deformation and metamorphism (Rivers, 2008, 2012).

1.3 Geology of the study area

This research work focused on the southern Mauricie and southwestern Portneuf area, located in the central part of the Grenville Province (Figures 1.1 and 1.3). This area is composed of rock units of the allochthonous medium–pressure belt and allochthonous low-pressure belt separated into the Mékinac–Taureau, Shawinigan and Portneuf–St. Maurice lithotectonic domains (Figure 1.3; Nadeau and Brouillette, 1994, 1995).

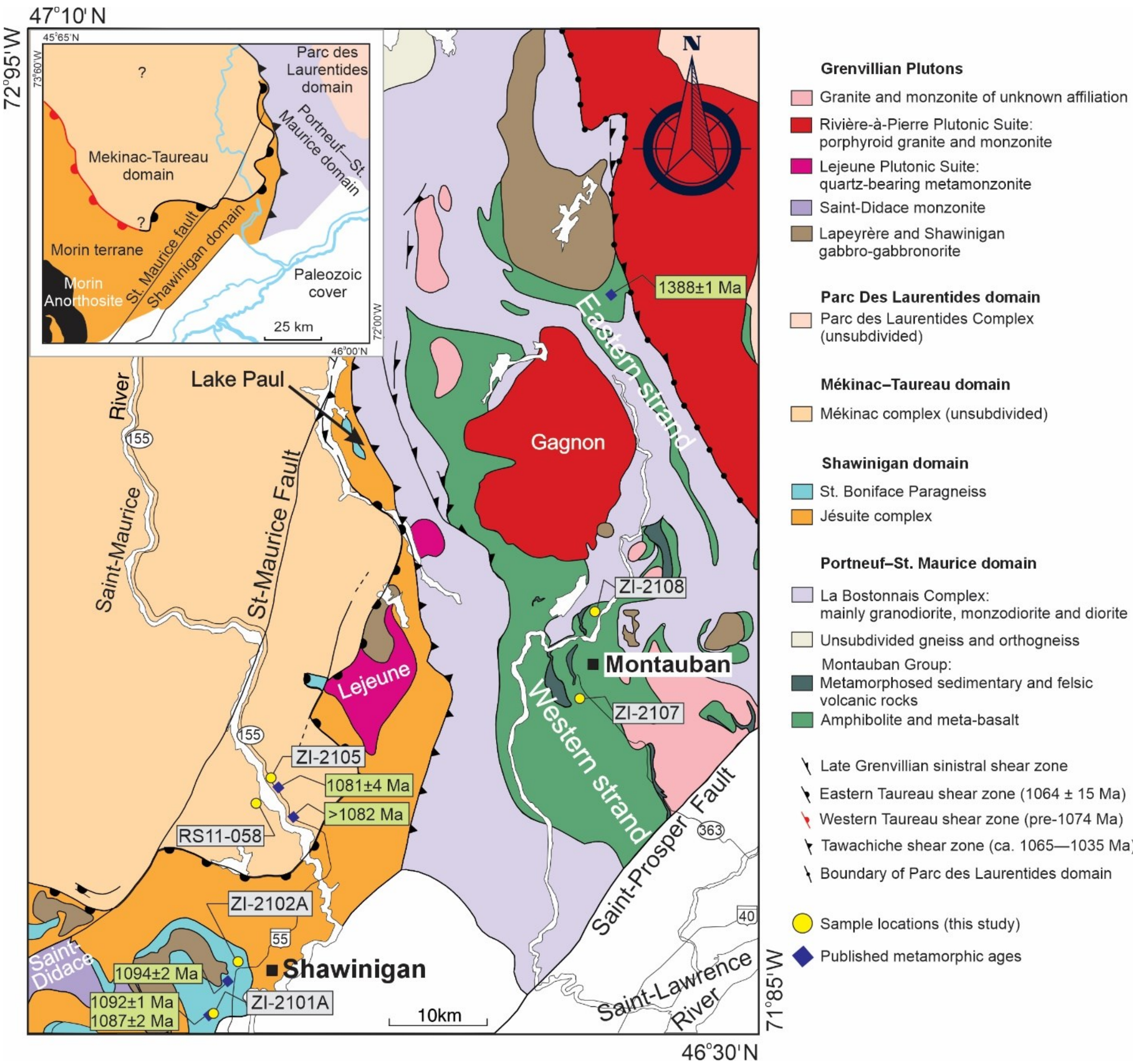

Figure 1.3 : Simplified geological map of the Mauricie area.

From Sappin et al. (2011) and Nadeau et al. (2009), modified from Nadeau and Brouillette (1995), and Nadeau et al. (2008). The >1082 Ma age (U-Pb on zircon from pegmatite) constrains the minimum age of metamorphism (Soucy La Roche et al., 2015). The 1081 ± 4 Ma, 1092 ± 1 Ma, 1094 ± 2 Ma, 1388 ± 1 Ma (U-Pb on monazite from metapelites), and 1087 ± 2 Ma (U-Pb on zircon from

metapelite), metamorphic ages are from Corrigan (1995). The Lake Paul granite is too small to be displayed on the map, but an arrow points to its location.

1.3.1 Mékinac–Taureau domain

The structurally lowest Mékinac–Taureau domain stretches ~ 80 km from the St. Maurice River to the Taureau Reservoir. The Mékinac–Taureau domain is predominantly composed of ca. 1370 Ma dioritic, granodioritic and granitic orthogneiss and local lenses of paragneiss (age from Nadeau and van Breemen, unpublished data reported in Corrigan and van Breemen, 1997; Nadeau and Brouillette, 1995). In the Mauricie area, the Mékinac–Taureau domain experienced peak P–T conditions of 1000—1100 MPa and 820—880 °C (garnet-biotite (GB) thermometry, garnet-sillimanite-plagioclase-quartz (GASP) baromometry and garnet-plagioclase-hornblende thermobarometry) before 1082 ± 20 Ma based on the crystallization age of a foliation-oblique granitic pegmatite that merges with stromatic leucosome (Table 1; Soucy La Roche et al., 2015). Corrigan (1995) reports a single grain 1081 ± 4 Ma monazite date in a metapelite acquired with isotope-dilution thermal ionisation mass spectrometry (ID–TIMS), which he attributed to cooling through 725 °C. The closure temperature for U–Pb isotopic diffusion in monazite was later demonstrated to be much higher (> 900 °C; Spear and Pyle, 2002; Cherniak et al., 2004; Engi, 2017 and references therein.), therefore, the significance of this date is equivocal. Metamorphism is likely due to northwestward thrusting during regional scale crustal stacking (Corrigan and van Breemen, 1997; Soucy La Roche et al., 2015). To the south and southeast, the Mékinac–Taureau domain lies in tectonic contact with the structurally higher Shawinigan domain of the Morin terrane along the 1064 ± 15 Ma normal–sense eastern Taureau shear zone, which was active under retrograde metamorphic conditions (≤ 600—700 MPa and ≤ 675—775 °C; Figure 1.3; Soucy La Roche et al., 2015).

1.3.2 Shawinigan domain

The Shawinigan domain represents the eastward extension of the Morin terrane, south of the Mékinac–Taureau domain (Figure 1.3). The Shawinigan domain is composed of the Jésuite complex and St. Boniface paragneiss (Corrigan, 1995; Nadeau and Brouillette, 1995). The Jésuite complex comprises ca. 1370 Ma orthogneiss (U-Pb zircon; protolith age) of tonalitic composition with local occurrences of granite and rare gabbro (Corrigan and van Breemen, 1997). The tectonically overlying St. Boniface paragneiss comprises metapelite interlayered with marble and quartzite with a maximum age of deposition of 1253 ± 11 Ma based on detrital zircon (Peck et al., 2019). Voluminous AMCG plutons, porphyritic granite, gabbro and monzonite intruded the Morin terrane (including the Shawinigan domain) during two distinct episodes of magmatic activity (Corrigan and van **Breemen, 1997). The first pulse encompasses the Morin anorthositic complex**

Litho-tectonic domain	Lithological units	Pressure-temperature (P-T) conditions	P-T interpretations	Method	Age interpretation and mineral dated	References
Mékinac–Taureau domain	Metapelite	1000—1100 MPa 820—880ºC	Peak	GB thermometry; GASP barometry; GPH thermobarometery	Peak metamorphism before 1082 ± 20 Ma (U-Pb zircon)	Soucy La Roche et al., 2015
	Paragneiss	600—688 °C 766—879 °C 770—1290 MPa	Peak	Grt-Opx thermometry Grt-Cpx thermometry GASP barometry		Corrigan, 1995
	Metapelite	705 °C 900 MPa	Peak	Grt-Cpx thermometry, GASP barometry		Corrigan, 1995
		~725°C	Cooling		1081±4 Ma on monazite	Corrigan, 1995
	Metapelite	775—675◦C; 800—650 MPa	Retrograde	GPH thermobarometery	At 1064 ± 15 Ma (U-Pb zircon)	Soucy La Roche et al., 2015
		<550—600◦C	Cooling		ca. 1030—1000 Ma (^{40}Ar-^{39}Ar amphibole)	Soucy La Roche et al., 2015
		<450◦C	Cooling		ca. 970—900 Ma (^{40}Ar-^{39}Ar biotite)	Soucy La Roche et al., 2015
		800-820◦C 900—1150 MPa		GB thermometry; GASP barometry		Levesque, 1995

Shawinigan domain	Metapelite	775—700◦C 850—625 MPa		GB thermometry; GASP barometry		Soucy La Roche et al., 2015
	Metapelite	836 °C 750 MPa	Near-peak	GB thermometry; GASP thermobarometry;	Melt crystallization at 1092 ± 1 Ma (monazite) and 1087 ± 2 Ma (zircon) from a leucosome; cooling age at 1094 ± 2 Ma (monazite)	Corrigan, 1995
	Metapelite	652—716 °C 719—841 °C 850 MPa	Retrograde	Grt-Opx thermometry Grt-Cpx thermometry GASP barometry		Corrigan, 1995
	Syn-thrusting mylonitic metapelite	510 °C 450 MPa	Retrograde	GB thermometry; GASP barometry		Corrigan, 1995
		550—600◦C	Cooling		~1000—1030 Ma (^{40}Ar-^{39}Ar amphibole)	Soucy La Roche et al., 2015
		< 450◦C	Cooling		~900—970 Ma (^{40}Ar-^{39}Ar biotite)	Soucy La Roche et al., 2015
		478 ± 22 °C 320 ± 40 MPa	Retrograde	GB thermometry; GASP barometry		Corrigan, 1995
		724—798°C 720—880 MPa		GB thermometry; GASP barometry		Levesque, 1995

Portneuf–St. Maurice domain (Eastern strand)	Metapelite	734 °C 758 °C 710 MPa 630 MPa		GB thermometry Grt-Crd thermometry GASP barometry Grt-Spl barometry		Corrigan, 1995
	Metapelite	758 ± 5°C 640 ± 3 MPa		Grt-Crd thermometry GASP barometry; Grt-Spl barometry Al-in Hbl barometry	ca. 1388 ± 1 Ma (U-Pb monazite)	Corrigan, 1995
		678—740°C 570-660 MPa		GB thermometry; GASP barometry		Levesque, 1995
		~ 550 °C			1020—1010 Ma ^{40}Ar-^{39}Ar hornblende cooling ages	Corrigan, 1995
Portneuf–St. Maurice domain (Western strand)	Metapelite	320—490 MPa 544—638°C		GB thermometry Al in Hbl barometry, GASP barometry		Corrigan, 1995

Table 1.1: Compilation of the published P-T-t data from Mékinac–Taureau, Shawinigan and Portneuf–St. Maurice domain in Mauricie area, Quebec.

Thermobarometry abbreviations: GB: garnet-biotite, GASP: garnet-sillimanite-plagioclase-quartz, GPH: garnet-plagioclase-hornblende, Grt-Opx: garnet-orthopyroxene, Grt-Cpx: garnet-clinopyroxene, Grt-Crd: garnet-cordierite, Grt-Spl: garnet-spinel, Al-in Hbl: aluminum in hornblende.

(ca. 1165—1135 Ma; Doig, 1991; Friedman and Martignole, 1995), the Lac Croche complex (ca. 1140 Ma; Barton and Doig, 1972), and the Lake Paul granite (1153 ± 2/1 Ma; Corrigan and van Breemen, 1997). The Lac Croche and Morin anorthositic complexes and the Lac Paul granite are located about 75—100 km west and approximately 30 km north, respectively, of my study area. The second magmatic pulse includes the Shawinigan norite (1077 ± 10/2 Ma; Corrigan and van Breemen, 1997), the Lejeune complex (1059 ± 2 Ma; Corrigan and van Breemen, 1997), and the St. Didace complex (1072 ± 2 Ma; Figure 1.3; Nadeau and van Breemen, unpublished data reported in Nadeau et al., 2008).

Pressure–temperature conditions of metamorphism in the Shawinigan domain are estimated at 850 to 625 MPa and 775 to 700 °C (GB and GASP thermobarometry; Table 1; Soucy La Roche et al., 2015), comparatively lower than the underlying Mékinac–Taureau domain. Melt crystallization occurred during the earliest Ottawan, based on U—Pb geochronology on monazite (1092 ± 1 Ma) and zircon (1087 ± 2 Ma) from a leucosome, whereas a 1094 ± 2 Ma monazite date from a quartzite was interpreted as a cooling age (Corrigan, 1995). However, the metamorphic evolution of the Shawinigan domain may be more complex because zircon and titanite metamorphic ages spanning from the Shawinigan Orogeny (ca. 1190—1140 Ma) to the Ottawan orogenic phase (ca. 1085—1075 Ma) were documented in the Morin terrane to the west (Peck, 2012, Peck and Quinan, 2022). The high–metamorphic grade of the rocks in the Morin terrane has been interpreted to result from local thermal heating during the ca. 1160—1135 Ma Morin AMCG magmatism (Martignole and Schrijver, 1970; Doig, 1991; Martignole et al., 2000). Alternatively, the lack of correlation between peak metamorphic temperatures and distance from AMCG plutons (Peck et al., 2005), and metamorphic fabrics crosscut by these plutons indicate that granulite facies in the Morin terrane may have resulted from regional metamorphism during the Shawinigan Orogeny (ca. 1190—1140 Ma; Peck and Quinan, 2022).

The eastern boundary of the Shawinigan domain is the ca. 1065 to 1035 Ma oblique–normal–sense Tawachiche shear zone that separates it from the Portneuf–St. Maurice domain (Figure 1.3; Corrigan, 1995; Corrigan and van Breemen, 1997).

1.3.3 Portneuf–St. Maurice domain

The Portneuf–St. Maurice domain structurally overlies the Shawinigan and Mékinac–Taureau domains along the Tawachiche shear zone (Figure 1.3). The Portneuf–St. Maurice domain comprises remnants of the accreted ca. 1450 Ma Montauban island arc and/or back–arc basin and associated metasedimentary rocks and the ca. 1400—1370 Ma calc–alkaline plutonic rocks of the La Bostonnais complex (Nadeau and Brouillette, 1995; Corrigan and van Breemen, 1997). Corrigan and van Breemen (1997) interpreted the La Bostonnais complex to be a possible low metamorphic–grade equivalent of the ca. 1370 Ma orthogneiss in the Mékinac–Taureau and Shawinigan domains. Rocks of the Portneuf–St. Maurice domain experienced dominantly middle to upper amphibolite–facies metamorphic conditions (320—500 MPa and 544—638 °C; Corrigan, 1995), except in the eastern segment, which recorded low to medium–pressure granulite facies conditions (570—710 MPa and 678—760 °C; GB, GASP, Grt-Crd, Grt-Spl thermobarometry; Table 1; Corrigan, 1995; Levesque, 1995). Timing of metamorphism is constrained to ca. 1390 Ma based on monazite U—Pb geochronology on a single sample (Corrigan, 1995). Metamorphism across the domain is inferred to result from the accretion of the Montauban arc, whereas Ottawan–aged metamorphism would have been limited, although ca. 1020—1010 Ma $^{40}Ar/^{39}Ar$ hornblende cooling ages indicate that temperature reached at least ~ 550 °C during the Ottawan phase (Corrigan, 1995). The Portneuf–St. Maurice domain was thus included in the allochthonous low-pressure belt by Rivers (2012).

1.4 Scientific problems and research objectives

The lithotectonic domains in the Mauricie region are thought to have preserved evidence of metamorphism and deformation related to pre-Grenvillian accretionary orogenies and to the Grenville Orogeny (e.g., Corrigan, 1995; Peck and Quinan, 2022). However, the exact timing and duration of metamorphism in these domains are poorly constrained. Granulite facies metamorphism in the Mékinac–Taureau domain was attained prior to 1082 ± 20 Ma; however, the timing of the earlier prograde metamorphism leading to peak conditions remains uncertain. Additionally, the culmination of granulite facies metamorphism is not well constrained; while subsequent cooling to temperatures ≤550–600 °C is inferred to have occurred at ca. 1000–1030 Ma, indicated by $^{40}Ar/^{39}Ar$ hornblende cooling ages (Corrigan, 1995; Soucy La Roche et al., 2015).

The maximum age of metamorphism in the Shawinigan domain was loosely constrained by the age of crystallization of igneous protoliths or the depositional age of metasedimentary units. For example, the St. Boniface quartzite in the Shawinigan domain has a maximum depositional age of 1250 ± 11 Ma (U—Pb on detrital zircon, Peck et al., 2019), which implies that metamorphism must be younger than the maximum age of deposition of the quartzite. Corrigan (1995) dated monazite (1092 ± 1 Ma, concordant date) and zircon (1087 ± 2 Ma upper intercept date from discordant fractions) from a deformed leucosome in a paragneiss layer adjacent to the quartzite, which constrains the crystallization age of the leucosome. The age of prograde and peak metamorphism and their duration are therefore unconstrained.

A high grade metapelite from the eastern strand of the Portneuf St. Maurice domain yielded a single 1388 ± 1 Ma metamorphic monazite date (Corrigan, 1995) that is the only constraint on the accretion of the Montauban arc to the extended SE Laurentian continental margin. This domain was at least partially overprinted during the Grenville Orogeny, as indicated by the resetting of $^{40}Ar/^{39}Ar$ hornblende cooling ages at ca. 1020–1010 Ma (Corrigan, 1995), however, the exact timing of Grenvillian metamorphism is not constrained. Grenvillian metamorphism in this domain may have resulted from the juxtaposition with the hotter underlying Shawinigan domain during its exhumation (Rivers, 2008, 2012). However, this model needs to be tested through detailed geochronological and metamorphic constraints.

This M.Sc. thesis aims to constrain the timing and metamorphic conditions of the Mauricie region (Figures 1.1 and 1.3) to provide new insights into the tectonometamorphic evolution of the central Grenville Province, Quebec. The research objectives outlined below are designed to address the gaps in geochronological and metamorphic understanding:

1. Characterize the timing of the prograde, peak, and post–peak segments along the P—T—t loop and identify their associated mineral assemblages within each domain.
2. Compare and contrast the metamorphic evolution in each domain, and integrate the new data into tectonic models of the central Grenville Province.

1.5 Methodology

1.5.1 Fieldwork

I visited more than 20 outcrops and collected 11 aluminous gneiss samples from the Mékinac–Taureau, Shawinigan and Portneuf–St. Maurice domains (Figure 1.3). Outcrops of aluminous gneiss with garnet, sillimanite and/or K-feldspar were selected based on the descriptions of Lévesque (1995), Corrigan (1995) and Soucy La Roche et al. (2015). Field observations included identification of lithological units and index minerals, and measurement of mesoscopic structures. Aluminous gneiss samples were collected for *in situ* U—Th—Pb petrochronology on monazite and xenotime as well as *in situ* Lu—Hf petrochronology on garnet.

1.5.2 Analytical techniques

A brief overview of analytical methods is provided here, and they are described in detail in section 2.4. Thin sections were cut normal to the foliation plane and parallel to the mineral lineation. Peak mineral assemblage, accessory phases, and mineral inclusions in metamorphic porphyroblasts were identified based on detailed petrography to constrain the metamorphic evolution qualitatively.

Micro X-ray fluorescence (μ—XRF) mapping of the thin sections was employed to identify major, minor and most accessory minerals and assess chemical zoning of major elements in garnet. Element maps were generated using a Bruker M4 Tornado at Université Laval.

Monazite, xenotime and apatite were identified in element maps of thin sections, acquired with a Cameca SX–Five Field Emission Electron Probe Microanalyzer (EPMA) equipped with five wavelength–dispersive spectrometers (WDS), housed at the Fipke Laboratory for Trace Element Research (FiLTER), University of British Columbia, Okanagan. Elemental maps were processed in ImageJ and overlaid on backscattered electron (BSE) images to characterize the textural setting of the petrochronometers.

The identification of monazite and xenotime grains along with their grain morphology, size and shape was confirmed with a Carl Zeiss EVO® 50 scanning electron microscope (SEM) equipped with an energy–dispersive spectroscopy (EDS) detector, housed at INRS–ETE. Image processing software Corel Photo–Paint was used to enhance BSE zoning to guide the placement of LA–ICP–MS analytical spots.

In situ U—Th—Pb analyses were conducted using laser ablation inductively coupled plasma mass spectrometry (LA–ICP–MS) at FiLTER. Target samples were ablated using an ESL NWR 193 excimer laser with a TwoVol3 cell paired with an Agilent 8900 inductively coupled plasma tandem mass spectrometer (ICP–MS/MS) operated in single MS mode, allowing for concurrent acquisition of isotopic ratios and trace elements.

Trace element mapping was conducted prior to *in situ* Lu—Hf dating to optimize laser spot placement and assess the spatial distribution of trace elements. *In situ* LA–ICP–MS analyses were conducted at the FiLTER using an ESL193 excimer laser ablation system paired with a TwoVol3 sample chamber and an Agilent 8900 ICP–MS/MS.

1.6 Thesis structure

This thesis is presented in a manuscript format in fulfillment of the requirements for the Master of Science (M.Sc.) degree in Earth Sciences at the Centre Eau Terre Environnement, Institut national de la recherche scientifique (INRS–ETE), Université du Québec. It comprises three main chapters, followed by a bibliography of the references cited in the thesis. Data tables and supplementary figures are provided in separate Excel and PDF files.

Chapter 1 introduces the research topic by outlining the regional geological background and summarizing previous work conducted in the study area. It identifies key scientific questions and knowledge gap that this research aims to address. The chapter concludes with a statement of the study objectives and an overview of the methodology employed to achieve the research objectives and fill the knowledge gap.

Chapter 2 consists of a manuscript prepared for submission to the journal "Precambrian Research", entitled: " *Constraining the Timing of Mesoproterozoic Metamorphism in the Central Grenville Province (Mauricie, Québec): A Petrochronological Study of Monazite, Xenotime and Garnet*", authored by M. Z. Iqbal, R. Soucy La Roche, and K. Larson. This manuscript forms the core of the thesis. It presents new geochronological results to constrain the timing of metamorphism in the Mauricie region, central Grenville Province. The study integrates petrographic observations with *in situ* U—Th—Pb monazite and xenotime petrochronology and *in situ* Lu—Hf garnet petrochronology from six aluminous gneiss samples. The results are interpreted in the context of regional tectonometamorphic evolution and compared with existing geochronological data to assess the temporal and spatial framework of metamorphism in the study area. The chapter concludes by discussing the broader tectonic implications of these new results to decipher the timing and metamorphic evolution of the central Grenville Province.

The contribution of each author are as follows:

1. M. Z. Iqbal (first author) conducted fieldwork, sample selection and preparation, petrographic observations, data acquisition and processing at FiLTER, University of British Columbia–Okanagan, and interpretation of the geochemical and geochronological datasets. He prepared all data tables and figures and wrote the entire manuscript/thesis.
2. R. Soucy La Roche helped with field planning, outcrop descriptions and sampling, sample selection, petrography, and provided guidance in data filtering, interpretation, and extensive editorial feedback on the figures, data tables, and the manuscript.

3. K. Larson provided guidance in data processing at the FiLTER, University of British Columbia, Okanagan, and revised the detailed methodology section in Chapter 2.

Chapter 3 provides a synthesis of the main findings presented in Chapter 2 and discuss their significance within the regional geological framework and how they meet the scientific objectives outlined in Chapter 1.

Supplementary materials include field photographs, mosaic images of selected thin sections, backscattered electron (BSE) images of monazite and xenotime with corresponding LA–ICP–MS spot locations, representative geochemical plots and age diagrams, LA–ICP–MS trace element maps of garnet, inverse isochron diagrams, laser spots on garnet grains, and complete datasets for all petrochronological analyses and representative μ–XRF maps. The data tables provided in the supplementary material include data for unknowns, and primary and secondary reference materials used in the isotopic analysis.

2 ARTICLE

Constraining the Timing of Mesoproterozoic Metamorphism in the Central Grenville Province (Mauricie, Québec): A Petrochronological Study of Monazite, Xenotime and Garnet

Muhammad Zahoor Iqbal[1]

Renaud Soucy La Roche[1]

Kyle Larson[2]

1 Centre Eau Terre Environnement, Institut national de la recherche scientifique, 490 rue de la Couronne, Québec, G1K 9A9, QC, Canada.

2 Department of Earth, Environmental and Geographic Sciences, University of British Columbia Okanagan, 3333 University Way, Kelowna, V1V 1V7, BC, Canada.

Corresponding author: Muhammad Zahoor Iqbal

Email: Mzahooriqbal@gmail.com

2.1 Abstract

Despite decades of research on the late Mesoproterozoic to early Neoproterozoic Grenville Orogeny, key aspects, such as the timing of initial continental collision and the duration of metamorphism, remain poorly resolved. In this study, we integrate *in situ* U–Th–Pb monazite and xenotime and *in situ* Lu–Hf garnet petrochronology with detailed microtextural observations to constrain the metamorphic evolution of aluminous gneiss from the Mékinac–Taureau, Shawinigan, and Portneuf–St. Maurice domains in the Mauricie region, Quebec, central Grenville Province. Three distinct metamorphic stages are recognized. Amphibolite facies prograde metamorphic conditions related to the onset of the continental collision are recorded as early as 1137 ± 13 | 24 Ma, predating the traditionally defined Ottawan phase (ca. 1090 Ma) of the Grenville Orogeny. Peak metamorphism occurred during Ottawan phase (ca. 1100–1050 Ma) under suprasolidus granulite facies conditions in the structurally lowest Mékinac–Taureau and Shawinigan domains and under subsolidus amphibolite facies conditions in the structurally highest Portneuf–St. Maurice domain. Retrograde metamorphism and cooling followed at ≤1045 Ma and continued until at least ca. 980 Ma. These results document a protracted metamorphic history spanning ~150 Myr, including ~50 Myr of high-temperature mid-crustal residence, supporting a long-lived, continental collisional Grenville Orogeny. Our new data do not readily fit in current geodynamic models. Future revised models must address more effectively the protracted evolution of the Grenville Orogeny, which initiated as early as 1137 ± 13 | 24 Ma, and its temporal overlap with the development of a major rift system within Laurentia.

Keywords: Continental collision onset, crustal thickening, protracted metamorphism, monazite petrochronology, *in situ* garnet geochronology

2.2 Introduction

The Grenville Province in central and western Quebec preserves evidence of multiple tectono-magmatic events along the long-lived southeastern continental active margin of Laurentia starting at ca. 1800 Ma until the final collision with Amazonia during the ca. 1090 to 980 Ma Grenville Orogeny (Figure 2.1; Rivers et al., 2012; Swanson–Hysell et al., 2023). Geochronological data are key to understand the timing and duration of metamorphic events (e.g., Labrousse et al., 2024), which is foundational to reconstruct tectonic models of the Grenville Province (Rivers et al., 2012).

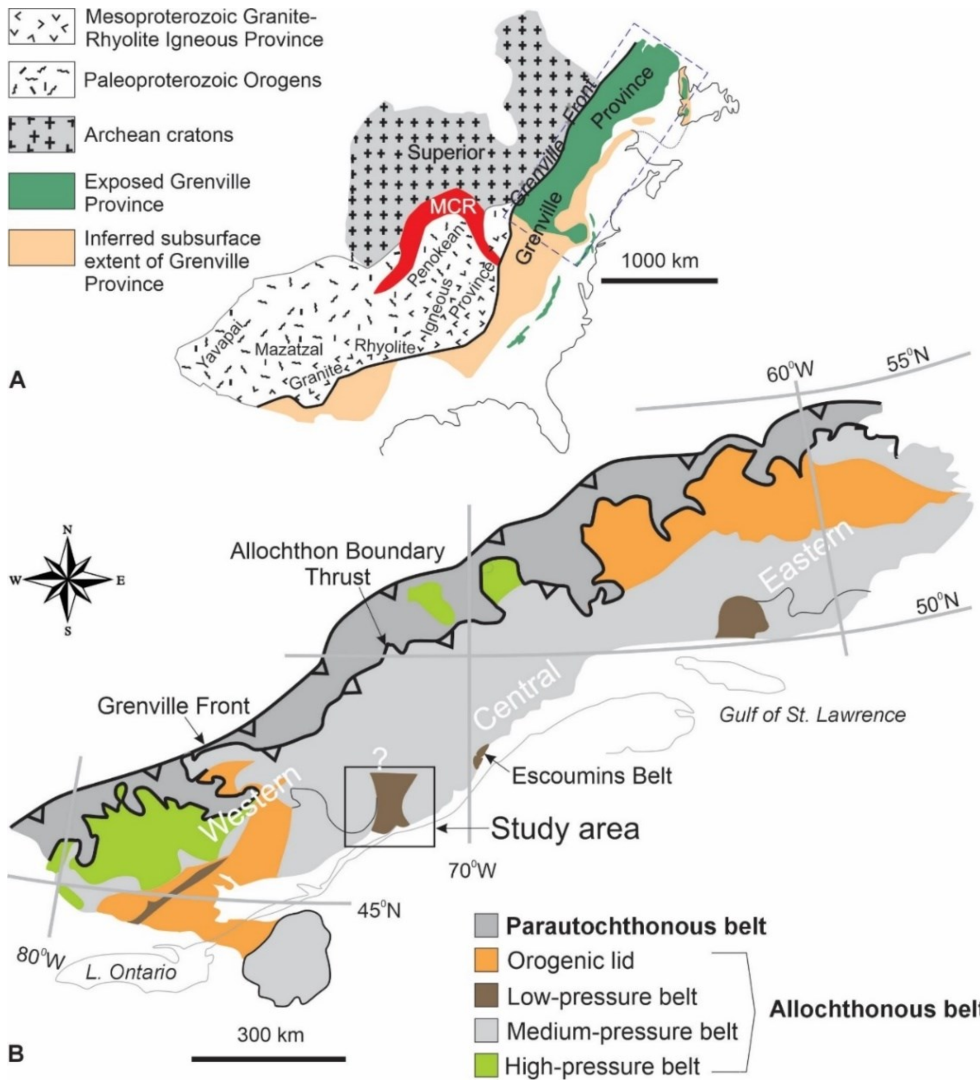

Figure 2.1: Precambrian tectonic framework of Laurentia and regional tectonic map of Grenville Province.

(A) Tectonic framework of Laurentia during the Precambrian, illustrating major cratonic and orogenic domains. From Rivers et al. (2012), modified from Hoffman (1989). (B) Enlarged view of the outlined area in (A), presenting a simplified geological map of the Grenville Province (modified from Rivers, 2008). The map delineates the distribution of Parautochthonous and Allochthonous belts. The study area is indicated by a black box.

Geochronological constraints across the Grenville Province have largely been derived from zircon and to a lesser extent monazite U-Pb ages (e.g., Corrigan, 1995; Corriveau and van Breemen, 2000; Indares and Dunning, 2001; Wodicka et al., 2004; Peck, 2012; Peck et al., 2013). Historically, zircon and monazite were dated using isotope dilution–thermal ionization mass spectrometry (ID-TIMS) or more rarely using sensitive high-resolution ion microprobe (SHRIMP) on mineral separates. Sparse U–Pb data (LA–ICP–MS analyses) are also available on monazite (e.g., Lasalle et al., 2014; McCarron et al., 2014), zircon (e.g., Marsh and Culshaw, 2014; Peck et al., 2019; Shinevar et al., 2021; Culshaw et al., 2023), and titanite (e.g., Peck and Quinan, 2022). However, the interpretation of geochronological data from mineral separates presents challenges, particularly due to the potentially complex growth and resorption histories of accessory minerals along the pressure–temperature (P–T) path. Although ID-TIMS provides highly precise dates, it lacks spatial resolution and several studies used multi-grain aliquots (e.g., Chiarenzelli and McLelland, 1991; McLelland et al., 2001, 2002), which may have lead to mixing of different age domains, thereby obscuring the timing of discrete metamorphic stages (Schoene, 2014). Whole-grain ID-TIMS dating is generally effective for igneous chronometers that crystallized during a single event with no metamorphic overprinting, but resolving metamorphic ages present greater challenges. Specifically, accessory chronometers (e.g., zircon and monazite) may crystallize over a range of metamorphic conditions. Zircon ages are traditionally interpreted in the Grenville Province to record prograde or peak metamorphic conditions (e.g., Corriveau and van Breemen, 2000; Cox et al., 2002; Schneider et al. 2013; Marsh and Culshaw, 2014; Culshaw et al., 2016). However, recent work using textural observations and trace element composition in conjunction with phase equilibrium modelling (Dyer et al., 2025) demonstrates that zircon growth in meta-granitoid samples from the SW Grenville Province results from melt crystallization and breakdown of titanomagnetite during retrograde metamorphism, which has important implications for tectonic models. Phase equilibria modeling in pelitic compositions suggest that zircon is likely to remain stable during prograde to near-peak conditions, but it is expected to undergo dissolution in melt under peak temperatures (Yakymchuk and Brown, 2014). Similarly, monazite may crystallize under subsolidus conditions, dissolve during anatexis and recrystalize during cooling and melt crystallization, and thus making it difficult to directly link U–Pb dates to specific metamorphic reactions or stages of the P-T loop (Spear and Pyle, 2002; Williams et al., 2007). Without integrating microtextural context to understand the growth of chronometers along the pressure–temperature (P–T) path, interpretations based solely on U–Pb dates may be misleading. Thus, ID-TIMS age interpretation of zircon and monazite in the Grenville Province are often ambiguous in the absence of detailed textural characterization and a clear link to specific metamorphic reactions. These challenges are magnified in long-lived orogenic systems, for instance, in the Grenville Orogen, where high-temperature metamorphism in the middle to lower crust persisted over tens of millions of years (Beaumont et al., 2006).

Other petrochronometers are also useful to complement our understanding of the metamorphic evolution. For example, Lu–Hf garnet dating offers a promising yet underutilized approach for constraining the timing of metamorphism in the Grenville Province. Garnet dating can be performed by isotope dilution with high precision (< 2.4% and as low as ~ 0.3%) but limited spatial resolution (Anczkiewicz et al., 2014; Gaidies e al., 2021; Godet et al., 2021; Lotout et al., 2023; Glorie et al., 2024), or by *in-situ* laser ablation with low precision (~15% and as low as ~1.5%) and high spatial resolution (Simpson et al., 2023; Godet et al., 2024; Larson et al., 2024). Recent studies in the Grenville Province have demonstrated the potential of isotope dilution (Lotout et al., 2023) and *in situ* laser ablation (Gaidies et al., 2024; Godet et al., 2024) Lu-Hf garnet petrochronology, underscoring the need for its broader application to improve temporal resolution in metamorphic studies. In these studies, Lu–Hf garnet dates are interpreted to represent the age of prograde and peak metamorphism. The Mauricie region, located in the central Grenville Province, offers an ideal geological setting to assess the timing of metamorphism associated with the Grenville Orogeny. The area is well characterized in terms of geology, structure and tectonic boundaries, and the three lithotectonic domains making up the area were interpreted to have been metamorphosed at different times and/or P-T conditions (Corrigan, 1995; Corrigan and van Breemen, 1997; Soucy La Roche et al., 2015; Peck et al., 2019). However, geochronological constraints supporting this interpretation are limited and often equivocal.

To address this knowledge gap, we combine *in situ* U—Th—Pb monazite and xenotime petrochronology and *in situ* Lu—Hf garnet petrochronology, aimed at providing reliable constraints on the timing of prograde, peak and retrograde metamorphism in the Mauricie region. This approach combines isotopic and trace element analysis of petrochronometers with detailed petrographic characterization of their microtextural relationships with metamorphic index minerals. Such integration allows us to link the crystallization of petrochronometers to the growth and resorption of index minerals during their metamorphic evolution, providing a more comprehensive view of the metamorphic evolution (Spear and Pyle, 2002; Pyle and Spear, 2003; Wing et al., 2003; Gibson et al., 2004; Rubatto et al., 2013; Mottram et al., 2014; Johnson et al., 2015; Engi, 2017; Weller et al., 2020; Soucy La Roche et al., 2022).

We present new petrochronological constraints on the timing of metamorphism in the Mauricie region. These results demonstrate that all three lithotectonic domains investigated—the Mékinac–

Taureau, Shawinigan, and Portneuf–St. Maurice domains—record a protracted metamorphic evolution associated with the Grenville Orogeny. In addition, no geochronological evidence supports upper amphibolite to granulite facies metamorphism attributable to the earlier Shawinigan accretionary Orogeny in this region. Furthermore, our data refined the timing of continental collision and constrained both the initiation and culmination of the Grenville Orogeny. These findings provide critical insights into a prolonged metamorphic evolution of the central Grenville Province and enhance our broader understanding of its tectonometamorphic history.

2.3 Geological setting

2.3.1 Grenville Province

The Grenville Province records multiple tectono–magmatic events along the long-lived southeastern margin of Laurentia from ca. 1800 Ma until the final collision with Amazonia during the ca. 1090 to 980 Ma Grenville Orogeny (Figure 2.1; Rivers et al., 2012; Swanson–Hysell et al., 2023). The pre–Grenvillian development of the southeastern Laurentian margin (present-day coordinates) was separated into regional scale orogenies, including the Labradorian (ca. 1710—1600 Ma; Gower and Krogh, 2002), Pinwarian (ca. 1520—1460 Ma; Tucker and Gower, 1990; Groulier et al., 2018a), Elsonian (ca. 1460—1230 Ma; Gower and Krogh, 2002; Groulier et al., 2018a), Elzevirian (ca. 1250—1180 Ma; Carr et al., 2000) and Shawinigan (ca. 1190—1140 Ma; Rivers et al., 2012) orogenies. The Elsonian, Shawinigan and Grenville orogenies are particularly important in the central Grenville Province, Quebec.

Although the Elsonian period (ca. 1460—1230 Ma) is associated with continental arc magmatism in large portions of the Grenville Province, especially in the eastern part (Emslie, 1978; Gower and Krogh, 2002), a tectonic event in the Mauricie area involved the ca. 1400—1390 Ma accretion of a peri–Laurentian arc system which is represented by the ca. 1450 Ma Montauban volcano–sedimentary belt (Corrigan and van Breemen, 1997; Sappin et al., 2009). Accretion was contemporaneous with the development of an Andean–type continental margin (Hanmer and McEachern, 1992; McEachern and van Breemen, 1993; Corrigan and van Breemen, 1997; Sappin et al., 2009, 2012; Groulier et al., 2020).

The Shawinigan Orogeny (ca. 1190—1140 Ma) is characterized by granulite facies metamorphism and deformation documented locally in the southwestern Grenville Province (Adirondack Highlands, western Quebec and Ontario) that has been interpreted as the result of an accretionary episode (Figure 2.2; Wodicka et al., 2000; Heumann et al., 2006; Chiarenzelli et al., 2011; McLelland et al., 2010, 2013; Darling and Peck, 2016; Markley et al., 2018; Peck et al., 2019; Valentino et al., 2019; Williams et al., 2019; Peck and Quinan, 2022). Between ca. 1180 and 1120 Ma, magmatic activity was widespread in the Grenville Province (Gower and Krogh, 2002; Heumann et al., 2006; Hynes and Rivers, 2010; Rivers et al., 2012). This magmatic activity was predominantly characterized by anorthosite–mangerite–charnockite–granite (AMCG) suites (Higgins et al., 2002; Hébert and van Breemen, 2004; McLelland et al., 2004, 2010). In the central and southwestern Grenville Province, these igneous bodies are thought to be caused by late–to post–orogenic tectonic processes following significant crustal thickening associated with the accretionary Shawinigan Orogeny. Possible mechanisms include the delamination of overthickened lithospheric mantle in a compressional orogen, lithospheric thinning and slab breakoff (Corrigan and Hanmer, 1997; McLelland et al., 2010).The Grenville Orogeny (ca. 1090—980 Ma) is characterized by a >100 Myr period of episodic crustal thickening followed by phases of extensional thinning, which mainly affected the partly reworked Laurentian crust (Hynes and Rivers, 2010; Rivers et al., 2012). It marks the continental collision between Laurentia and Amazonia (Rivers, 1997; Carr et al., 2000; Swanson–Hysell et al., 2023), although this final collision has also been interpreted to have occurred at ca. 1030 Ma following a period of shortening in a micro-continent outboard of Laurentia (Gervais et al., 2023, 2024; c.f. Slagstad et al., 2023). The Grenville Orogeny includes the Ottawan phase (ca. 1090—1020 Ma) and the Rigolet phase (ca. 1005—980 Ma; Rivers et al., 2012). The Ottawan phase is characterized by widespread high–grade metamorphism and penetrative deformation, preserved in the Allochthonous belt in the orogenic hinterland, where the study area is located, whereas the ca. 1005—980 Ma Rigolet phase mainly affected the Parautochthonous belt in the NW part of the Grenville Orogen (Figure 2.1; Rivers et al., 2012; River, 2021). These belts are separated by the Allochthon Boundary Thrust (Figure 2.1; Rivers et al., 1989; Rivers et al., 2012).

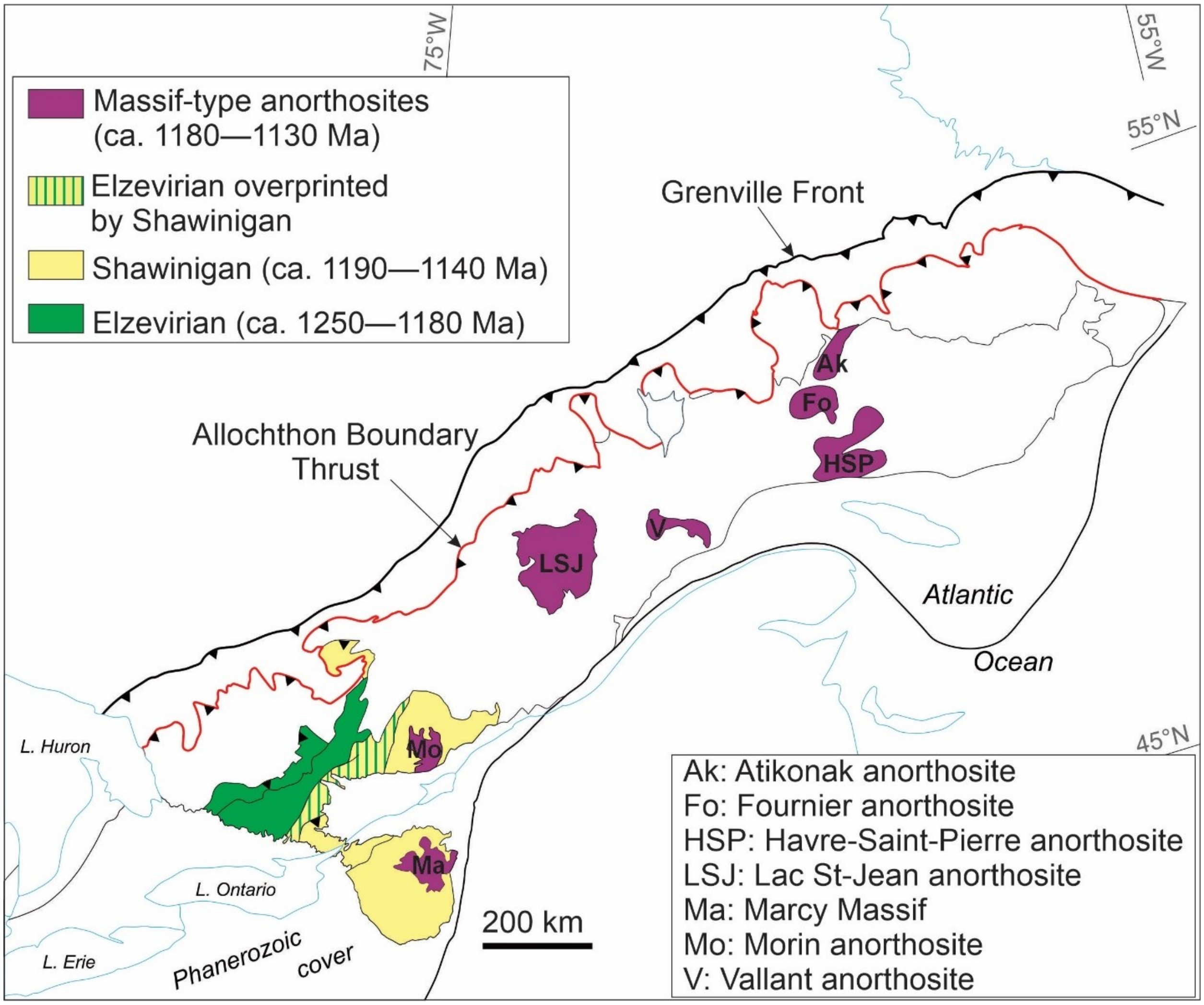

Figure 2.2: Map of the Grenville Province.

Spatial extent of Elzevirian and Shawinigan metamorphism, and the distribution of ca. 1180—1130 Ma anorthosite bodies. Modified from Rivers et al. (2012), Corrigan (2024) and Indares (2024).

Ottawan metamorphism persisted for at least ca. 30—40 Myr, though its exact timing varied across the Grenville Orogen (Jamieson et al., 2007; Rivers, 2012). The Allochthonous belt is subdivided into four distinct belts, based on their relative positions in the orogenic crust during the Ottawan phase (Rivers, 2008, 2012). The deepest part of the Ottawan orogenic infrastructure is represented by the Allochthonous high–pressure belt, located structurally above the Allochthon Boundary Thrust (Figure 2.1). In western Grenville Province, mafic rock units are characterized by relict ca. 1090 Ma (early Ottawan) eclogite facies metamorphism overprinted by ca. 1080—1040 Ma granulite facies metamorphism (Marsh and Culshaw, 2014). In the central Grenville

Province, high–pressure granulite and locally eclogite facies metamorphism occurred during the mid to late Ottawan (ca. 1050—1020 Ma; Indares et al., 2000; Lotout et al., 2023).

The Allochthonous medium–pressure belt represents the mid–crustal level of the Ottawan orogenic infrastructure and is the most widely exposed belt, stretching along the entire length of the Grenville Province (Figure 2.1; Rivers, 2008, 2012; Indares, 2020). This belt is characterized by medium–pressure granulite facies metamorphism that occurred between ca. 1080 and 1040 Ma (e.g., central Grenville Province: Dunning and Indares, 2010; western Grenville Province: Slagstad et al., 2004).

The Allochthonous low-pressure belt represents the highest structural level of the Ottawan orogenic infrastructure and is sparsely distributed along the southern, central and western portions of the Grenville Province (Rivers, 2008, 2012; Groulier et al., 2018a). Rock units in the Allochthonous low-pressure belt are reported from the Escoumins supracrustal belt and the Mazinaw, Portneuf–St. Maurice, and Natashquan domains (Rivers, 2008; Groulier et al., 2018a, b). The Allochthonous low-pressure belt is juxtaposed with the Allochthonous medium–pressure belt along late–Ottawan extensional shear zones (Corrigan and van Breemen, 1997; Rivers, 2008, 2012; Soucy La Roche et al., 2015). The Allochthonous low-pressure belt records metamorphic conditions during the Ottawan ranging from greenschist metamorphic facies (e.g., Natashquan and Mazinaw domains; Wodicka et al. 2004) to amphibolite facies (e.g., Escoumins supracrustal belt; Groulier et al., 2018a) and low-pressure granulite facies (e.g., Portneuf–St. Maurice domain, although the age of granulite facies metamorphism in the latter has also been interpreted to be ca. 1400 Ma (Corrigan, 1995; Corrigan and van Breemen, 1997).

Finally, the Ottawan Orogenic Lid forms the Ottawan orogenic suprastructure in the hinterland (Rivers, 2008, 2012). The rock units of the Ottawan Orogenic Lid (OOL), largely exposed in the SW and NE parts of the Grenville Province, escaped Ottawan penetrative deformation and metamorphism (Figure 2.1; Rivers, 2008, 2012).

2.3.2 Geology of the Mauricie region

This research work focused on the southern Mauricie and southwestern Portneuf area, located in the central part of the Grenville Province (Figures 2.1 and 2.3). The study area is composed of rock units of the Allochthonous medium–pressure and low-pressure belts separated into the Mékinac–Taureau, Shawinigan and Portneuf–St. Maurice lithotectonic domains (Figure 2.3; Nadeau and Brouillette, 1994, 1995).

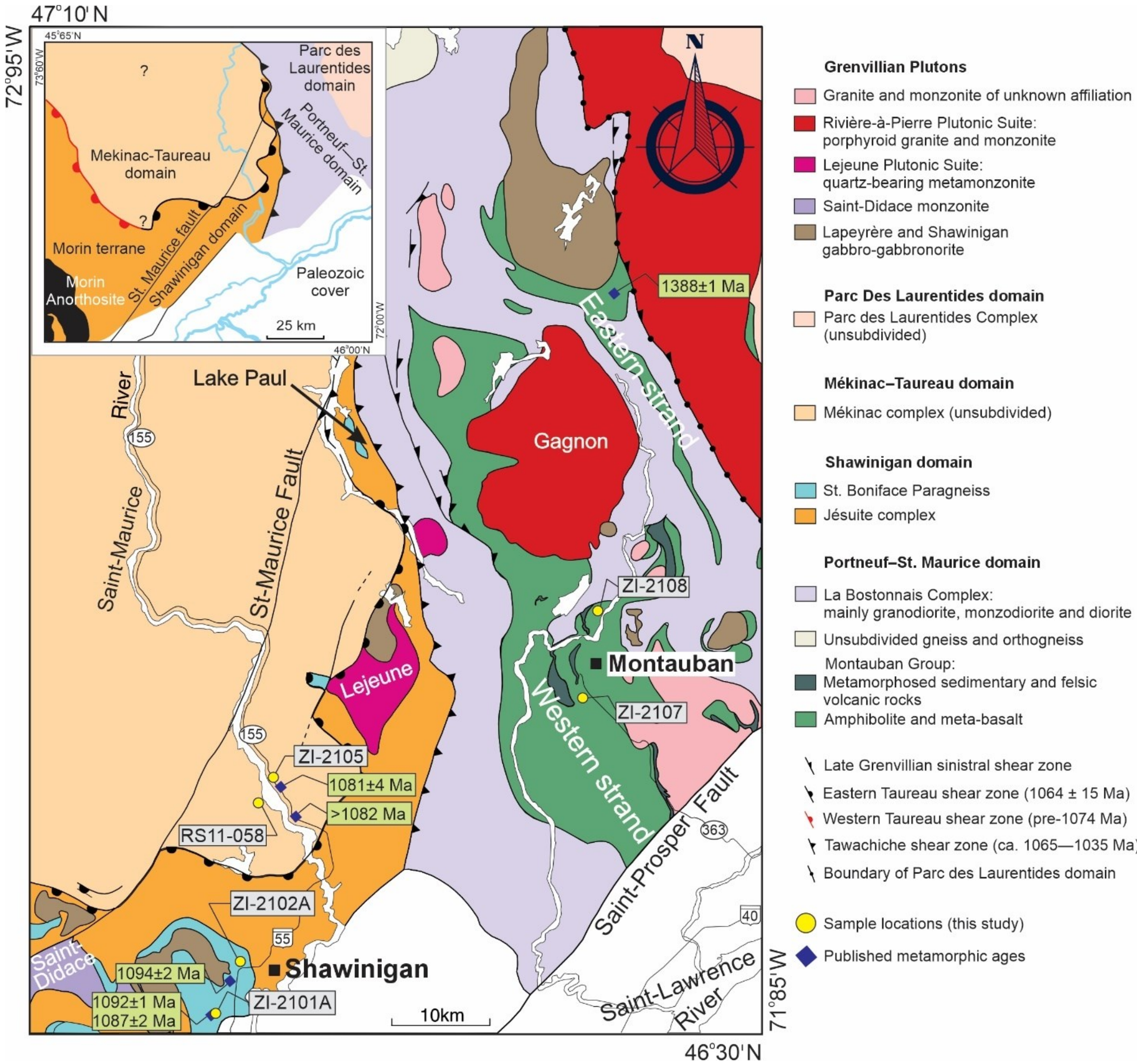

Figure 2.3: Simplified geological map of the Mauricie area.

From Sappin et al. (2011) and Nadeau et al. (2009), modified from Nadeau and Brouillette (1995), and Nadeau et al. (2008). The >1082 Ma age (U-Pb on zircon from pegmatite) constrains the minimum age of metamorphism (Soucy La Roche et al., 2015). The 1081 ± 4 Ma, 1092 ± 1 Ma, 1094 ± 2 Ma, 1388 ± 1 Ma (U-Pb on monazite from metapelites), and 1087 ± 2 Ma (U-Pb on zircon from metapelite), metamorphic ages are from Corrigan (1995). The Lake Paul granite is too small to be displayed on the map, but an arrow points to its location.

2.3.2.1 Mékinac–Taureau domain

The structurally lowest Mékinac–Taureau domain stretches ~ 80 km from the St. Maurice River to the Taureau Reservoir. It is predominantly composed of ca. 1370 Ma dioritic, granodioritic and granitic orthogneiss and local lenses of paragneiss (age from Nadeau and van Breemen, unpublished data reported in Corrigan and van Breemen, 1997; Nadeau and Brouillette, 1995).

In the Mauricie area, the Mékinac–Taureau domain experienced peak P–T conditions of 1000—1100 MPa and 820—880 °C (garnet-biotite (GB) thermometry, garnet-sillimanite-plagioclase-quartz (GASP) baromometry and garnet-plagioclase-hornblende thermobarometry) before 1082 ± 20 Ma, based on the crystallization age of a foliation-oblique granitic pegmatite that merges with stromatic leucosome (Soucy La Roche et al., 2015). Corrigan (1995) reports a single–grain ID–TIMS 1081 ± 4 Ma monazite date in a metapelite, which he attributed to cooling through 725 °C. The closure temperature for U–Pb isotopic diffusion in monazite was later demonstrated to be much higher (> 900 °C; Spear and Pyle, 2002; Cherniak et al., 2004; Engi, 2017 and references therein), therefore, the significance of this date is ambiguous. Metamorphism is likely due to northwestward thrusting during regional scale crustal stacking (Corrigan and van Breemen, 1997; Soucy La Roche et al., 2015). Cooling through ~550–600 °C and ~450 °C occurred at ca. 1030–985 Ma and ca. 970–920 Ma based on hornblende and biotite cooling ages, respectively (Corrigan, 1995; Soucy La Roche et al., 2015). To the south and southeast, the Mékinac–Taureau domain lies in tectonic contact with the structurally higher Shawinigan domain of the Morin terrane along the 1064 ± 15 Ma normal–sense eastern Taureau shear zone, which was active under retrograde metamorphic conditions (≤ 600—700 MPa and ≤ 675—775 °C; (Figure 2.3; Soucy La Roche et al., 2015).

2.3.2.2 Shawinigan domain

The Shawinigan domain represents the eastward extension of the Morin terrane, south of the Mékinac–Taureau domain (Figure 2.3). The Shawinigan domain is composed of the Jésuite complex and St. Boniface paragneiss (Corrigan, 1995; Nadeau and Brouillette, 1995). The Jésuite complex comprises ca. 1370 Ma orthogneiss (U-Pb zircon; protolith age) of tonalitic composition with local occurrences of granite and rare gabbro (Corrigan and van Breemen, 1997). The tectonically overlying St. Boniface paragneiss comprises metapelite interlayered with marble and quartzite with a maximum age of deposition of 1253 ± 11 Ma (detrital zircon; Peck et al., 2019). Voluminous AMCG plutons, porphyritic granite, gabbro and monzonite intruded the Shawinigan domain (including the Morin Terrane) during two distinct episodes of magmatic activity (Corrigan and van Breemen, 1997). The first pulse encompasses the Morin anorthositic complex (ca. 1165—1135 Ma; Doig, 1991; Friedman and Martignole, 1995), the Lac Croche complex (ca. 1140 Ma; Barton and Doig, 1972), and the Lake Paul granite (1153 ± 2/1 Ma; Corrigan and van Breemen, 1997). The Lac Croche and Morin anorthositic complexes and the Lac Paul granite are located about 75–100 km west and approximately 30 km north, respectively, of our study area.

The second magmatic pulse includes the Shawinigan norite (1077 ±10/2 Ma; Corrigan and van Breemen, 1997), the Lejeune complex (1059 ± 2 Ma; Corrigan and van Breemen, 1997), and the St. Didace complex (1072 ± 2 Ma; Figure 2.3; Nadeau and van Breemen, unpublished data reported in Nadeau et al., 2008).

Pressure–temperature conditions of metamorphism in the Shawinigan domain are estimated at 850 to 625 MPa and 775 to 700 °C (GB and GASP thermobarometry; Soucy La Roche et al., 2015), comparatively lower than the underlying Mékinac–Taureau domain. Melt crystallization occurred during the earliest Ottawan, based on U—Pb geochronology on monazite (1092 ± 1 Ma) and zircon (1087 ± 2 Ma) from a leucosome, whereas a 1094 ± 2 Ma monazite date from a quartzite was interpreted as a cooling age (Corrigan, 1995). Zircon and titanite metamorphic ages spanning from the Shawinigan Orogeny (ca. 1190—1140 Ma) to the Ottawan orogenic phase (ca. 1085—1075 Ma) were documented in the Morin terrane to the west (Peck, 2012, Peck and Quinan, 2022). Granulite facies metamorphism there has been interpreted to result from local thermal heating during the ca. 1160—1135 Ma Morin AMCG magmatism (Martignole and Schrijver, 1970; Doig, 1991; Martignole et al., 2000). Alternatively, the lack of correlation between peak metamorphic temperatures and distance from AMCG–suite plutons (Peck et al., 2005) and metamorphic fabrics crosscut by these plutons indicate that granulite facies in the Morin terrane resulted from regional metamorphism during the Shawinigan Orogeny (ca. 1190—1140 Ma; Peck and Quinan, 2022). The extent of ca. 1190—1140 Ma metamorphism in the Shawinigan domain has not been constrained. Cooling of the Shawinigan domain below ~550–600 °C and ~450 °C is constrained at ca. 1030–1020 Ma and ca. 930–905 Ma based on hornblende and biotite cooling ages, respectively (Soucy La Roche et al., 2015). The eastern boundary of the Shawinigan domain is the ca. 1065 to 1035 Ma oblique–normal–sense Tawachiche shear zone that separates it from the Portneuf–St. Maurice domain (Figure 2.3; Corrigan, 1995; Corrigan and van Breemen, 1997).

2.3.2.3 Portneuf–St. Maurice domain

The Portneuf–St. Maurice domain structurally overlies the Shawinigan and Mékinac–Taureau domains along the Tawachiche shear zone (Figure 2.3). The Portneuf–St. Maurice domain comprises remnants of the accreted ca. 1450 Ma Montauban island arc and/or back–arc basin and associated metasedimentary rocks and the ca. 1400—1370 Ma calc–alkaline plutonic rocks of the La Bostonnais complex (Nadeau and Brouillette, 1995; Corrigan and van Breemen, 1997). Corrigan and van Breemen (1997) interpreted the La Bostonnais complex to be a possible low metamorphic–grade equivalent of the ca. 1370 Ma orthogneiss in the Mékinac–Taureau and Shawinigan domains. Rocks of the Portneuf–St. Maurice domain experienced dominantly middle to upper amphibolite facies metamorphic conditions (320—500 MPa and 544—638 °C; Corrigan, 1995), except in the eastern segment, which recorded low to medium–pressure granulite facies conditions (570—660 MPa and 678—750 °C; GB and GASP thermobarometry; Corrigan, 1995; Levesque, 1995). Timing of metamorphism is constrained to ca. 1390 Ma based on monazite U—Pb geochronology on a single sample (Corrigan, 1995). Metamorphism across the domain is thus inferred to result from the accretion of the Montauban arc to the Laurentian margin, whereas Ottawan–aged metamorphism would have been limited, although ca. 1020—1010 Ma $^{40}Ar/^{39}Ar$ hornblende cooling ages indicate that temperature reached at least ~550—600 °C during the Ottawan (Corrigan, 1995). The Portneuf–St. Maurice domain was thus included in the Allochthonous low-pressure belt by Rivers (2012).

2.4 Analytical Methods

2.4.1 Micro—X-ray fluorescence (μ—XRF)

Micro X-ray fluorescence (μ—XRF) mapping of entire thin sections was employed to identify major, minor and most accessory minerals and assess chemical zoning of major elements in garnet. Element maps were generated using a Bruker M4 Tornado at Université Laval. Analytical conditions were an accelerating voltage of 50 kV, a beam current of 600 mA, a step size of 20 μm, and a dwell time of 5 ms. The elements analyzed included ^{27}Al, ^{40}Ca, ^{140}Ce, ^{52}Cr, ^{56}Fe, ^{39}K, ^{24}Mg, ^{56}Mn, ^{23}Na, ^{59}Ni, ^{31}P, ^{32}S, ^{28}Si, ^{49}Ti, ^{65}Zn, and ^{90}Zr.

2.4.2 Electron probe microanalyzer geochemical mapping

Monazite, xenotime and apatite were identified in element maps of entire thin sections acquired with a Cameca SX–Five Field Emission Electron Probe Microanalyzer (EPMA) equipped with five wavelength–dispersive spectrometers (WDS), housed at the Fipke Laboratory for Trace Element Research (FiLTER), University of British Columbia, Okanagan. Maps were collected with a 15 kV accelerating voltage, a 200 nA current, a step size and beam diameter of approximately 40 μm, and a dwell time of 25 ms. The mapping lines employed were Ce–Lα, Y–Lα, P–Kα, Ca–Kα, and Ti–Kα. Monazite, xenotime and apatite were identified based on the co-occurrence of Ce and P (without Ca), Y and P (without Ce) and P and Ca, respectively. Element maps were processed in ImageJ and overlaid on backscattered electron images (collected concomitantly) to characterize the textural setting of the petrochronometers.

2.4.3 Scanning electron microscopy

The identification of monazite and xenotime grains was confirmed with a Carl Zeiss EVO® 50 scanning electron microscope (SEM) equipped with an energy–dispersive spectroscopy (EDS) detector, housed at INRS–ETE. Analytical conditions were set to 20 keV accelerating voltage, a beam intensity of 4.2 nA, and a variable working distance of 8.5 to 9.5 mm, depending on the size of the grains. Data acquisition and processing were performed using the ESPRIT software (version 2.2.0.3007). High-resolution BSE images of monazite and xenotime were acquired with the same SEM to examine grain morphology, size, shape, and inclusions, if present. Inclusions in monazite and xenotime were identified with EDS. Image processing software Corel Photo–Paint was used to enhance BSE zoning to guide the placement of LA–ICP–MS analysis.

2.4.4 *In situ* U—Th—Pb petrochronology on monazite and xenotime

In situ U—Th—Pb analyses were conducted using laser ablation inductively coupled plasma mass spectrometry (LA–ICP–MS) at FiLTER. Carbon coating was removed from all samples prior to ablation. Target samples were ablated using an ESL NWR 193 excimer laser with a TwoVol3 cell paired with an Agilent 8900 inductively coupled plasma tandem mass spectrometer (ICP–MS/MS) operated in single MS mode, allowing for concurrent acquisition of isotopic ratios and trace elements. Spot analyses of monazite and xenotime were carried out with a laser diameter of 15 µm with a fluence of ~1.5 J cm^{-2} and a repetition rate of 8 Hz. Analyses were carried out using a traditional bracketing technique with analyses of reference materials every 10-15 unknowns. Corrections for background, instrumental drift, mass bias, and downhole fractionation were applied using the Iolite v4 software package (Paton et al., 2011). Six samples were analyzed across two analytical runs (run_1 = RS11-058, ZI-2105 and ZI-2101A and run_2 = ZI-2102A, ZI-2107 and ZI-2108), using the same reference materials.

Isotopic data were normalized to the primary reference monazite "44069" ($^{206}Pb/^{238}U$ ID–TIMS age of 424.9 ± 0.4 Ma; Aleinikoff et al., 2006), with Trebilcock (ca. 273 Ma, Tomascak et al., 1996) and Bananeira (also referred to as Stern, 508 ± 1 Ma; Kylander-Clark et al., 2013) used as secondary reference materials. Analyses of Trebilcock yielded a weighted mean ^{207}Pb-corrected $^{206}Pb/^{238}U$ date of 270.7 ± 2.1 Ma (MSWD = 1.6, n = 19/19) in run_1 and 272.7 ± 2.5 Ma (MSWD = 1.9, n = 15/15) in run_2. Analyses of Bananeira in run_1 yielded a weighted mean ^{207}Pb-corrected $^{206}Pb/^{238}U$ date of 509 ± 3 Ma (MSWD = 0.86, n = 20/20) while run_2 produced a weighted mean ^{207}Pb-corrected $^{206}Pb/^{238}U$ date of 502 ± 3 Ma (MSWD = 0.9, n = 14/15). The calculated dates were within uncertainty of the accepted values, consistent with the systematic uncertainties of the LA–ICP–MS U-Pb method (Horstwood et al, 2016).

Trace element concentrations were normalized relative to analyses of Bananeira (Kylander-Clark et al. 2013) based on assumed stoichiometric P as such, are interpreted only for relative changes. The isotopes analyzed included ^{49}Ti, ^{51}V, ^{89}Y, ^{90}Zr, ^{93}Nb, ^{139}La, ^{140}Ce, ^{141}Pr, ^{146}Nd, ^{147}Sm, ^{153}Eu, ^{157}Gd, ^{159}Tb, ^{163}Dy, ^{165}Ho, ^{166}Er, ^{169}Tm, ^{172}Yb, and ^{175}Lu.

The acquired isotopic and trace element data were carefully filtered to ensure data quality and reliability. Analyses were excluded if they were > 4% discordant or >4% reversely discordant, ablated micro inclusions (identified based on abnormal chemical composition), overlapped chemically distinct domains, or were off the targeted grains due to laser drifting during acquisition. To avoid potential excess dispersion based on slight matrix difference between reference materials and unknown monazite, dates reported in this study reflect the ^{207}Pb/^{206}Pb system. Subsets of dates with similar chemical compositions and textural associations, which are interpreted to have crystallized at approximately the same time, are combined in weighted averages. All geochronological calculations and plots were made using IsoplotR (Vermeesch, 2018). For comparison with previously published dates, we added 1% uncertainty to the final ^{206}Pb/^{207}Pb dates based on long-term reproducibility at FiLTER. This uncertainty is reported as the second value in date notations in the format: date ± α | β Ma (without | with propagation of long-term systematic uncertainty). We use the terms “date” and “age” for analytical results and their interpretation in a geological context, respectively.

2.4.5 Trace elements mapping and *in situ* Lu—Hf petrochronology on garnet

Trace element mapping of representative garnet was conducted in the FiLTER facility, prior to *in situ* Lu-Hf dating to optimize laser spot placement and assess the spatial distribution of trace elements. LA–ICP–MS mapping targeted ^{27}Al, ^{40}Ca, ^{140}Ce, ^{52}Cr, ^{163}Dy, ^{167}Er, ^{56}Fe, ^{178}Hf, ^{165}Ho, ^{39}K, ^{139}La, ^{7}Li, ^{175}Lu, ^{24}Mg, ^{55}Mn, ^{23}Na, ^{93}Nb, ^{31}P, ^{207}Pb, ^{45}Sc, ^{119}Sn, ^{88}Sr, ^{181}Ta, ^{159}Tb, ^{232}Th, ^{48}Ti, ^{169}Tm, ^{238}U, ^{51}V, ^{89}Y, ^{172}Yb, and ^{91}Zr. For sample ZI–2107, two entire garnet grains were fully mapped due to their relatively small size (~ 10 mm in diameter), while for ZI–2108, mapping focused on the central cross-sections of two garnet grains, due to the large grain size (~ 20 mm in diameter). Mapping used a square 15 x 15 µm spot with a fluence of 4 $J \cdot cm^{-2}$, a repetition rate of 25 Hz, and a scan speed of 70 µm/s. Reference glasses NIST610 and NIST612 (Jochum et al., 2011) were measured under the same conditions, bracketing the garnet maps to correct for signal drift and quantify element concentrations using the Iolite v.4 software package (Paton et al., 2011). Element maps were generated using logarithmic color scaling in Iolite v.4 (Paton et al., 2011).

In situ LA–ICP–MS Lu—Hf analyses were conducted at the FiLTER, using an ESL193 excimer laser ablation system paired with a TwoVol3 sample chamber and an Agilent 8900 ICP–MS/MS following the method described in Larson et al. (2024), based on that outlined in Simpson et al. (2021, 2023).

Specimens were analyzed in one analytical session. A standard–sample bracketing technique was applied, and each batch of 10-15 unknown analyses were bracketed by a series of primary and secondary reference materials to monitor and correct for background, instrument drift and primary ratio calibrations using a custom data reduction scheme (Larson, 2024) in Iolite (v. 4; Paton et al. 2011). Garnet analyses were performed using a 150 µm circular laser spot, operating at a fluence of 4.5 $J \cdot cm^{-2}$ and a repetition rate of 10 Hz. The Högsbo reference garnet (Simpson et al., 2021), however, was analyzed using smaller spot sizes of 63–65 µm. The standard reference material NIST610 glass (Jochum et al., 2011; Nebel et al., 2009) was utilized for primary calibration standard and to correct for instrumental drift. NIST610 analyses were conducted using both 30 µm and 60 µm spot sizes to ensure signal to be above and below the $^{175}Lu^{+}$ detector crossover threshold (see Glorie et al., 2024), thereby minimizing potential calibration inaccuracies between pulse and analogue modes (e.g., Pullen et al., 2018). After primary correction, analyses of the Högsbo garnet reference material (1029 ± 1.7 Ma, U–Pb on columbite; Romer and Smeds, 1996) were used for secondary matrix correction. Excess dispersion, determined from NIST610 analyses using the spot size not employed for primary ratio calibration, was propagated through all isotopic ratios using quadrature. All reported dates incorporate the propagated relative uncertainties based on measurements from the Högsbo garnet reference standard (e.g., Glorie et al., 2024). Analyses of three reference garnets, GWA-1 (1267 ± 3 Ma; Ribeiro et al., 2024), GWA–2 (934.7 ± 1.4 Ma; Ribeiro et al., 2024) and Granite Mountain (ca. 2630 Ma; C. McFarlane Pers. Comm), reproduced expected dates. GWA-1 returned a date of 1327 ± 84 Ma (MSWD = 0.61, n = 15), GWA-2 returned a date of 957 ± 59 Ma (MSWD = 0.61, n = 15), while Granite Mountain analyses define an isochron at 2646 ± 117 Ma (MSWD = 0.89, n = 14/15).

Following the approach of Larson et al. (2024), data were filtered based on Zr and Ce concentrations (> 500 ppm) to minimize potential Hf contributions from zircon or monazite, despite the minimal impact zircon inclusions may have (Simpson et al., 2023). As garnet can incorporate substantial amounts of HREE and Y (Moore et al., 2013; Smit et al., 2013), often displaying pronounced zoning in these elements, a uniform cutoff for Y and Yb concentrations to filter out possible xenotime contamination was not applied. Instead, analyses were excluded if Y and Yb concentrations exceeded two standard deviations from the median. Lu—Hf data were plotted using inverse isochrons (Li and Vermeesch, 2021) with IsoplotR (Vermeesch, 2018).

2.5 Sample descriptions

Eleven aluminous gneiss samples were collected during targeted fieldwork in the Mauricie area along well-exposed road cuts (Figures 2.3, S1 and Table 2). Samples were cut perpendicular to the foliation and parallel to the lineation, where present. Six samples (two from each domain) were selected for petrochronology based on their metamorphic assemblages, prioritizing those including index minerals such as garnet, sillimanite, cordierite and K–feldspar that are more likely to provide approximate insights into the metamorphic conditions of the study area. Samples RS11–058 and ZI–2105 are from the Mékinac–Taureau domain; samples ZI–2101A and ZI–2102A are from the Shawinigan domain; samples ZI–2107 and ZI–2108 are from the western strand of the Portneuf–St. Maurice domain (Figures 2.3 and Table 2). Most samples contain abundant monazite or more rarely xenotime as well as garnet porphyroblasts suitable for *in situ* petrochronology. They also contain biotite, K–feldspar (absent in ZI–2107), sillimanite (absent in ZI–2105 and ZI–2107) and cordierite (only in ZI–2108). All samples are coarse-grained porphyroblastic aluminous gneiss with a well–developed foliation. Overall, the six analyzed samples cover a wide geographic area and are representative of most metamorphic assemblages that we and previous workers (e.g., Corrigan, 1995; Corrigan and van Breemen, 1997; Soucy La Roche et al., 2015) have identified in aluminous gneiss samples in the Mauricie area.

Lithotectonic domain	Sample	Latitude	Longitude	Mineral assemblages
Mékinac–Taureau domain	RS11-058	46°42'1.24"N	72°45'16.43"W	Grt, Bt, Sil, Kfs, Pl, Qz, Py, Rt, Fe-oxide, Gr, Mnz, Ap, Zrn
	ZI-2105	46°42'53.60"N	72°44'58.47"W	Grt, Bt, Kfs, Pl, Qz, Py, Rt, Ilm, Gr, Mnz, Zrn, Xtm, Chl
Shawinigan domain	ZI-2101A	46°31'2.99"N	72°49'5.84"W	Grt, Bt, Sil, Kfs, Pl, Qz, Ilm, Rt, Fe-oxide, Mnz, Ap, Zrn
	ZI-2102A	46°33'31.22"N	72°46'52.78"W	Grt, Bt, Sil, Kfs, Pl, Qz, Ilm, Rt, Gr, Fe-oxide, Mnz, Ap, Zrn
Portneuf–St. Maurice domain	ZI-2107	46°47'52.6"N	72°21'27.3"W	Grt, Bt, Ap, Pl, Qz, Ilm, Fe-oxide, Py, Gr, Mnz, Xtm
	ZI-2108	46°51'58.58"N	72°19'47.12"W	Grt, Bt, Pl, Qz, Crd, Ilm, Wm, Kfs, Sil, Xtm

Table 2.1 : Sample locations and mineral assemblages in each lithotectonic domain in Mauricie area, Quebec.

Mineral abbreviations: Ap: apatite, Bt: biotite, Chl: chlorite, Crd: cordierite, Gr: graphite, Grt: garnet, Ilm: ilmenite, Kfs: K-feldspar, Mnz: monazite, Pl: plagioclase, Py: pyrite, Rt: rutile, Qz: quartz, Sil: sillimanite, Wm: white mica, Xtm: xenotime, Zrn: zircon.

2.5.1 Mékinac–Taureau domain

Sample RS11–058

RS11–058 was sampled from the western side of the St. Maurice River within the Mékinac–Taureau domain and was first investigated by Soucy La Roche et al. (2015). This paragneiss contains centimeter–scale leucosome layers and pockets. The sample consists of garnet, biotite, sillimanite, K–feldspar, plagioclase, quartz, pyrite, rutile, Fe–oxide, graphite, monazite, apatite, and zircon. The thin section displays alternating layers rich in plagioclase, K-feldspar and biotite with lesser amounts of quartz and scattered sillimanite, layers rich in large garnet porphyroblasts wrapped by biotite and sillimanite, with lesser amounts of K-feldspar, plagioclase and quartz, and one large quartz ribbon (Figure S2A). Euhedral to subhedral garnet porphyroblasts contain inclusions of biotite, sillimanite, K–feldspar, plagioclase, quartz, and minor Fe–oxide, along with accessory monazite, apatite, and zircon (Figure 2.4A). Subspherical or elongated inclusions composed of K–feldspar, plagioclase and quartz (granitic composition), are sporadically distributed throughout the garnet grains (Figure 2.4A). Such inclusions are interpreted as pseudomorphs of former silicate melt pockets (e.g., Holness and Sawyer, 2008; Cesare et al., 2009, 2015). Garnet porphyroblasts are partially embayed and replaced by biotite, prismatic sillimanite, quartz and plagioclase. Garnet displays homogenous major element distribution (Ca, Fe, Mn and Mg; S3). Large polygonal quartz grains form matrix and co-exist with K-feldspar and plagioclase.

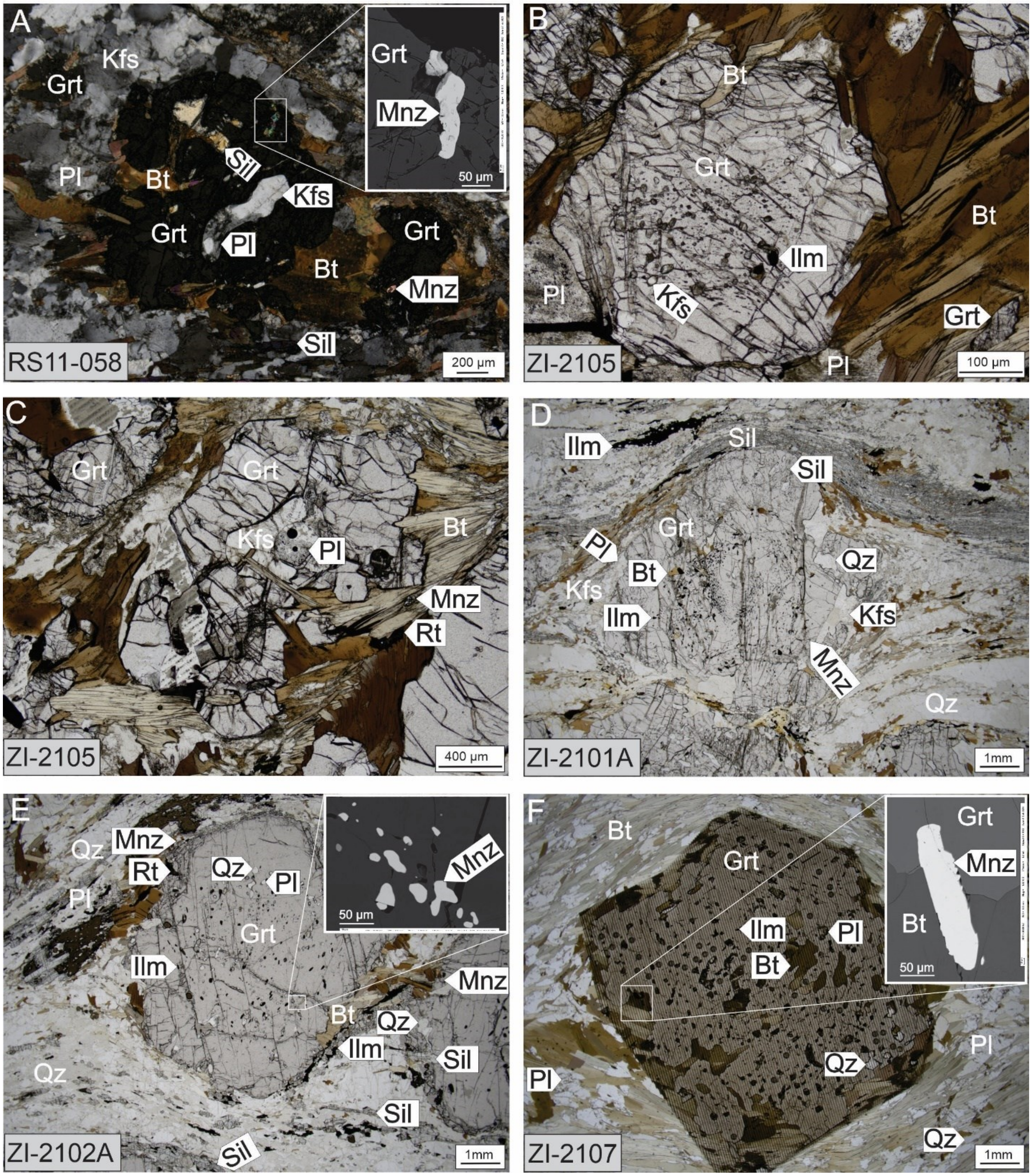

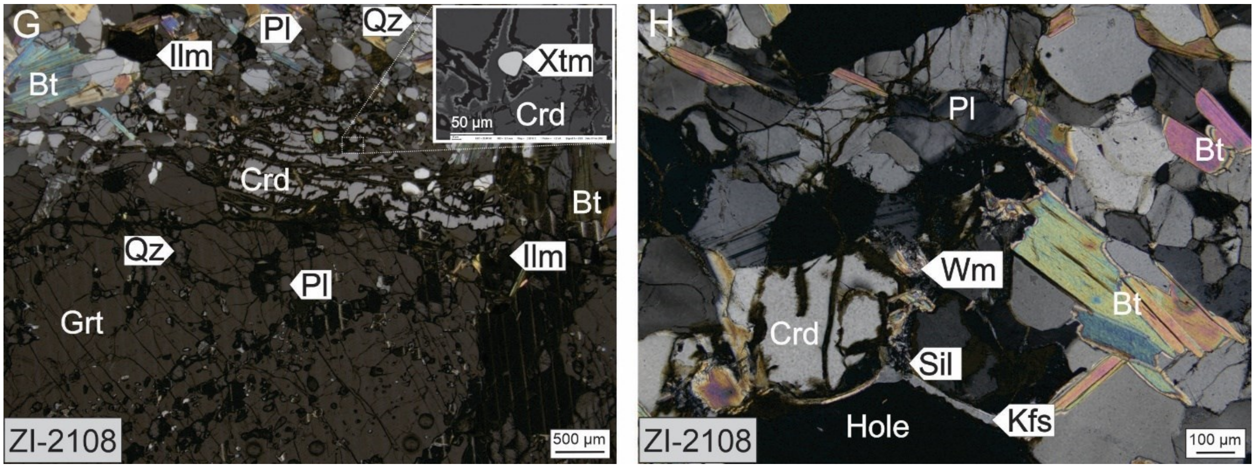

Figure 2.4: Photomicrographs of metamorphic minerals under plane-polarized light (PPL), cross-polarized light (XPL), and back-scattered electron (BSE) images.

(A) Sample RS11-058, euhedral garnet with inclusions of Mnz, Bt, Sil, Pl and former melt composed of Kfs and Pl (XPL); the upper-right inset shows monazite inclusion in garnet along a microcrack. (B) Sample ZI-2105, garnet displaying an inclusion-rich core containing K-felspar and ilmenite, and inclusion-poor rim. (C) Sample ZI-2105, garnet with K-feldspar and plagioclase inclusions interpreted as pseudomorphs after melt (PPL). (D) Sample Z-2101A, large garnet porphyroblast with inclusion-rich core containing Ilm, Bt, Qz and Mnz inclusions. Sillimanite and biotite wrap around the garnet (PPL). (E) Sample ZI-2102A, garnet porphyroblast with inclusion-rich core (Ilm, Qz, Pl, Mnz) and inclusion-poor rim (Sil; PPL). The upper-right inset shows monazite inclusions in garnet core (BSE image). (F) Sample ZI-2107, euhedral garnet porphyroblast with core containing abundant inclusions of Ilm, Bt, Pl and Qz (PPL). The upper-right inset shows a monazite inclusion partially enclosed within the garnet rim and biotite surrounding the garnet (BSE image). (G) Sample ZI-2108, cordierite rims around partially resorbed garnet (XPL). The upper-right inset shows xenotime inclusion in cordierite (BSE image). (H) Sample ZI-2108, sillimanite needles, white mica and K-feldspar in association with cordierite (XPL). Mineral abbreviations: Bt: biotite, Crd: cordierite, Ilm: ilmenite, Kfs: K-feldspar, Mnz: monazite, Pl: plagioclase, Qz: quartz, Sil: sillimanite, Wm: white mica, Xtm: xenotime.

Prismatic sillimanite and biotite in the matrix are foliation-parallel and mostly present around garnet porphyroblasts. In places, sillimanite porphyroblasts are partly replaced by biotite in the matrix. They contain monazite, apatite, and zircon inclusions. K–feldspar contains sillimanite needles and more rarely prismatic sillimanite and co-exists with quartz and plagioclase. Monazite grains (ranging in size from ≤ 30 µm to ~100 µm) are moderately abundant within K–feldspar, plagioclase, biotite, and sillimanite in the matrix, and rarely form inclusions in garnet. All but one monazite inclusion in garnet are located along microcracks (Figure 2.4A; Figure S4).

Sample ZI–2105

ZI–2105 was sampled from the eastern side of the St. Maurice River within the Mékinac–Taureau domain. This paragneiss contains centimeter–scale leucosome layers and pockets. It contains garnet, biotite, K–feldspar, plagioclase, quartz, pyrite, rutile, ilmenite, graphite, monazite, zircon, xenotime, and chlorite. The thin section contains two distinct layers based on mineral proportions

(Figure S2B). The lower layer contains abundant euhedral garnet porphyroblasts surrounded by large biotite flakes, while the upper layer is less garnetiferous, with biotite present predominantly in garnet strain shadows.

In both layers, garnet is typically euhedral and inclusion–free or contains rare inclusions of euhedral biotite, pyrite and graphite. A few garnet crystals display an inclusion–rich core that contains tiny, randomly oriented inclusions of quartz, plagioclase, K–feldspar and rare biotite (Figure 2.4B). Subspherical Kfs and Pl pseudomorphs after silicate melt pockets are preserved mostly within and around garnet grains that are otherwise devoid of inclusions (Figure 2.4C). No significant chemical zoning of major elements (Ca, Fe, Mn and Mg) was observed in garnet (Figure S3).

Chlorite replaces biotite in the matrix around garnet. K–feldspar exhibits perthitic flame textures and quartz–plagioclase myrmekite at the edges. No sillimanite was identified in this specimen. Numerous large zircon grains are present within the matrix and garnet porphyroblasts. Monazite inclusions are found within inclusion–poor portions of garnet grains and are absent from the inclusion–rich cores (Figure S4). Monazite grains are also present in matrix biotite. A single xenotime grain is located within a matrix biotite adjacent to garnet.

2.5.2 Shawinigan domain

Sample ZI–2101A

Sample ZI–2101A was collected from the St. Boniface unit within the Shawinigan domain. This paragneiss contains centimeter–scale leucosome layers and pockets. It contains garnet, biotite, sillimanite, K–feldspar, plagioclase, quartz, ilmenite, rutile, Fe–oxide, monazite, apatite and rare zircon. Garnet porphyroblasts reach up to ~10 mm in diameter and most display textural zoning (Figure 2.4D). Cores contain abundant ilmenite inclusions forming curved trails at various angles to the matrix foliation, and less abundant biotite and quartz inclusions (Figure 2.4D). The abundance and size of ilmenite inclusions increase towards the edge of the core (μ—XRF Ti map in Figure S5A). Sillimanite is absent from garnet cores. Garnet cores are separated from inclusion–free mantles by a sharp subhedral boundary. Garnet mantles are separated from rims by a gradational boundary. Garnet rims host numerous sillimanite needles, rare ilmenite, rutile and biotite, and a few monazite and apatite inclusions (Figure 2.4D). Bulbous and lobate quartz inclusions in garnet rims frequently contain sillimanite needles. Pseudomorphs of former silicate melt pockets (Pl and Qz) are preserved within the garnet rims and plagioclase locally forms thin films near the edges of the garnet. Garnet porphyroblasts are wrapped by interlayered sillimanite and biotite within quartzofeldspathic layers. Large ilmenite grains (up to 500 μm across) are present in the matrix. Rutile in the matrix is partially replaced by ilmenite. Mn in two large garnet porphyroblasts gradually decreases from the ilmenite-rich core to the rim, whereas Ca increases slightly from core to rim (Figure 2.5A; Figures S3, S6). Other grains that display textural evidence of a distinct core and rim lack zoning in major elements (Ca, Fe, Mn and Mg; Figure S3).

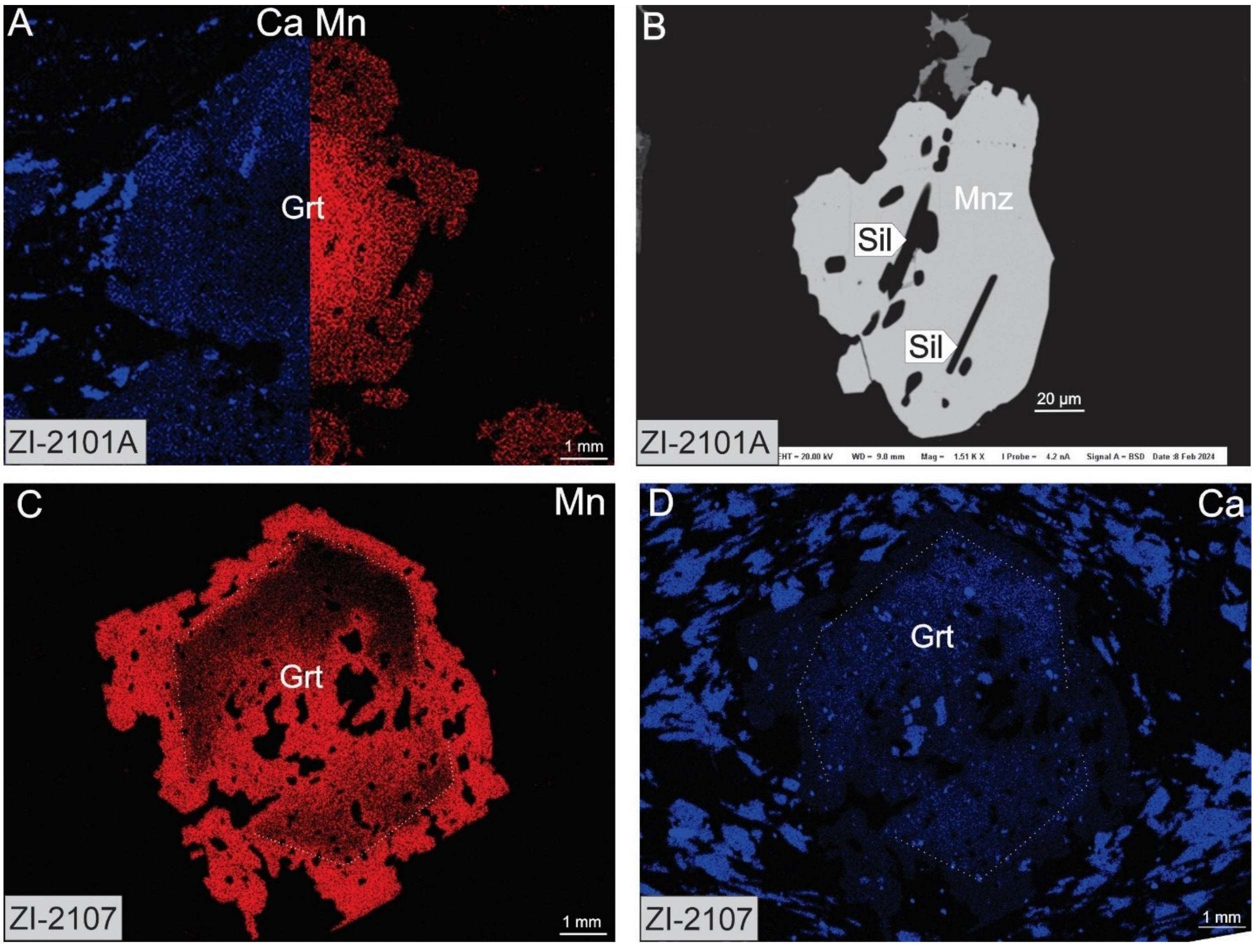

Figure 2.5: Micro-X-Ray fluorescence (μ-XRF) maps and back-scattered electron (BSE) image.

(A) Ca and Mn zoning of the same garnet (μ-XRF maps) as in Figure 4D. (B) Matrix monazite grain hosting sillimanite inclusions (BSE image). (C, D) μ-XRF Mn and Ca maps of garnet. Mineral abbreviations: Mnz: monazite, Sil: sillimanite.

Monazite inclusions in garnet are found exclusively in the rims. Monazite grains are also present in matrix K–feldspar, sillimanite, quartz, and biotite. Monazite inclusions within garnet rims rarely contain ~4 μm sillimanite inclusions (Figure S4). Some of the matrix monazite grains (ranging from ~50 μm to ~100 μm across) contain sillimanite inclusions measuring up to 40 μm long (Figures 2.5B; S4).

Sample ZI–2102A

Sample ZI–2102A was collected from the St. Boniface unit within the Shawinigan domain, approximately 6 km NNE of sample ZI–2101A (Figure 2.3). This paragneiss contains centimeter–scale leucosome layers and pockets (Figure S1D). It is composed of garnet, biotite, sillimanite, K–feldspar, plagioclase, quartz, ilmenite, rutile, graphite, Fe–oxide, monazite, apatite, and zircon. Garnet porphyroblasts reach up to ~10 mm in diameter and most display textural zoning (Figure 2.4E). Cores contain abundant, anhedral ilmenite inclusions aligned at an angle to the matrix foliation, along with occasional small inclusions of plagioclase, quartz, and monazite (Figure 2.4E). The abundance and size of ilmenite inclusions increase towards the edge of the core (µ—XRF Ti map in Figure S5B). Sillimanite is absent from garnet cores. Garnet cores are overgrown by rims separated by a sharp boundary. Garnet rims host numerous sillimanite needles, large rutile, fewer inclusions of ilmenite, quartz, K–feldspar, monazite, apatite and zircon, and rare biotite. Bulbous and lobate quartz inclusions in garnet rims frequently contain sillimanite needles. Garnet porphyroblasts are wrapped by the matrix foliation defined by prismatic sillimanite, biotite, ilmenite and graphite interlayered in quartzofeldspathic layers. Rutile in the matrix is partially replaced by ilmenite. Garnet porphyroblasts that display textural evidence of a distinct core and rim reveal no systematic variation in Fe, Mn and Mg across the grain. In contrast, Ca exhibits a subtle gradational increase from the core to the rim (Figure S3).

Monazite forms inclusions in garnet cores and rims (Figure 2.4E). Monazite (up to 60 µm across) in garnet rims encloses ~10 µm sillimanite inclusions (Figure S4). Monazite grains are also present in matrix K–feldspar, sillimanite, biotite, and quartz.

2.5.3 Portneuf–St. Maurice domain

Sample ZI–2107

Specimen ZI–2107, a paragneiss from the western segment of the Portneuf–St. Maurice domain contains garnet, biotite, apatite, plagioclase, quartz, ilmenite, Fe–oxide, pyrite, rare graphite, monazite and xenotime. No leucosome was observed in the hand specimen and on the outcrop. The thin section features two large euhedral garnet porphyroblasts (~10 mm across) with cores containing abundant ilmenite, biotite, plagioclase and quartz inclusions (Figure 2.4F). Biotite and ilmenite inclusions in the garnet core form curved inclusion trails and are at an angle to the matrix foliation that wraps the garnet (Figure S7A). Ilmenite increases in size and abundance with distance from core except in the inclusion–poor rim where they are not present (Figure S7A). A few small (~ 500 µm across), euhedral garnet grains contain inclusions of biotite and quartz. Mn content in garnet porphyroblasts gradually decreases from the inner core to the outer core and increases sharply at the core–rim boundary (Figures 2.5C, S3, S8A). Ca content in the garnet core increases toward the outer edge of the core and decreases sharply at the core–rim boundary (Figure 2.5D, S3, S8B). Fe and Mg are homogeneous across the garnet grains (Figure S3). Biotite defines the matrix foliation, wrapping around garnet porphyroblasts, and also forms moderately oriented inclusions within garnet, matrix quartz and plagioclase. Quartz and sericitized plagioclase co-exist with biotite in the matrix. No sillimanite was observed in this specimen. A single monazite inclusion is partially enclosed by the outermost edge of a large garnet grain and by matrix biotite (Figure 2.4F), while other monazite and xenotime grains are present in matrix biotite, plagioclase, and quartz.

Sample ZI–2108

Specimen ZI–2108, a paragneiss from the western segment of the Portneuf–St. Maurice domain comprises garnet, biotite, plagioclase, quartz, cordierite, ilmenite, and rare white mica, K–feldspar, sillimanite and xenotime. No leucosome was observed in the hand specimen and on the outcrop. The thin section contains two large anhedral garnet porphyroblasts (~ 20 mm across) with abundant inclusions of quartz, minor inclusions of biotite, ilmenite and two xenotime inclusions. Mn and Ca in garnet decrease slightly and gradually from core to rim (Figures S3, S7B). Fe and Mg are homogeneous across the garnet grains (Figure S3).

Altered cordierite rims partially resorbed garnet (Figure 2.4G). Rare sillimanite needles occur with K–feldspar and intergrown white mica and biotite next to cordierite (Figure 2.4H). Ilmenite mostly occurs as inclusions in the garnet core. Xenotime occurs as tiny inclusions (< 30 μm) in cordierite and within matrix biotite, plagioclase and quartz along the resorbed garnet rims. Xenotime also forms rare inclusions located along microcracks within garnet rims. No monazite was identified in this specimen.

2.6 Metamorphic evolution based on petrographic observations

2.6.1 Mékinac–Taureau domain

In sample RS11–058, the peak metamorphic assemblage is composed of garnet, sillimanite, biotite, plagioclase, quartz, Fe–oxide, rutile and K–feldspar. The presence of Qz–Pl–Kfs polymineralic inclusions in the cores and rims of garnet indicates that whole garnet porphyroblasts grew in the presence of melt (e.g. Goncalves et al., 2021), likely from the biotite dehydration melting reaction

Sil + Bt + Pl + Qz → Grt + Kfs + Liq (1; Vielzeuf and Holloway, 1988).

In sample ZI–2105, the peak metamorphic assemblage is identical, except for the lack of sillimanite. The presence of abundant tiny K–feldspar inclusions in a few garnet cores, along with quartz, plagioclase, and biotite, is consistent with the crystallization of these cores in the stability field of K–feldspar (>650 °C for metapelitic compositions; e.g., Spear et al. 1999; Yakymchuk et al., 2017). Relatively inclusion–poor garnet porphyroblasts commonly contain Kfs–Pl polymineralic inclusions that are interpreted as crystallized melt pockets, indicating these garnet grains grew under suprasolidus conditions.

2.6.2 Shawinigan domain

The peak metamorphic assemblage of samples ZI–2101A and ZI–2102A is composed of garnet, biotite, sillimanite, quartz, K–feldspar, plagioclase and rutile. The cores of garnet porphyroblasts in both samples are clouded with abundant, small inclusions of ilmenite, biotite, quartz, plagioclase, and (in sample ZI–2102A) monazite that are oriented at an angle to the matrix foliation. In contrast, garnet rims contain numerous sillimanite needles, rutile, rare ilmenite and biotite, quartz, K–feldspar, and a few monazite inclusions. The core–rim textural transition is associated with a chemical variation in one garnet porphyroblast in sample ZI–2101A (Mn decrease and Ca increase from core to rim), whereas other porphyroblasts in this sample are chemically homogeneous. Garnet grains in ZI–2102A are characterized by a subtle increase in Ca between the core and the rim. These textural and chemical observations suggest two growth generations of garnet at distinct P–T conditions. The lack of former melt inclusions and minerals that form at high temperature (>650 °C, e.g. K-feldspar and sillimanite) in garnet cores, which are rich in inclusions aligned at an angle to the matrix foliation, is consistent with subsolidus crystallization (e.g., Soret et al., 2019; Jiang et al., 2022). In contrast, abundant sillimanite, K–feldspar and former melt inclusions in garnet rims are consistent with garnet growth under suprasolidus conditions via Reaction 1 (e.g., Godet et al., 2021, Bartoli et al., 2013).

2.6.3 Portneuf–St. Maurice domain

In sample ZI–2107, the peak metamorphic assemblage is composed of garnet, biotite, quartz and plagioclase. Garnet cores containing abundant ilmenite, biotite, plagioclase and quartz inclusions, whereas rims are inclusion poor. Mn content in garnet porphyroblasts gradually decreases from the inner core to the outer core and increases sharply at the core–rim boundary. Ca displays the opposite zoning pattern. This textural and geochemical evidence indicates a change in P–T conditions and/or that a metamorphic reaction was crossed during the growth of garnet cores and rims. The disappearance of ilmenite inclusions in garnet rim (ilmenite-consuming reaction) is consistent with the increase in Mn in garnet rim, as ilmenite may have sequestered a significant amount of Mn (e.g., Pownceby et al., 1987; McCarron et al., 2019). Fe and Mg zoning are more subdued, likely due to homogenization during peak metamorphism and Fe–Mg exchange reaction between garnet and biotite (e.g., Spear, 1991). The lack of former melt inclusions across garnet and microtextural evidence, such as aligned inclusions of ilmenite forming an internal foliation at an angle to the matrix biotite foliation in the garnet cores indicate that garnet cores and rims likely formed at subsolidus metamorphic conditions (e.g., Soret et al., 2019; Jiang et al., 2022).

In sample ZI–2108, the peak metamorphic assemblage is composed of garnet, biotite, plagioclase, and quartz. Garnet in ZI–2108 lacks textural evidence of a distinct core and rim, and chemical zoning is consistent with relict growth zoning (slight gradual decrease in Mn and Ca from core to rim). Garnet grew during prograde subsolidus conditions in the absence of high temperature minerals such as sillimanite and K-feldspar. Garnet is partially replaced by cordierite with rare sillimanite, white mica and K–feldspar, which indicates garnet resorption under low-pressure conditions along the retrograde P–T path (Yakymchuk et al., 2017). Partial resorption of garnet rims promoted crystallization of xenotime inclusions in cordierite around garnet.

2.7 Results

2.7.1 Monazite and xenotime U—Th—Pb dates and trace elements

In situ U—Th—Pb petrochronology was performed on monazite in four samples, on both monazite and xenotime in one sample, and on xenotime in one sample. Results are presented in Figures 2.6, 2.7, S9, S10 and Table S1. Locations of analyzed grains in thin section and BSE images are presented in Figure S4.

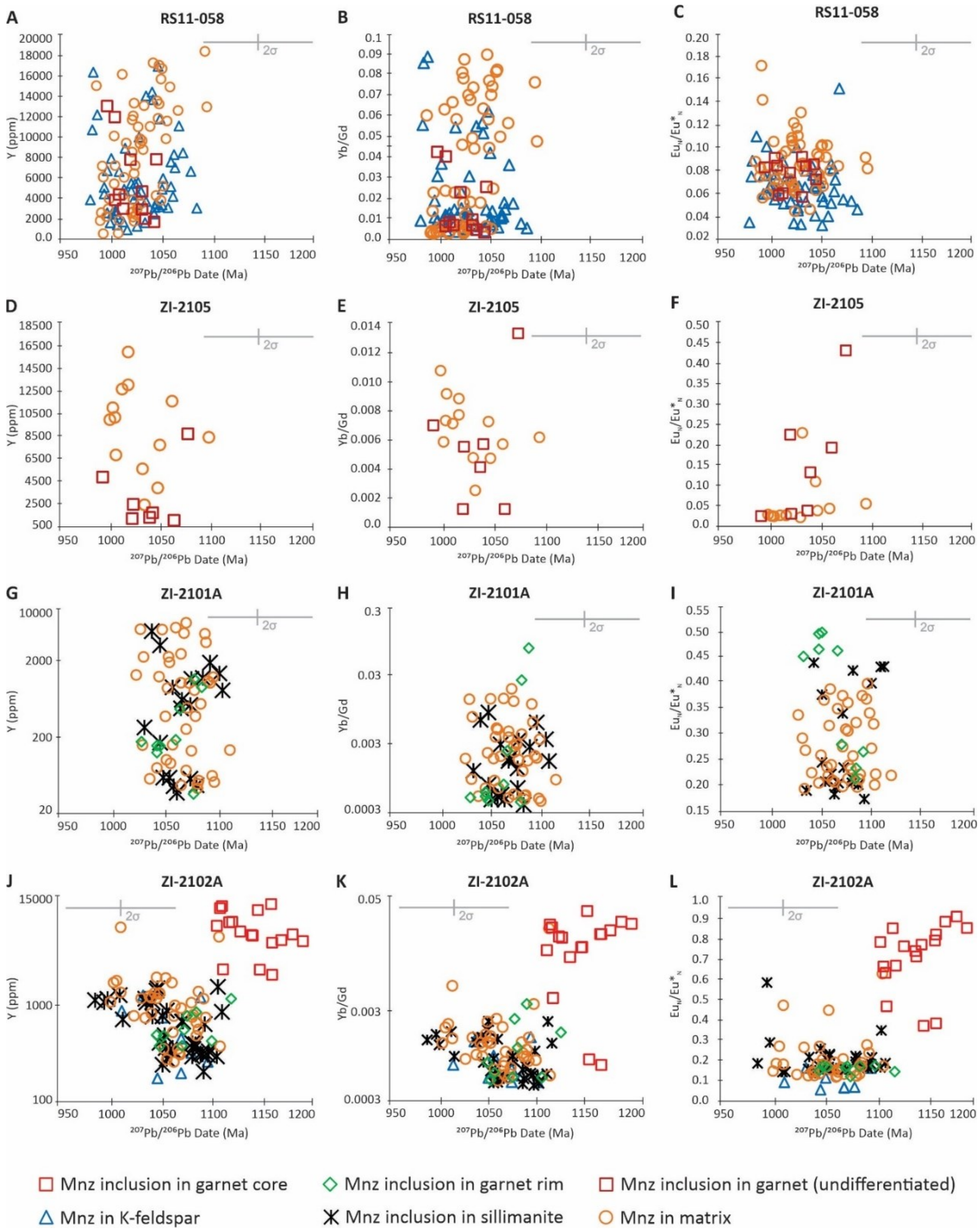

Figure 2.6: Y, Yb/Gd, and Eu$_N$/Eu*$_N$ versus ^{207}Pb/^{206}Pb dates (Ma) in monazite.

(A-F) samples RS11-058 and ZI-2105 from the Mékinac-Taureau domain; (G–L) samples ZI-2101A and ZI-2102A from the Shawinigan domain. Inclusions within metamorphic index minerals typically represent the maximum crystallization age of the host mineral. However, in certain cases, microtextural and/or geochemical evidence indicates that some inclusions have been recrystallized after the crystallization of the host mineral. See text for details. Error bars on

each plot represent the average 2SE uncertainty on the $^{207}Pb/^{206}Pb$ dates (Ma) and chemical composition.

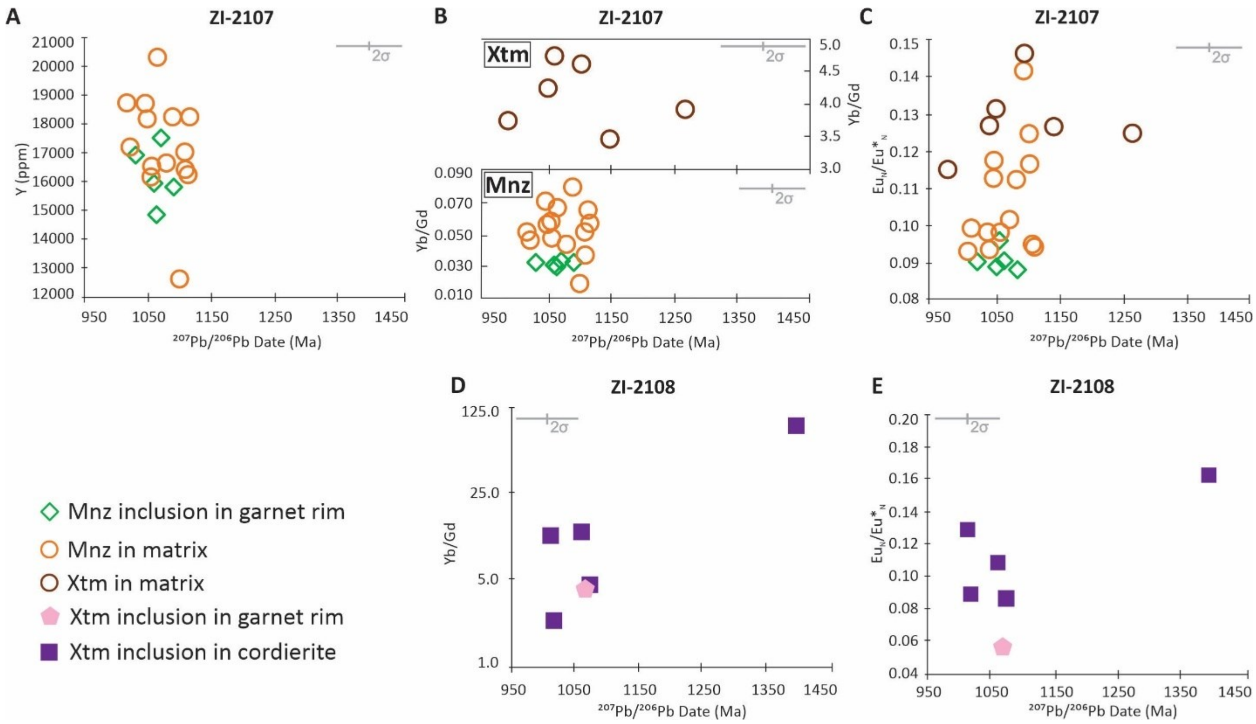

Figure 2.7: Y, Yb/Gd, and Eu_N/Eu^*_N versus $^{207}Pb/^{206}Pb$ dates (Ma) in monazite and xenotime.

(A–E) samples ZI-2107 and ZI-2108 from the Portneuf–St. Maurice domain. Inclusions within metamorphic index minerals typically represent the maximum crystallization age of the host mineral. However, in certain cases, microtextural and/or geochemical evidence indicates that some inclusions have been recrystallized after the crystallization of the host mineral. See text for details. Error bars on each plot represent the average 2SE uncertainty on the $^{207}Pb/^{206}Pb$ dates (Ma) and chemical composition.

2.7.1.1 Mékinac–Taureau domain

Sample RS11–058

One hundred and twenty dates on 25 monazite grains range from 1098 ± 54 Ma to 981 ± 42 Ma (Figure S9; Table S1). Eleven dates from six monazite inclusions in garnet (Figures S9, S10) range from 1047 ± 54 Ma to 999 ± 51 Ma and yield a weighted mean of 1024 ± 15 | 25 Ma (MSWD = 0.5, n = 11). Seven monazite inclusions in K–feldspar yield 54 dates between 1088 ± 51 Ma and 981 ± 42 Ma. Twelve matrix monazite grains yield 55 dates ranging from 1098 ± 54 Ma to 987± 85 Ma.

The thin section displays alternating layers rich in plagioclase, K-feldspar and biotite with lesser amounts of quartz and scattered sillimanite, layers rich in large garnet porphyroblasts wrapped by biotite and sillimanite, with lesser amounts of K-feldspar, plagioclase and quartz, and one large quartz ribbon (Figure S2A).

Yttrium and Yd/Gb in monazite are variable and do not vary systematically with dates or textural settings (in the matrix or inclusions in garnet or K-feldspar, Figure 2.6A–C). However, the position within the thin section influences Y and Yd/Gb in monazite (Figure S11). In the upper portion of the thin section which displays alternating layers rich in plagioclase, K-feldspar and biotite with minor quartz and sillimanite, three monazite grains in a garnet-poor and plagioclase, K-feldspar and biotite rich layer are characterized by higher Y and Yb/Gd compared to grains that are close to garnet and elsewhere in the thin section. In contrast, monazite grains in a layer rich in large garnet porphyroblasts wrapped by biotite and sillimanite in the middle of the thin section display low Y and Yb/Gd. In the lower part of the thin section, however, the position within feldspar-biotite rich and garnet-biotite-sillimanite rich layers does not control monazite chemical composition, and a few grains contain both high and low Y and Yb/Gd domains. Eu anomalies ($Eu_N/Eu^*_N = Eu_N/(Sm_N{*}Gd_N)^{0.5}$, N = normalized to the chondrite values of O'Neill, 2016) are strongly negative (Eu_N/Eu^*_N between 0.02–0.20) and Eu_N/Eu^*_N increase subtly with decreasing dates (Figure 2.6C). Eu anomalies from all textural settings overlap, but on average monazite inclusions in K–feldspar have more pronounced negative Eu anomalies compared to contemporaneous monazite in the matrix (Figure 2.6C).

Sample ZI–2105

Twenty dates on eight monazite grains range from 1096 ± 78 Ma to 992 ± 74 Ma (Figure S9, Table S1). Seven dates from five monazite inclusions in garnet range from 1076 ± 57 Ma to 992 ± 74 Ma. Excluding the oldest analysis that has a different chemical composition, they yield a weighted mean of 1028 ± 26 | 36 Ma (MSWD = 0.4, n = 6, Figures S9, S10). Four matrix monazite grains yield 13 dates ranging between 1096 ± 78 Ma and 999 ± 45 Ma. Y and Yb/Gd increases weakly with decreasing date, and in general, monazite inclusions in garnet have lower Y and Yb/Gd compared to monazite in the matrix (Figure 2.6D–F). The 1076 ± 57 | 68 Ma monazite inclusion in garnet is characterized by higher Y and Yb/Gd, and less negative Eu anomaly ($Eu_N/Eu^*_N = 0.43$), compared to other inclusions and matrix monazite (Figure 2.6D–F). Eu anomalies are strongly negative ($Eu_N/Eu^*_N < 0.25$) in matrix monazite and all other inclusions in garnet. The single xenotime grain did not yield a reliable date and was excluded from age calculation and interpretations.

2.7.1.2 Shawinigan domain

Sample ZI–2101A

Sixty–eight dates on 16 monazite grains range from 1115 ± 53 Ma to 1025 ± 98 Ma (Figure S9, Table S1). Nine dates from three monazite inclusions in garnet rims range from 1088 ± 57 Ma to 1030 ± 74 Ma and yield a weighted mean of 1060 ± 19 | 30 Ma (MSWD = 0.41, n = 9, Figures S9, S10). Five monazite inclusions in sillimanite yield 19 dates ranging between 1108 ± 65 Ma and 1033 ± 52 Ma. Nine matrix monazite grains yield 40 dates between 1115 ± 53 Ma and 1025 ± 98 Ma. Y, Yb/Gd and Eu_N/Eu^*_N do not vary systematically with dates in most monazite grains (Figure 2.6G–I). Y and Yb/Gd in monazite inclusions in garnet rims decrease slightly with decreasing dates, whereas Eu_N/Eu^*_N increases (Figure 2.6G–I).

Sample ZI–2102A

One hundred and nine dates on 28 monazite grains range from 1190 ± 120 Ma to 987 ± 50 Ma (Figure S9, Table S1). Seventeen dates from nine monazite inclusions in garnet cores range between 1190 ± 120 Ma and 1106 ± 55 Ma and yield a weighted mean of 1137 ± 13 | 24 Ma (MSWD = 0.71, n = 17, Figures S9, S10). Nine dates on three monazite inclusions in garnet rims range between 1120 ± 110 Ma and 1047 ± 43 Ma and yield a weighted mean of 1071 ± 18 | 29 Ma (MSWD = 0.62, n = 9, Figures S9, S10). A single monazite inclusion in K–feldspar yields nine dates ranging between 1097 ± 60 Ma and 1013 ± 58 Ma. Four monazite inclusions in sillimanite yield 35 dates between 1111 ± 59 Ma and 987 ± 50 Ma. Eleven matrix monazite yield 39 dates between 1109 ± 41 Ma and 1002 ± 45 Ma.

Monazite composition varies systematically with dates and textural settings (Figure 2.6J–L). Monazite inclusions in garnet cores (ca. 1190–1100 Ma) are characterized by high Y, Yb/Gd and Eu_N/Eu^*_N. Ca. 1100–1045 Ma monazite inclusions in garnet rims, in sillimanite and in K–feldspar, and monazite grains in the matrix are characterized by low Y, Yb/Gd and Eu_N/Eu^*_N. Monazite younger than 1045 Ma displays a mild increase in Y and Yb/Gd (Figures 2.6K, L).

2.7.1.3 Portneuf–St. Maurice domain

Sample ZI–2107

Twenty–five dates on six monazite and five xenotime grains range between 1260 ± 140 Ma and 985 ± 54 Ma. A single monazite grain partially enclosed in garnet rim yields 5 dates between 1089 ± 44 Ma and 1029 ± 41 Ma and a weighted mean of 1060 ± 21 | 32 Ma (MSWD = 1, n = 5, Figures

S9, S10). Five matrix monazite grains yield 14 dates between 1114 ± 57 Ma and 1015 ± 40 Ma. Five matrix xenotime grains yield six dates between 1260 ± 140 Ma and 985 ± 54 Ma. Overall, trace element compositions do not show systematic trends with date (Figure 2.7A–C). The monazite inclusion in garnet rim is characterized by lower Y, Yb/Gd and Eu_N/Eu^*_N compared to monazite in the matrix. Xenotime show less negative Eu_N/Eu^*_N compared to monazite (Figure 2.7C).

Sample ZI–2108

Six dates on six xenotime grains range between 1394 ± 43 Ma and 1012 ± 52 Ma. A single xenotime inclusion in garnet rim yields a 1068 ± 93 Ma date. Excluding the oldest analysis that has a different chemical composition, four xenotime inclusions in cordierite around partially resorbed garnet yield four dates between 1073 ± 63 Ma and 1012 ± 52 Ma and yield a weighted mean of 1039 ± 24 | 34 Ma (MSWD = 1.4, n = 4, Figure S9, S10). A single analysis from xenotime in cordierite yields a significantly older date at 1394 ± 43 Ma. Xenotime trace element composition does not vary systematically with dates or textural settings, except for the 1394 Ma xenotime that is characterized by higher Yb/Gd and Eu_N/Eu^*_N (Figure 2.7D,E).

2.7.2 Garnet trace element distribution and *in situ* Lu—Hf petrochronology

In situ Lu–Hf garnet dating lacks precision compared to traditional solution-based methods, but this approach offers the advantage of easily analyzing garnet zones that may not have crystallized at the same time (Larson et al., 2024). This *in situ* technique is particularly useful for dating garnets from polymetamorphic terranes, where garnet may preserve multiple growth generations reflecting distinct metamorphic events (e.g. Tamblyn et al., 2022; Simpson et al., 2023; Larson et al., 2024). In the Portneuf–St. Maurice domain, Corrigan (1995) reported a ca. 1390 Ma metamorphic age based on U–Pb dating of monazite from a single sample. However, most of our monazite and xenotime dates are <1100 Ma. Because garnet displays textural and compositional evidence for distinct cores and rims, and the potentially polyphase metamorphic evolution, we applied *in situ* Lu–Hf dating of garnet to verify if garnet crystallized during the ~1390 Ma event, the Grenvillian Orogeny, or both.

2.7.2.1 Portneuf–St. Maurice domain

Samples ZI–2107 and ZI–2108

In sample ZI–2107, garnet is characterized by a core-rim transition defined by a sharp increase in Mn, a decrease in Ca, and the disappearance of ilmenite inclusions (Figures 2.5C, D). Two garnet porphyroblast cores exhibit concentric zoning and relatively low Y, MREE and HREE that decrease outward typical of growth zoning (Figures 2.8A-H, S12). The core-rim transition is marked by an increase in Y and Dy, a Lu-rich annulus, and a decrease in Cr (Figures 2.8A-H, S12). The resorbed outer edge of garnet is characterized by high Y, Lu and Dy. The Lu-rich outer edge is interpreted to result from back-diffusion of Lu inside garnet during garnet resorption because it follows the irregular shape of the resorbed edge and not growth faces. Lu–Hf dates therefore exclude analyses located on the Lu-rich edge. Since cores and rims display variations in texture, major elements (Mn and Ca) and trace element composition, Lu—Hf analyses were separated by zone to assess any age difference between cores and rims. Cores yield a Lu—Hf date of 1075 ± 169 Ma (Hf_0 = 0.287 ± 0.011; MSWD = 1.1, n = 49), statistically indistinguishable from the 1091 ± 139 Ma rim date (Hf_0 = 0.288 ± 0.033, MSWD = 0.73, n = 13, Figure S13, Table S2). Lu—Hf isotopic data from cores and rims define a regression with a Lu—Hf date of 1089 ± 96 Ma (initial $^{176}Hf/^{177}Hf$ isotope composition (Hf_0) = 0.2865 ± 0.0091; MSWD = 0.98; n = 62/80; Figure 2.9A).

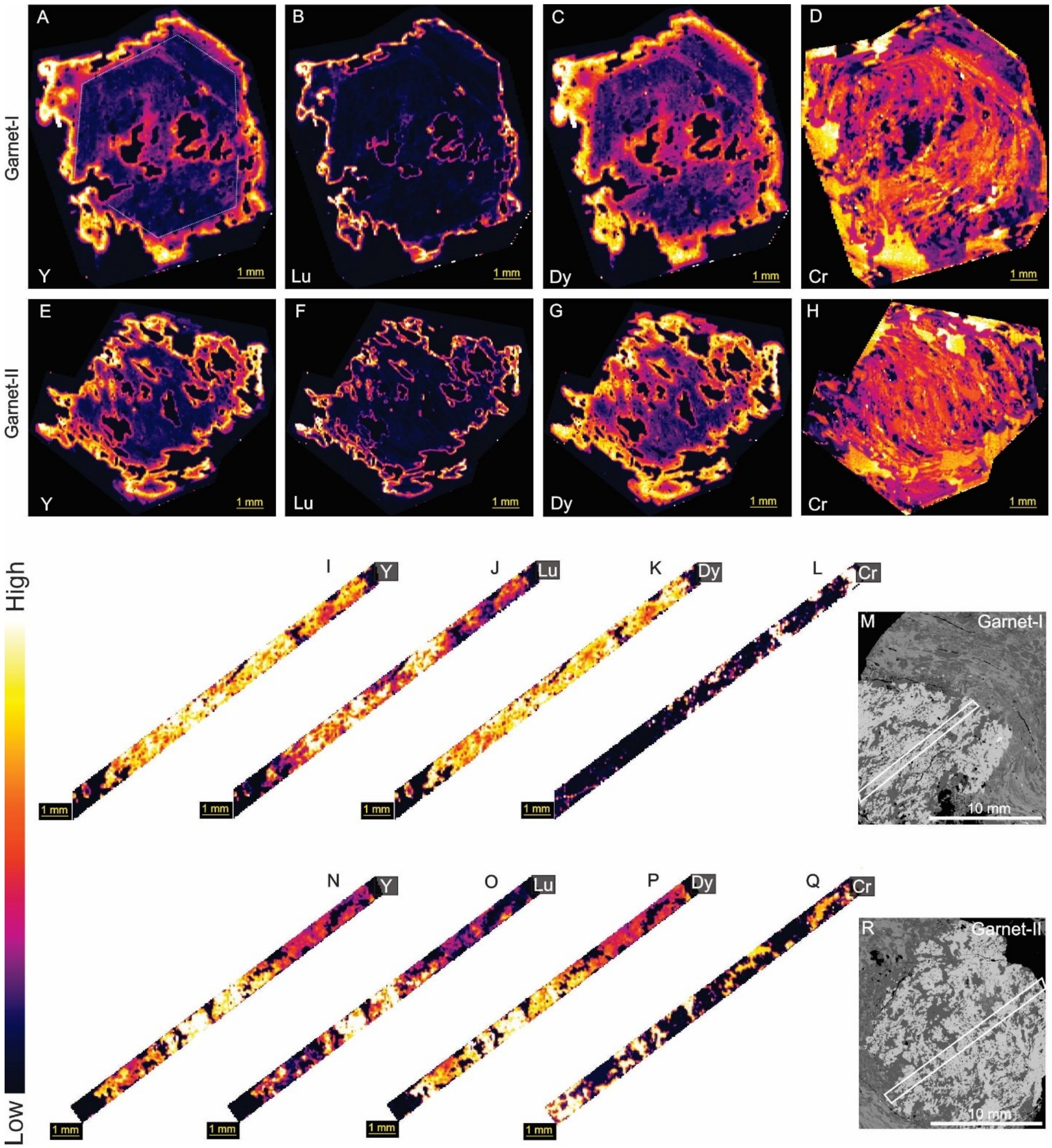

Figure 2.8: LA-ICP-MS trace element maps of (A—D) garnet-I and (E—H) garnet-II in sample ZI-2107, and (I—L) for garnet-I and (N—Q) for garnet-II in sample ZI-2108, respectively.

In figure 8A, the garnet core-rim boundary is marked by a white dotted line. In sample ZI-2107, two entire garnet grains were mapped due to their relatively small size (~ 10 mm in diameter). For ZI-2108, mapping focused on central cross-sections of two garnet grains, due to the large grain size (~ 20 mm in diameter) and are presented on BSE images (M, R). Element maps were generated using logarithmic color scaling using Thermal %ile99 color scheme.

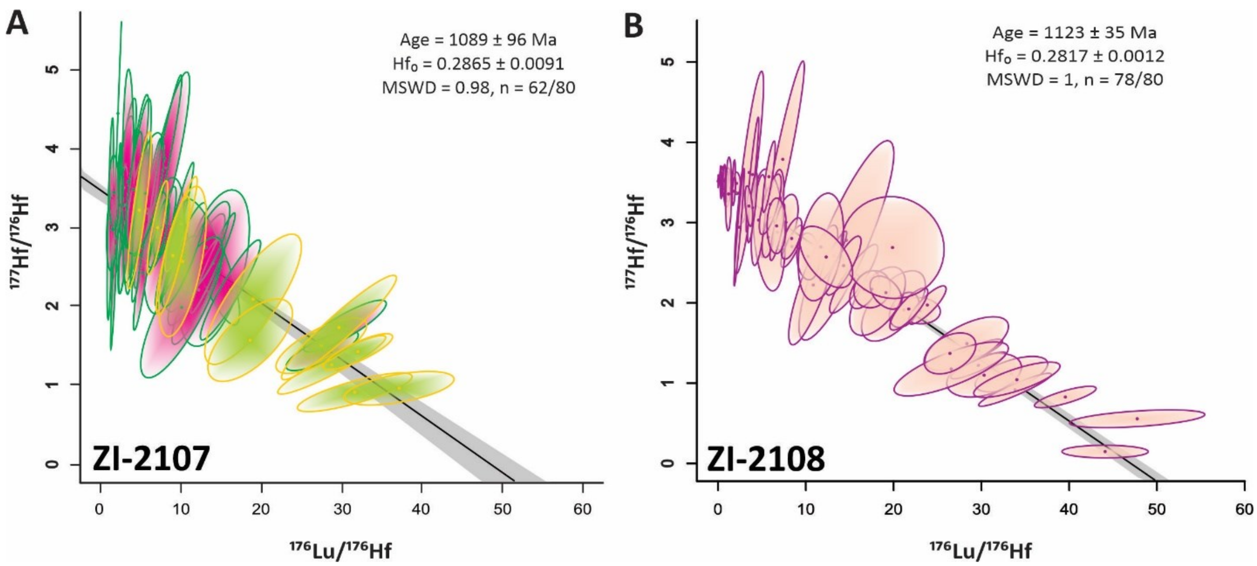

Figure 2.9: Inverse isochrons of two representative garnet porphyroblasts per sample in ZI-2107 and ZI-2108 from the Portneuf–St. Maurice domain.

Inverse isochron regression are used due to the high error correlation between the $^{176}Hf/^{177}Hf$ and $^{176}Lu/^{177}Hf$ isotopic ratios in conventional isochrons (Simpson et al., 2023). Error ellipses are shown at the ±2 standard error (2SE) level. Lu—Hf dates are reported with 95% confidence intervals. Cores and rims in sample ZI-2107 are texturally and chemically distinct and are differentiated by color (cores shown as pink ellipses with emerald borders; rims as green ellipses with yellow borders), but they yield statistically indistinguishable Lu—Hf dates that are shown in Figure S13.

In sample ZI–2108, two garnet porphyroblasts display a different zoning pattern. Y and HREE decrease slightly from core to rims and display concentric zoning (Figures 2.8I-L, N-Q, S12), typical of growth zoning (Baxter et al., 2017). MREE do not show significant zoning. All analyses define a regression with a Lu—Hf date of 1123 ± 35 Ma (Hf_0 = 0.2817 ± 0.0012, MSWD = 1, n = 78/80; Figure 2.9B, Table S2).

2.8 Interpretation of petrochronology results

The integration of trace element data—particularly Y, HREE, and Eu anomalies—from monazite and xenotime, in conjunction with detailed petrographic observations, enables a nuanced petrochronological approach that links dates with the evolution of the metamorphic mineral assemblage (e.g., the presence, absence, growth or breakdown of garnet, K-feldspar, sillimanite, or cordierite; see Gibson et al., 2004; Mottram et al., 2014; Regis et al., 2016; Engi, 2017; Weller et al., 2020; Soucy La Roche et al., 2022; Volante et al., 2024). These trace elements function as proxies for the stability or breakdown of coexisting phases. Specifically, monazite that crystallizes contemporaneously with garnet, or in a rock where garnet is already present, typically exhibits lower Y concentrations and Yb/Gd ratios (a proxy for HREE fractionation) because garnet preferentially uptakes these elements. Conversely, monazite that forms prior to garnet crystallization or following garnet breakdown (e.g., during retrogression or melt crystallization) tends to display higher Y and HREE contents. Likewise, the stability of xenotime is sensitive to garnet growth and resorption; it often reacts out while garnet is growing and may crystallize following garnet breakdown as garnet liberates Y (Pyle and Spear, 1999; Zhu et al., 1999; Pyle et al., 2001; Foster et al., 2002; Spear and Pyle, 2002; Engi, 2017). Eu anomalies are strongly influenced by feldspar stability, as feldspar crystallization and breakdown play a key role in controlling Eu partitioning between major and accessory minerals (Holder et al., 2020). For example, a pronounced negative Eu anomaly in monazite is commonly associated with feldspar crystallization (e.g., Rubatto et al., 2006; Holder et al., 2015; Regis et al., 2016; Weller et al., 2020). The partitioning of Eu is particularly notable in K–feldspar (Bea et al., 1994).

Textural relationships between petrochronometers and metamorphic index minerals offer additional insights to interpret monazite and xenotime dates and chemical composition (Foster et al., 2002; Foster et al., 2003; Kelly et al., 2006; Rubatto et al., 2013; Warren et al., 2019; Weller et al., 2020). Monazite and xenotime inclusions in porphyroblasts can constrain the age, or maximum age, of metamorphic mineral growth, assuming that they were shielded by the porphyroblast and did not react subsequently with the matrix (e.g. monazite inclusions in garnet; Pyle et al., 2001; Jiao et al., 2013; Warren et al., 2019; Weller et al., 2020; Soucy La Roche et al., 2022). Inclusions of metamorphic index minerals in petrochronometers can also provide a timing constraint on their growth (e.g. sillimanite inclusions in monazite). Finally, petrochronometers located preferentially in resorption coronas can constrain the age of resorption of the porphyroblast.

Anatexis also plays a role on the stability of monazite. Phase equilibrium modelling predicts that monazite dissolves in melt in metapelitic compositions (e.g. Yakymchuk et al., 2014, 2017), as supported by experimental studies (Rapp and Watson, 1986). These models, however, do not incorporate phosphorus in anatectic melt, which can significantly influence monazite stability (Duc-Tin and Keppler, 2015). Apatite is the main sink for phosphorous and LREE in metapelitic rocks, and experimental studies show that apatite solubility in melt increases with increasing aluminium saturation index (Wolf and London, 1994), which commonly increases during anataxis (Johnson et al., 2015). Apatite dissolution in melt saturates it in LREE, promoting monazite crystallization (Wolf and London, 1995). Results from natural samples also suggest that monazite in migmatitic metapelites can crystallize during prograde, peak (i.e., during melt production), and retrograde stages (i.e., during melt crystallization; e.g., Harlov et al., 2007; Mottram et al., 2014; Johnson et al., 2015; Holder et al., 2024).

If monazite and xenotime are rare or absent, garnet offers an alternative tool to provide absolute timing constraints on metamorphism (Baxter et al., 2017; Simpson et al., 2021). As a common rock-forming mineral in aluminous metamorphic rocks, garnet provides valuable insight into linking geochronology to metamorphic processes (e.g., Baxter et al., 2017). It typically grows with increasing pressure and temperature during prograde metamorphism, both under subsolidus and suprasolidus conditions. Due to its preferential incorporation of heavy rare earth elements (HREE), garnet is ideal for Lu–Hf isotopic dating (Duchêne et al., 1997; Scherer et al., 2000; Smit et al., 2013; Simpson et al., 2023). The Lu–Hf system in garnet has a high closure temperature (≥ 900 °C), enabling the preservation of isotopic signatures even under anatectic conditions for geologically significant timescales (Smit et al., 2013; Bloch and Ganguly, 2015; Bloch et al., 2020). As a result, Lu–Hf ages generally record garnet growth during prograde or peak metamorphism rather than cooling (Smit et al., 2013).

2.8.1 Mékinac–Taureau domain

Garnet in samples RS11–058 and ZI–2105 from the Mékinac–Taureau domain is texturally and chemically homogeneous. It contains abundant inclusions of biotite, K–feldspar, plagioclase, quartz, and sillimanite (absent in ZI–2105), and accessory monazite, apatite, and zircon. Notably, garnets contain pseudomorphs of former melt, preserved as polymineralic assemblages of plagioclase, K–feldspar, and quartz, indicating that garnet porphyroblasts grew under suprasolidus conditions.

In sample RS11–058, all monazite in garnet are located along microcracks, maintaining direct connectivity with the matrix (Figure S4). The 1024 ± 15 | 25 Ma weighted average from monazite in garnet is significantly younger than published constraints on peak metamorphism (> ca. 1080 Ma; Corrigan, 1995; Soucy La Roche et al., 2015). This suggests that monazite inclusions in garnet likely (re)crystallized after garnet growth. Y and Gd/Yb in monazite vary with spatial position within the thin section (Figure S11), rather than with date or textural relationship with metamorphic index minerals, which limits their usefulness for monazite date interpretations in this sample. Eu_N/Eu^*_N values in monazite, however, are systematically low (<0.1 with a few outliers at 0.1–0.2), suggesting that K–feldspar was already stable even during the crystallization of the oldest monazite grains in this sample. We therefore interpret 1098 ± 54 Ma to 981 ± 42 Ma monazite in this sample to have (re)crystallized as a results of melt crystallization after the formation of the suprasolidus garnet, K-feldspar, sillimanite, biotite, plagioclase peak assemblage.

In sample ZI–2105, a single monazite inclusion fully enclosed in garnet is characterized by a different composition and older age (1076 ± 57 | 68 Ma) compared to other analyses. We interpret the higher Y, Yb/Gd and Eu_N/Eu^*_N to reflect monazite crystallization likely during a late prograde stage prior to peak metamorphism and under conditions where garnet and K-feldspar were stable. Other monazite inclusions in garnet are located next to microcracks and may have crystallized from interactions with the matrix after garnet and K-feldspar growth between 1062 ± 87 Ma and 992 ± 74 Ma, based on their low Y, Yb/Gd and Eu_N/Eu^*_N. Matrix monazite dates are interpreted similarly. The weak increase in Y and Yb/Gb in <1020 Ma matrix monazite may be related to garnet breakdown.

New monazite petrochronological data in the Mékinac-Taureau domain thus provides limited information about the metamorphic evolution. Prograde metamorphism is imprecisely constrained to 1076 ± 57 | 68 Ma by a single analysis, whereas almost all monazite (1098 ± 54 Ma to 981 ± 42 Ma) in the two samples (re)crystallized during post-peak metamorphism when biotite, K–feldspar and sillimanite were present in the rock and after partial breakdown of garnet.

2.8.2 Shawinigan domain

Textural evidence in samples ZI–2101A and ZI–2102A suggests two growth generations of garnet: 1) garnet cores crystallized at prograde subsolidus metamorphism, as suggested, by the lack of former melt inclusions, sillimanite and K-feldspar and the preservation of an internal foliation at an angle to the matrix foliation (e.g., Soret et al., 2019; Jiang et al., 2022), and 2) peritectic garnet rims crystallized under suprasolidus conditions, as evidenced by the presence of sillimanite, K–feldspar, and former melt inclusions (e.g., Godet et al., 2021). Peak metamorphism reached the granulite facies based on thermobarometry by previous studies (e.g., Lévesque, 1995; Soucy La Roche et al., 2015).

Monazite in sample ZI–2102A covers the largest range in dates and chemical composition. The oldest monazite inclusions (1190 ± 120 Ma to 1106 ± 55 Ma; weighted mean of 1137 ± 13 | 24 Ma) are restricted to garnet cores. These monazite grains are characterized by high Y and Yb/Gd, and weakly negative Eu anomalies, consistent with monazite crystallization prior to significant garnet growth and in the absence of K–feldspar and sillimanite. These monazite inclusions constrain the maximum age of subsolidus garnet core growth to 1137 ± 13 | 24 Ma. These older monazite grains were not identified in the matrix, which suggest that they were probably completely consumed at suprasolidus conditions after the crystallization of garnet cores (Hermann and Rubatto, 2003; Yakymchuk and Brown, 2014; Wang et al., 2017). At ca. 1100 Ma, monazite composition is characterized by a sharp decrease in Y, Yb/Gd and Eu_N/Eu^*_N, which we interpret to reflect the rock reaching suprasolidus conditions with abundant peritectic garnet and K-feldspar crystallization (Figure 2.6J–L). These monazite grains commonly contain inclusions of sillimanite, indicating that sillimanite was also part of the assemblage during their crystallization. Furthermore, nine analyses on three monazite inclusions in garnet rims range between 1120 ± 110 Ma and 1047 ± 43 Ma (weighted mean of 1071 ± 18 | 29 Ma) and are characterized by low Y, Yb/Gd and pronounced negative Eu anomalies, consistent with crystallization during garnet rim growth (Figure 2.6J–L). These monazite inclusions thus crystallized at suprasolidus conditions (e.g., Godet et al., 2021) and provide a robust maximum age constraint on peak metamorphism at 1071 ± 18 | 29 Ma. Monazite younger than ca. 1045 Ma displays a modest increase in Y and Yb/Gd, interpreted to reflect post–peak crystallization following garnet resorption, possibly during melt crystallization.

Despite petrographic similarities between samples ZI–2101A and ZI–2102A, monazite in ZI–2101A does not provide as much information about the metamorphic evolution. No monazite inclusions are preserved in the subsolidus garnet cores, and monazite form a single generation yielding dates between 1115 ± 53 Ma and 1025 ± 98 Ma. Any prograde monazite, if ever present, must have dissolved in melt. Monazite inclusions in garnet rims range from 1088 ± 57 Ma to 1030 ± 74 Ma (weighted mean of 1060 ± 19 | 30 Ma), which we interpret to date peritectic garnet growth at or near peak metamorphic conditions (e.g., Bartoli et al., 2013), similar within uncertainty to peak monazite in sample ZI-2102.

The two samples analyzed in the Shawinigan domain outline a similar metamorphic evolution, but one of them (ZI-2102A) contains monazite that crystallized over a longer portion of the metamorphic evolution, while the other preserves mainly peak or near peak metamorphic monazite. Prograde, subsolidus garnet growth is constrained to 1137 ± 13 | 24 Ma. Suprasolidus conditions in the stability field of garnet, K–feldspar and sillimanite just before or at peak metamorphism were attained at 1071 ± 18 | 29 Ma. Garnet resorption, possibly during melt crystallization, occurred after ca. 1045 Ma. Overall, monazite data highlight a metamorphic evolution spanning over 100 Myr, with a prolonged residence of ~ 50 Myr at mid-crustal levels.

2.8.3 Portneuf–St. Maurice domain

In sample ZI–2107, a single monazite inclusion (1089 ± 44 Ma—1029 ± 41 Ma; weighted mean of 1060 ± 21 | 32 Ma) is partially enclosed in garnet rim and characterized by lower Y, Yb/Gd and Eu_N/Eu^*_N compared to monazite in the matrix. The portion of the monazite grain outside of garnet is in an embayment, and thus may have been entirely enclosed by garnet before garnet resorption (Figure 2.4F). The textural setting and chemical composition of monazite are consistent with synchronous crystallization with garnet rim, and thus constrains the maximum age of garnet rim growth under subsolidus, amphibolite facies conditions (based on the mineral assemblage in this study, in agreement with mineral paragenesis and thermobarometery from Levesque and Nadeau, 1994 and Corrigan, 1995). Xenotime grains in matrix overlap in age (1260 ± 140 Ma to 985 ± 54 Ma) and are located away from garnet; their relationship with garnet growth and resorption history is therefore ambiguous. Two garnet porphyroblast cores display concentric zoning, with relatively low concentrations of Y, MREE, and HREE that decrease outward. In contrast, the rims display an increase in Y, MREE, and HREE and are separated from the cores by a sharp contact parallel to crystal faces. Narrow Y, Lu and Dy-rich annuli are preserved in the core close to the rim. These features are characteristic of growth zoning and suggest that Lu remained immobile and reflect the Lu concentrations during garnet core and rim growth. The resorbed edge is enriched in Lu and Y, which are interpreted to have back-diffused into garnet during resorption, and the edge is therefore not considered in age calculations. Lu—Hf dates from garnet cores and rims in sample ZI–2107 are indistinguishable. We therefore use the combined age of all analyses as the best crystallization age (1089 ± 96 Ma; Figure 2.9A) during prograde to peak metamorphism at lower to middle amphibolite facies conditions. This garnet crystallization age is equivalent within uncertainty with the 1060 ± 21 | 32 Ma age of a monazite inclusion that grew synchronously with the garnet rim.

In sample ZI-2108, a xenotime inclusion within cordierite surrounding garnet yields a1394 ± 43 Ma date, significantly older than other xenotime grains dated in this sample. The grain is characterized by higher Yb/Gd and Eu_N/Eu^*_N, but its origin is not clear. It could be a detrital grain or it may be related to the ca. 1390 Ma metamorphic age previously reported by Corrigan (1995), attributed to the accretion of the Montauban arc to the SE Laurentian margin. Other xenotime grains are also located within the cordierite corona around partially resorbed garnet. Xenotime (1073 ± 63 Ma—1012 ± 52 Ma; weighted mean of 1039 ± 24 | 34 Ma) thus constrain partial garnet resorption during retrograde metamorphism. Rare sillimanite, white mica and K–feldspar along with cordierite indicate that retrograde metamorphism occurred under low-pressure conditions at a minimum temperature of ~650 °C (e.g., Palin and Dyck, 2021). A single 1068 ± 93 Ma xenotime inclusion within the garnet rim is interpreted to have (re)crystallized after garnet growth because it has the same age and chemical composition as xenotime grains within the cordierite corona around garnet and is located along a microcrack that may have facilitated interaction with the matrix. Prograde and peak metamorphism are thus unconstrained by the monazite and xenotime petrochronology dataset but were assessed with Lu-Hf garnet petrochronology. Garnet displays concentric zoning and a general decrease in Y and HREE from core to rim (Figures 2.8I-L, N-Q, S12), consistent with growth zoning (see Baxter et al., 2017). It yields a 1123 ± 35 Ma Lu—Hf crystallisation age, which we interpret to be the best estimate for the timing of prograde to near-peak metamorphism (Figure 2.9B).

In the Portneuf–St. Maurice domain, prograde to peak metamorphism at lower to middle amphibolite facies conditions occurred between 1123 ± 35 Ma and 1060 ± 21 Ma. The discrepancy between these ages may indicate diachronous metamorphism across this lithotectonic domain, or protracted metamorphism in which the 1123 ± 35 Ma garnet crystallization age in ZI-2108 reflects early garnet growth (garnet is partially resorbed and this age does not reflect rim growth), compared to the 1060 ± 21 Ma monazite age that dates garnet rim growth in ZI-2107. The large uncertainty on the 1089 ± 96 Ma garnet date in ZI-2107 hinders a meaningful comparison of garnet crystallization ages. Peak metamorphism was followed by decompression in the cordierite stability field (e.g., Corrigan, 1995; Smit et al., 2001) and barely reaching the sillimanite and K-feldspar (due to their very low modal proportion, <<1%) stability fields at 1039 ± 24 | 34 Ma.

2.9 Regional tectonic implications

Our petrochronological results and interpretations from six aluminous gneiss samples across the three lithotectonic domains reveal overlapping ages of amphibolite to granulite facies metamorphism, suggesting broadly synchronous metamorphic evolution across the region. Petrochronometers in the Shawinigan and Portneuf–St. Maurice domains record a more complete metamorphic evolution, encompassing prograde, peak, and retrograde metamorphic stages. In contrast, monazite from the Mékinac–Taureau domain predominantly preserves dates associated with the post-metamorphic peak evolution.

2.9.1 Prograde to peak metamorphism (1137 ± 13 | 24 —1100 Ma)

Monazite dates from inclusions within subsolidus garnet cores in the Shawinigan domain and a Lu–Hf garnet date in the Portneuf–St. Maurice domain constrain the onset of burial of supracrustal sequences and crustal thickening during prograde metamorphism to 1137 ± 13 | 24 Ma and 1123 ± 35 Ma, respectively. Such old dates in the Mauricie area have not been reported before, although it was inferred that metamorphism started prior to ca. 1080 Ma and possibly as early as 1120 Ma in the Mékinac-Taureau and Shawinigan domains (Corrigan, 1995; Corrigan and van Breemen, 1997; Soucy La Roche et al., 2015). In the Morin terrane to the west, Peck and Quinan (2022) dated titanite from mineral separates at ca. 1120-1100 Ma in seven samples. They tentatively attributed these dates to partial resetting of older ca. 1190-1140 Ma dates during the Ottawan Orogeny, but they could be consistent with early prograde growth at the onset of the Ottawan Orogeny, as described herein. Interpretation of these titanite dates is however hindered by the lack of trace element data or textural information. Elsewhere in the Grenville Orogen, the tectonometamorphic event closest in time is the 1190—1140 Ma Shawinigan Orogeny. Evidence for this orogeny is preserved across the western Grenville Province, including the Adirondack Highlands (Heumann et al., 2006; Chiarenzelli et al., 2010; Peck et al., 2019; Williams et al., 2019), the Parry Sound domain (Jamieson et al., 1992; Wodicka et al., 2000), the Morin Terrane and the Central Metasedimentary Belt (Markley et al., 2018; Peck and Quinan, 2022, Peck and Lin, 2025). The Shawinigan Orogeny is characterized by crustal thickening and granulite-facies metamorphism (>725—825 °C, >600—900 MPa; Williams et al., 2019). In contrast, our petrochronological data point to a prograde metamorphic stage under amphibolite-facies conditions at 1137 ± 13 | 24 Ma leading to Ottawan-aged granulite-facies metamorphism. The age of prograde metamorphism in the Mauricie area therefore appears several tens of Myr younger than the age of peak granulite facies during the Shawinigan orogeny. Our older metamorphic ages therefore cannot be readily attributed to the Shawinigan Orogeny in the study area.

Alternatively, metamorphism during the 1190–1140 Ma interval has also been interpreted as the result of contact metamorphism associated with voluminous syn- to post-Shawinigan AMCG suites documented across the western Grenville Province, including the Marcy Massif in the Adirondacks (McLelland et al., 2010), and the Morin (Martignole and Schrijver, 1970; Doig, 1991; Martignole et al., 2000) and Lac-Saint-Jean anorthosites (Corriveau, 1982; Higgins and van Breemen, 1992, 1996; Hébert et al., 2005; Lin and Sawyer, 2019) in Quebec. Such AMCG bodies have not been identified within our study area; the nearest ones, the Lac Croche and Morin anorthosites and the Lac Paul granite, are situated approximately 75–100 km to the west and ~30 km to the north of our study area, respectively, while the Lac-Saint-Jean anorthosite lies ~200 km to the north. Therefore, it is unlikely that these plutonic bodies could have provided sufficient heat to drive the early metamorphism at 1137 ± 13 | 24 to 1100 Ma.

Instead, a regional tectonic mechanism must be responsible for the early metamorphism. The most plausible explanation is that continental collision began earlier than the previously inferred timing of ca. 1090 Ma. Based on thermomechanical models anchored to available geochronological constraints from the Grenville Orogen, Jamieson et al. (2010) proposed that the orogen progressively evolved into a thickened, thermally mature, and ductile system, with mid-crustal temperatures exceeding 700 °C ~40 Myr after the onset of the collision. Widespread anatexis is predicted to occur as temperatures reach ≥800 °C after ~60 Myr, with incipient channel flow developing within the melt-weakened mid-crust thereafter. Suprasolidus and granulite facies conditions in the Mauricie region as early as 1090-1080 Ma (this study, Corrigan, 1995, Soucy La Roche et al., 2015) is therefore consistent with continental collision initiating at 1150-1140 Ma as we documented in this study.

2.9.2 Early to Middle Ottawan peak metamorphism (ca. 1100—1050 Ma)

Suprasolidus metamorphism at granulite facies conditions occurred in the Mékinac–Taureau and Shawinigan domains during earliest to middle Ottawan (1100–1050 Ma), marking the culmination of the Ottawan thermal peak. Previous studies indicated that peak metamorphic conditions in the Mékinac–Taureau domain reached 1000–1100 MPa and 820–880 °C prior to 1082 ± 20 Ma (Soucy La Roche et al., 2015). The 1081 ± 4 Ma monazite age reported by Corrigan (1995), which was initially interpreted as cooling age, is in agreement (within uncertainty) with most monazite dates in our study and likely reflects peak P–T conditions. As noted by both these studies, migmatization in the Mékinac–Taureau domain likely outlasted deformation leading to the formation of the regional foliation. Estimated P–T conditions in the Shawinigan domain range from 850 to 625 MPa and 775 to 700 °C (Soucy La Roche et al., 2015). Corrigan (1995) obtained monazite ages at 1092 ± 1 Ma and zircon at 1087 ± 2 Ma from a leucosome, which he interpreted to reflect melt crystallization whereas peak metamorphism would have occurred before the early Ottawan. This interpretation was also supported by a 1094 ± 2 Ma monazite date from a quartzite that he interpreted as a cooling age. The 1100–1050 Ma date range from monazite in our study rather implies the persistence of suprasolidus conditions in the Mékinac–Taureau and Shawinigan domains for ~50 Myr, indicating prolonged residence in the middle crust, although peak condition were likely already attained at the beginning of the Ottawan orogenic phase.

In contrast, peak metamorphism (1060 ± 21 | 32 Ma) in the western strand of the Portneuf–St. Maurice domain occurred at middle amphibolite facies conditions without partial melting. Corrigan (1995) reported a single monazite metamorphic age at 1388 ± 1 Ma from the eastern strand of the Portneuf–St. Maurice domain and metamorphism in this domain was inferred to be the result of the accretion of the Montauban arc to southeast Laurentian margin. Corrigan and van Breemen (1997) further proposed that the Portneuf–St. Maurice domain remained at upper crustal levels during the Ottawan Orogeny and that metamorphic overprint at that time was limited. We found only limited evidence of metamorphism related to the ca. 1400 Ma Montauban arc accretion in the samples studied herein (one xenotime date at 1394 ± 43 Ma that could be detrital or linked to this event). This indicates that the metamorphic evolution of the Portneuf–St. Maurice domain is heterogeneous, as our data support the formation of garnet-bearing peak metamorphic mineral assemblages during the Grenville Orogeny.

2.9.3 Middle Ottawan to Rigolet post–peak metamorphism and cooling (ca. 1050—980 Ma)

Petrochronometers that crystallized during post–peak and retrograde metamorphism are well preserved in all three domains. Almost all monazite dates from the Mékinac–Taureau domain are interpreted to reflect post–peak metamorphism during middle Ottawan to Rigolet (1098 ± 54 Ma to 981 ± 42 Ma with a majority younger than 1050 Ma). In the Shawinigan domain, sample ZI-2102A contains monazite with a retrograde signature after 1045 Ma. Cooling under 550–600 °C was constrained to 1030–985 Ma and 1030–1020 Ma in the Mékinac–Taureau and Shawinigan domains, respectively, based on $^{40}Ar/^{39}Ar$ cooling ages (Corrigan, 1995; Soucy La Roche et al., 2015), consistent with our retrograde monazite dates. Furthermore, these authors identified a general younging trend from higher to lower structural levels, which they attributed to progressive cooling downwards from the Tawachiche and eastern Taureau shear zones. Post-peak monazite dates in the Mékinac–Taureau domain are more abundant and relatively younger than those from the Shawinigan domain (Figure 2.6). The Mékinac–Taureau domain therefore likely remained at lower and hotter crustal conditions for a more prolonged period, resulting in continued monazite (re)crystallization along a younger segment of its evolution compared to the Shawinigan domain.

In the Portneuf–St. Maurice domain, 1020—1010 Ma $^{40}Ar/^{39}Ar$ hornblende cooling ages indicate that temperature reached at least ~ 550 °C during the Ottawan Orogeny (Corrigan, 1995). Since peak metamorphism in this domain was attributed to the accretion of the Montauban arc to Laurentia at 1400 Ma, Corrigan and van Breemen (1997) interpreted these dates to represent reheating during the juxtaposition of the cold upper–crustal rocks of the Portneuf–St. Maurice domain against the hotter, deeper crustal levels of the Shawinigan domain along the ca. 1065—1035 Ma Tawachiche shear zone. At the scale of the Grenville Province, Rivers (2012) suggested that metamorphism in the Allochthonous low-pressure belt, which comprises the Portneuf–St. Maurice domain, was the result of conductive heating following juxtaposition with the exhumed hot middle crust. Our monazite and garnet petrochronology demonstrate that at least part of the Portneuf–St. Maurice domain records regional metamorphism as early as 1123 ± 35 Ma and reached peak metamorphic conditions during the early Ottawan (see previous sections), synchronous with structurally lower domains, which is at odds with Rivers' model predictions. However, one sample from the Portneuf–St. Maurice domain contains cordierite coronas around garnet, which we dated at 1039 ± 24 | 34 Ma based on xenotime grains that formed during garnet breakdown. Replacement of garnet by cordierite with rare sillimanite and K-feldspar is consistent with low-pressure metamorphism or decompression and possibly heating to <400 MPa and ~ 650 °C since sillimanite and K-feldspar were not part of the peak, garnet-stable mineral assemblage (320—500 MPa and 544—638 °C; Corrigan, 1995). Low-pressure metamorphism is commonly attributed to contact metamorphism (Loosveld, 1989; Best, 2002; Miyashiro, 2012). The closest mid- to late- Ottawan pluton is the ~15x20 km 1056 ± 2 Ma Gagnon pluton (Figure 2.3; Corrigan and van Breemen, 1997), located ~8 km north of the sampled outcrop, which is farther than the width of a typical contact aureole (McFarlane et al., 2003; Bucher, 2023). Heat during the late Ottawan may thus have been provided by juxtaposition with the underlying Shawinigan domain, as predicted by the orogenic collapse of Rivers (2012). Decompression recorded by this sample further requires that the Portneuf–St. Maurice domain was also exhumed at that time, but tectonic structures have not been identified.

2.10 Tectonic significance of an older onset of the Grenville Orogeny

Swanson–Hysell et al. (2023) estimated the timing of substantial crustal shortening and thickening during the Grenville Orogeny through bootstrapped resampling of published age data from igneous and metamorphic suites. They estimated the onset of Grenvillian orogenesis at ca. 1089 Ma based on combined monazite and zircon metamorphic ages, whereas zircon-only datasets yielded a younger estimate of ca. 1070 Ma. They explained this discrepancy by the early crystallization of prograde monazite before zircon captured the age of peak metamorphism (e.g. as in the original monazite interpretation of Markley et al., 2018). However, the absence of textural context and the lack of constraints on compositional variations with age for most datasets hampers the ability to confidently link isotopic dates to specific stages of metamorphism in this compilation. We rather applied an *in situ* approach combining isotopic and trace element analyses with an assessment of the microtextural context of petrochronometers that highlighted the crystallization of prograde monazite and garnet between 1137 ± 13 | 24 and 1100 Ma, indicating that Ottawan metamorphism started several tens of million years earlier than generally accepted. These results are consistent with those of Dyer et al. (2025) who dated retrograde zircon at 1100–1070 Ma, implying an older metamorphic peak.

Shifting the onset of the Grenville Orogeny by several tens of million years has profound implications for tectonic models describing the late Mesoproterozoic evolution of the SE margin of Laurentia. Just before the presumed onset of the Grenville Orogeny, the Midcontinent Rift marks a period of significant lithospheric extension, and voluminous mafic magmatism between 1109 and 1084 Ma in the Great Lakes area of the USA and near Thunder Bay in Canada (Cannon, 1992; Swanson-Hysell et al., 2019; Woodruff *et al.,* 2020). Rifting was so important that it could have lead to the break-up of Laurentia if it did not fail (Swanson-Hysell et al., 2023). The transition from an extensional to a compressional tectonic regime resulted in the structural inversion of the Midcontinent Rift through northwest-directed thrusting along pre-existing extensional faults (Cannon, 1994). Rift inversion and termination of magmatic and extensional activity have been attributed to the onset of the Grenville Orogeny because it apparently coincided with it (Cannon, 1994; Swanson-Hysell et al., 2023). Our older monazite and garnet dates, however, overlap temporally with the initiation and the cessation of the Midcontinent Rift. This indicates that the Midcontinent Rift must have entirely developed while parts of the Grenville Orogen were undergoing shortening and crustal thickening. This may point to a diachronous collisional evolution along the margin of Laurentia, but additional robust geochronological data to constrain the onset of the orogeny along-strike are needed to fully resolve this issue. Alternatively, another tectonic model may be required.

Gervais et al. (2023) pointed out the apparent inconsistency between high-precision volcanic ages in the Midcontinent Rift (1105.60 ± 0.32 Ma to 1083.52 ± 0.23 Ma; Swanson-Hysell et al., 2019) and the age of eclogite-facies metamorphism in the hanging wall of the Allochthon Boundary Thrust (1100 ± 7 Ma to 1088 ± 5 Ma; Marsh and Culshaw, 2014). This and other arguments lead them to propose a new tectonic model for the Grenville Orogeny based on compiled global geochronological and geochemical datasets. They proposed that at ca. 1170–1150 Ma, a distinct microcontinent termed “Shawiniga” formed offshore of Laurentia through the accretion of mature arc terranes during the Shawinigan Orogeny. Slab avalanche beneath Shawiniga likely induced the rapid southward movement of Laurentia towards Shawiniga from 1110 to 1080 Ma, and potentially resulted in shortening and metamorphism in the upper plate, which would correspond to the first part of the Ottawan phase of the Grenville Orogeny (ca. 1090–1050 Ma). Shawiniga then collided with Laurentia at ca. 1030 Ma, which is interpreted to mark the final continent-continent collision. It is, however, unclear how shortening in the upper plate above a slab avalanche could lead to crustal thickening and anataxis at the scale of the entire Grenville Province for such an extended time. Accretionary orogenies—such as the Caledonian–Appalachian—are typically short-lived, with durations of approximately 20—50 Myr (Dewey, 2005). The extensive duration of prograde burial and heating (~60 Myr), followed by prolonged residence at deep crustal levels and anatexis (~50 Myr) rather support a long-lived continent–continent collision for the Grenville Orogeny. Moreover, if crustal shortening in Shawiniga is the result of a slab avalanche and rapid motion of the downgoing plate (>27 cm/a; Swanson-Hysell et al., 2019), extending the duration of the Ottawan Orogeny to ca. 1150 Myr (i.e. 40 Myr earlier) would require Laurentia to travel >10,800 km during that interval, i.e. more than a quarter of Earth's circumference, which is unsupported by paleogeographic reconstructions (Swanson-Hysell et al., 2019, 2023). The driving force for ca. 1150-1050 Ma Ottawan Orogeny in the model of Gervais et al. (2023) is thus unclear.

Existing geodynamic models offer valuable insights about the evolution of the Grenville Province, nevertheless each model appears to fall short in fully reconciling all available geological and geochronological observations. Improved future models must explain both the long-lived nature of the Grenville Orogeny, including its onset as early as 1137 ± 13 | 24 Ma, and its synchronicity with the development of a major rift system in Laurentia.

2.11 Conclusions

This study integrates *in situ* U—Th—Pb monazite and xenotime petrochronology and *in situ* Lu–Hf garnet petrochronology to constrain the timing of metamorphism across three lithotectonic domains in the Mauricie region, central Grenville Province. We reconstruct a prolonged metamorphic evolution, consistent with a long-lived continent–continent collision. Prograde metamorphism began as early as 1137 ± 13 | 24 Ma, marking the onset of burial and heating at amphibolite facies conditions and lasted until ca. 1100 Ma. Peak metamorphism at suprasolidus granulite facies metamorphism were attained between ca. 1100 and ca. 1050 Ma, marking the culmination of Ottawan metamorphism and suggests ~50 Myr of mid-crustal residence.

Retrograde metamorphism and exhumation occurred between ca. 1045 Ma and ca. 985 Ma during decompression. The timing of metamorphic stages is best preserved in the Shawinigan and Portneuf–St. Maurice domains, while monazite in the Mékinac–Taureau domain preserved only the post-peak late stage evolution. This illustrates that, despite a careful petrochronological approach, it is not always possible to characterize the entire metamorphic evolution of granulite facies rocks. We highlight that the incomplete record of metamorphism has certainly led to an incomplete understanding of the Grenville Orogeny.

3 GENERAL DISCUSSION

The Grenville Province in central and western Quebec preserves a protracted history of tectono-magmatic events along the southeastern margin of Laurentia, spanning from ca. 1800 Ma until the final collision with Amazonia during the Grenville Orogeny (ca. 1090–980 Ma; Rivers et al., 2012; Swanson-Hysell et al., 2023). Within the central Grenville Province, the Mauricie region encompasses the Mékinac–Taureau, Shawinigan, and Portneuf–St. Maurice lithotectonic domains, which form parts of the allochthonous medium and low-pressure belts (Figure 2.3, Nadeau and Brouillette, 1994, 1995). These domains preserve structural and metamorphic signatures linked to both pre-Grenvillian accretionary orogenies and the Grenville Orogeny (Corrigan, 1995; Peck and Quinan, 2022). However, the timing and duration of metamorphism and metamorphic conditions associated with these events was poorly resolved prior to my study.

Geochronological data from the Grenville Province have largely been derived from zircon and to a lesser extent, monazite, using ID-TIMS or SHRIMP methods (e.g., Corrigan, 1995; Corriveau and van Breemen, 2000; Indares and Dunning, 2001; Wodicka et al., 2004; Peck, 2012; Peck et al., 2013) and more rarely LA-ICP-MS on monazite (e.g., Lasalle et al., 2014; McCarron et al., 2014), zircon (e.g., Marsh and Culshaw, 2014; Peck et al., 2019; Shinevar et al., 2021; Culshaw et al., 2023), and titanite (e.g., Peck and Quinan, 2022). Yet, interpretations based on zircon and monazite ages from mineral separates remain ambiguous due to the complex growth and resorption histories of accessory phases during metamorphism, insufficient characterization of the textural context and the lack of correlation with specific P–T conditions and metamorphic reactions.

This M.Sc. thesis aimed to constrain the timing of metamorphism of high grade metamorphism of the rock units (aluminous gneiss) exposed in the Mauricie region to improve our understanding of the tectonometamorphic evolution of the central Grenville Province. The primary objective was to constrain the timing of the prograde, peak, and post-peak metamorphic stages during the metamorphic evolution and to associate them with their mineral assemblages in each lithotectonic domain. Another goal was to compare the metamorphic evolution among the three lithotectonic domains and integrate the results into broader tectonic models of the central Grenville Province.

To achieve these goals, I employed *in situ* U–Th–Pb monazite and xenotime petrochronology, and *in situ* Lu–Hf garnet petrochronology using LA-ICPMS. Isotopic and trace element analyses were contextualized through detailed textural characterization, linking the growth and resorption of petrochronometers to the growth and resorption of index minerals during the metamorphic evolution. This combined petrochronological approach provided robust constraints on the timing of prograde, peak, and retrograde metamorphism.

I performed *in situ* U—Th—Pb petrochronology on six aluminous gneiss samples (monazite in RS11-058, ZI-2105, ZI-2101A, ZI-2102A, monazite and xenotime in ZI-2107, and xenotime in ZI-2108). In addition, *in situ* Lu–Hf garnet petrochronology was performed on two samples, ZI-2107 and ZI-2108, which helped to provide timing constraints on the age of garnet growth in these samples in which monazite and xenotime U-Pb data were limited.

This combined approach allowed me to deduce a prolonged metamorphic evolution, consistent with a long-lived continent–continent collision. Results indicate that prograde metamorphism began as early as 1137 ± 13 | 24 Ma in the Shawinigan domain based on the dates from monazite inclusions in garnet cores, and at 1123 ± 35 Ma in the Portneuf–St. Maurice domain based on the Lu-Hf garnet date. Elsewhere in the Grenville Orogen, metamorphism in the ca. 1190—1140 Ma interval is attributed to the Shawinigan Orogeny that is characterized by granulite facies conditions (e.g., Jamieson et al., 1992; Wodicka et al., 2000; Heumann et al., 2006; Chiarenzelli et al., 2010; Markley et al., 2018; Peck et al., 2019; Williams et al., 2019; Peck and Quinan, 2022, Peck and Lin, 2025). However, our petrochronological data point to prograde metamorphism under amphibolite-facies conditions at 1137 ± 13 | 24 —1100 Ma leading to Ottawan-aged granulite-facies metamorphism. These older metamorphic ages therefore cannot be readily attributed to the Shawinigan Orogeny in the Mauricie region.

Suprasolidus, granulite-facies metamorphism occurred between ca. 1100 and 1050 Ma, as recorded by monazite inclusions in garnet rims from the Shawinigan domain. The 1100–1050 Ma monazite date range implies the persistence of suprasolidus conditions in the Mékinac–Taureau and Shawinigan domains for ~50 Myr, indicating prolonged residence in the middle crust. Furthermore, the Mékinac–Taureau domain likely remained at lower and hotter crustal conditions for a more prolonged period, resulting in continued monazite (re)crystallization along a younger segment of its evolution compared to the Shawinigan domain.

Petrochronometers that crystallized during post–peak metamorphism are well preserved in all three domains. Retrograde metamorphism and exhumation occurred between ca. ca. 1045 and ca. 985 Ma. Most monazite dates from the Mékinac–Taureau domain reflect post-peak metamorphism as the majority are younger than 1050 Ma and are characterized by textural relationships and chemical compositions consistent with post-peak crystallization. In the Portneuf–St. Maurice domain, 1039 ± 24 | 34 Ma xenotime is associated with cordierite coronas around garnet and linked to garnet breakdown during low-pressure metamorphism or decompression and possibly heating.

Collectively, the metamorphic record is best preserved in the Shawinigan and Portneuf–St. Maurice domains, whereas monazite in the Mékinac–Taureau domain mainly reflects post-peak evolution. This demonstrates that even with careful petrochronology, the full metamorphic evolution is not always captured in granulite-facies terranes, leading to an incomplete understanding of the Grenville Orogeny.

The new petrochronological results presented above have significant implications for tectonic models of late Mesoproterozoic evolution along the southeastern margin of Laurentia, as these dates shift the initiation of the Grenville Orogeny by several tens of millions of years—from the traditionally accepted ca. 1090 Ma to 1137 ± 13 | 24 Ma (this study). Swanson-Hysell et al. (2023) used bootstrapped resampling of published age data to estimate the onset of the Grenville Orogeny at ca. 1089 and ca. 1070 Ma. However, the lack of detailed textural and compositional context limits confident linkage of dates to specific metamorphic stages. Gervais et al. (2023) highlighted the apparent inconsistency between high-precision volcanic ages from the Midcontinent Rift (1105.60 ± 0.32 to 1083.52 ± 0.23 Ma; Swanson-Hysell et al., 2019) and eclogite-facies metamorphism in the Allochthon Boundary Thrust (1100 ± 7 to 1088 ± 5 Ma; Marsh and Culshaw, 2014). I further demonstrated that the Midcontinent Rift formed entirely during the onset of the Grenville Orogeny, which requires modifications to conventional Grenville tectonic models (e.g. Rivers et al., 2012, Swanson-Hysell et al., 2023). To reconcile these observations, Gervais et al. (2023) proposed a new tectonic model for the Grenville Orogeny based on compiled global geochronological and geochemical datasets and invoking the formation of a microcontinent, "Shawiniga," offshore Laurentia at ca. 1170–1150 Ma. A slab avalanche beneath Shawiniga possibly drove the southward motion of Laurentia (1110–1080 Ma), triggering shortening and metamorphism corresponding to the early Ottawan phase (1090–1050 Ma), with final collision at ca. 1030 Ma. However, this model does not account for the prolonged prograde burial and heating (~60 Myr) and mid-crustal residence (~50 Myr) inferred from my data. These prolonged timescales, along with evidence of metamorphism as early as 1137 ± 13 | 24 Ma, emphasize a protracted and more complex evolution of the Grenville Orogeny than is captured by existing geodynamic models. Such models, though insightful, fail to fully reconcile all available geological and geochronological constraints. Future models must address the long-lived nature of the Grenville Orogeny, including early metamorphism (as early as 1137 ± 13 | 24 Ma) and its overlap with the development of a major rift system in Laurentia like the Midcontinent Rift.

3.1 Future directions

Corrigan (1995) dated a single 1388 ± 1 Ma metamorphic monazite from a high-grade metapelite in the eastern segment of the Portneuf–St. Maurice domain, and attributed metamorphism in this domain to the accretion of the Montauban arc to the SE Laurentian continental margin. I have not found evidence of metamorphism at that time in the two samples investigated form the western segment. *In situ* petrochronology (monazite, xenotime, garnet) in and around the area investigated by Corrigan (1995) could further resolve the metamorphic evolution associated with the accretion of the Montauban arc. Garnet in the two samples I collected in the Portneuf–St. Maurice domain yielded Lu-Hf crystallization ages consistent with growth during a single metamorphic event despite their texturally and chemically distinct cores and rims. Bulk-grain isotope dissolution technique is often limited because garnet zones are often too thin to mechanically isolate (Nesheim et al., 2012; Dragovic et al., 2015; Larson et al., 2024; Du et al., 2024). *In situ* LA-ICP-MS Lu–Hf dating provides a viable dating approach to resolve such complexities, particularly in polymetamorphic terranes, but lacks analytical precision. Future work should use isotope dissolution dating methods on carefully characterized garnet grains that crystallized during a single event, such as those investigated herein, to obtain higher-precision Lu-Hf garnet dates and better constrain the timing of metamorphism in the Portneuf–St. Maurice domain.

The Escoumins Supracrustal Belt, located in the southern central Grenville Province, is interpreted as a remnant volcanic arc within the allochthonous low-pressure belt (Figure 2.1, Groulier et al., 2018; Dickin et al., 2023). Monazite dates of 1056 ± 19 Ma and 984 ± 9 Ma (Costello et al., 2018) attest metamorphism related to the Grenville Orogeny. However, an older Lu–Hf garnet date (1123 ± 35 Ma; this study) suggests earlier prograde metamorphism in the Portneuf–Mauricie domain that is also part of the allochthonous low-pressure belt. Detailed petrochronology in the Escoumins Supracrustal Belt would help clarify its evolution and potential correlation with the Portneuf–St. Maurice domain, and possibly to better understand the cryptic accretion of an arc system to the Laurentian margin at ca. 1400 Ma.

The Midcontinent Rift represents a major Mesoproterozoic tectonomagmatic event, characterized by extensive lithospheric extension and voluminous mafic magmatism between 1109 and 1084 Ma in the Great Lakes region of the USA and near Thunder Bay, Canada (Cannon, 1992; Swanson-Hysell et al., 2019; Woodruff et al., 2020). The western arm of the rift, extending beneath Phanerozoic cover in the Great Plains region to Lake Superior, where rift-associated rocks are well exposed (Van Schmus and Hinze, 1985). Its eastern arm, southeast of the lake, estimated to contain ~0.2 × 106 km^3 of volcanic rocks over ~700 km (Swanson et al., 2023). Early plateau-stage magmatism (ca. 1109–1105 Ma; Miller and Vervoort, 1996; Woodruff et al., 2020) produced mafic intrusions and picritic to tholeiitic basalts, forming lava sequences exceeding ~3 km in thickness in northern Lake Superior (Hollings et al., 2007; Swanson-Hysell et al., 2014). This was followed by a limited volcanic "latent" stage (Miller et al., 2013), after which the main rift stage (ca. 1098–1091 Ma) accumulated >9 km of basaltic flows in northern Minnesota and up to 20 km beneath Lake Superior (Cannon, 1992; Green et al., 2011). Post-rift sedimentation, represented by the Oronto Group, reflects thermal subsidence and fluvial-lacustrine deposition, including the Copper Harbor Conglomerate (ca. 1085 Ma) and the Nonesuch Formation (ca. 1075 Ma), followed by the >4 km-thick Freda Formation (Elmore et al., 1989; Swanson-Hysell et al., 2019).

Rift inversion occurred prior to complete lithospheric separation, driven by a transition from extensional to compressional tectonics (Swanson-Hysell et al., 2023). This inversion produced northwest-directed thrusting along pre-existing extensional faults and transpressional faulting within accommodation zones (Cannon, 1994; Zhang et al., 2016). The Montreal River monocline, the largest structure associated with this contraction, uplifted and tilted a 35-km-thick sequence of Archean, Paleoproterozoic, and rift-related lithologies along a major reverse fault, with Rb-Sr biotite dates indicating deformation at ca. 1050 Ma, coeval with the middle Ottawan phase of the Grenville Orogeny (Cannon et al., 1993). U-Pb dating of detrital zircon on late-kinematic calcite veins (CA-ID-TIMS) from the Jacobsville Formation yielded a maximum depositional age of 992.51 ±0.64/1.21 Ma. When considered together with a lower-precision U-Pb age of 985.5 ± 35.8 Ma obtained from calcite in the Keweenaw fault breccia, these data collectively constrain the terminal phase of Midcontinent Rift inversion to the Rigolet phase of the Grenville Orogeny (Hodgin et al., 2022).

The close temporal correlation between cessation of rift volcanism (ca. 1091 Ma) and the onset of the Ottawan phase of the Grenville Orogeny (ca. 1090 Ma; Corrigan and van Breemen, 1997) supports far-field Grenvillian compression as the principal driver of rift termination, rather than successful separation of a conjugate continent (Stein et al., 2014). The importance of rifting is emphasized by the fact that, had it succeeded, Laurentia may have fragmented (Swanson-Hysell et al., 2023). Although rift-related magmatism and extension largely coincide with Grenville Orogeny, monazite and garnet prograde ages (1137 ± 13 | 24—1100 Ma) from this study indicate that parts of the Grenville Orogen were already undergoing crustal thickening during the development of the Midcontinent Rift. This suggests a diachronous, along-strike collisional evolution of Laurentia's margin, highlighting the need for additional robust geochronology data to resolve apparent temporal inconsistencies or to evaluate alternative geodynamic models.

4 BIBLIOGRAPHY

Aleinikoff, J. N., Schenck, W. S., Plank, M. O., Srogi, L., Fanning, C. M., Kamo, S. L., and Bosbyshell, H. (2006). Deciphering igneous and metamorphic events in high-grade rocks of the Wilmington Complex, Delaware: Morphology, cathodoluminescence and backscattered electron zoning, and SHRIMP U-Pb geochronology of zircon and monazite. *Geological Society of America Bulletin*, 118(1–2), 39–64.

Anczkiewicz, R., Chakraborty, S., Dasgupta, S., Mukhopadhyay, D., and Kołtonik, K. (2014). Timing, duration and inversion of prograde Barrovian metamorphism constrained by high resolution Lu–Hf garnet dating: A case study from the Sikkim Himalaya, NE India. *Earth and Planetary Science Letters*, 407, 70-81.

Augland, L. E., Moukhsil, A., Solgadi, F., and Indares, A. (2015). Pinwarian to Grenvillian magmatic evolution in the central Grenville Province: new constraints from ID–TIMS U–Pb ages and coupled Lu–Hf S–MC–ICP–MS data. *Canadian Journal of Earth Sciences*, 52(9), 701–721.

Bartoli, O., Tajčmanová, L., Cesare, B., and Acosta-Vigil, A. (2013). Phase equilibria constraints on melting of stromatic migmatites from Ronda (S. Spain): insights on the formation of peritectic garnet. *Journal of Metamorphic Geology*, 31(7), 775-789.

Barton Jr, J. M., and Doig, R. (1972). Rb–Sr Isotopic Studies of the Lac Croche Complex Grenville Province, Quebec. *Canadian Journal of Earth Sciences*, 9(9), 1180–1186.

Battisti, M. A., Konopásek, J., Bitencourt, M. D. F., Sláma, J., Percival, J. J., De Toni, G. B., and Trubač, J. (2024). Petrochronology of the Dom Feliciano Belt foreland in southernmost Brazil reveals two distinct tectonometamorphic events in the western central Kaoko–Dom Feliciano–Gariep orogen. *International Journal of Earth Sciences*, 113(4), 973–1004.

Baxter, E. F., Caddick, M. J., and Dragovic, B. (2017). Garnet: A rock-forming mineral petrochronometer. *Reviews in Mineralogy and Geochemistry*, 83(1), 469–533.

Bea, F., Pereira, M. D., and Stroh, A. (1994). Mineral/leucosome trace-element partitioning in a peraluminous migmatite (a laser ablation-ICP-MS study). *Chemical Geology*, 117(1–4), 291–312.

Beaumont, C., Nguyen, M. H., Jamieson, R. A., and Ellis, S. (2006). Crustal flow modes in large hot orogens. *Geological Society, London, Special Publications*, 268, 91–145. Bingen, B., Viola, G., Möller, C., Vander Auwera, J., Laurent, A., and Yi, K. (2021). The Sveconorwegian orogeny. *Gondwana Research*, 90, 273–313.

Best, M. G. (2002). Igneous and metamorphic petrology. John Wiley and Sons. 564-607.

Bloch, E., and Ganguly, J. (2015). 176Lu–176Hf geochronology of garnet II: numerical simulations of the development of garnet–whole-rock 176Lu–176Hf isochrons and a new method for constraining the thermal history of metamorphic rocks: *Contributions to Mineralogy and Petrology*, 169(12), 1–18.

Bloch, E.M., Jollands, M.C., Devoir, A., Bouvier, A.S., Ibañez-Mejia, M., and Baumgartner, L.P., (2020). Multispecies Diffusion of Yttrium, Rare Earth Elements and Hafnium in Garnet. *Journal of Petrology*, 61(7), 1–61.

Boggs, K.J.E., and Corriveau, L. (2004). Granulite-facies P-T-t paths and the influence of retrograde cation diffusion during polyphase orogenesis, western Grenville Province, Quebec. *Geological Society of America*, 197, 35–64.

Brown, D. A., Simpson, A., Hand, M., Morrissey, L. J., Gilbert, S., Tamblyn, R., and Glorie, S. (2022). Laser-ablation Lu-Hf dating reveals Laurentian garnet in subducted rocks from southern Australia. *Geology*, 50(7), 837–842.

Cannon, W. F. (1992). The Midcontinent rift in the Lake Superior region with emphasis on its geodynamic evolution. *Tectonophysics*, 213(1–2), 41–48.

Cannon, W. F., Peterman, Z. E., and Sims, P. K. (1993). Crustal-scale thrusting and origin of the Montreal River monocline-A 35-km-thick cross section of the midcontinent rift in northern Michigan and Wisconsin. *Tectonics*, 12(3), 728-744.

Cannon, W. F. (1994). Closing of the Midcontinent rift-A far—field effect of Grenvillian compression. *Geology*, 22(2), 155-158.

Carr, S. D., Easton, R. M., Jamieson, R. A., and Culshaw, N. G. (2000). Geologic transect across the Grenville orogen of Ontario and New York. *Canadian Journal of Earth Sciences*, 37(2–3), 193–216.

Cesare, B., Ferrero, S., Salvioli-Mariani, E., Pedron, D., and Cavallo, A. (2009). "Nanogranite" and glassy inclusions: The anatectic melt in migmatites and granulites. *Geology*, 37(7), 627-630.

Cesare, B., Acosta-Vigil, A., Bartoli, O., and Ferrero, S. (2015). What can we learn from melt inclusions in migmatites and granulites?. *Lithos*, 239, 186-216.

Cherniak, D. J., Watson, E. B., Grove, M., and Harrison, T. M. (2004). Pb diffusion in monazite: a combined RBS/SIMS study. *Geochimica et Cosmochimica Acta*, 68(4), 829–840.

Chiarenzelli, J. R., and McLelland, J. M. (1991). Age and regional relationships of granitoid rocks of the Adirondack Highlands. *The Journal of Geology*, 99(4), 571-590.

Chiarenzelli, J., Regan, S., Peck, W. H., Selleck, B. W., Cousens, B., Baird, G. B., and Shrady, C. H. (2010). Shawinigan arc magmatism in the Adirondack Lowlands as a consequence of closure of the Trans-Adirondack backarc basin. *Geosphere*, 6(6), 900–916.

Chiarenzelli, J., Valentino, D., Lupulescu, M., Thern, E., and Johnston, S. (2011). Differentiating Shawinigan and Ottawan orogenesis in the central Adirondacks. *Geosphere*, 7(1), 2–22.

Corfu, F., and Easton, R. M. (1995). U–Pb geochronology of the Mazinaw terrane, an imbricate segment of the Central Metasedimentary Belt, Grenville Province, Ontario. *Canadian Journal of Earth Sciences*, 32(7), 959-976.

Corrigan, D., and van Breemen, O. (1997). U–Pb age constraints for the lithotectonic evolution of the Grenville Province along the Mauricie transect, Quebec. *Canadian Journal of Earth Sciences*, 34(3), 299–316.

Corrigan, D., Rivers, T. and Dunning, G. (2000). U-Pb constraints for the plutonic and tectonometamorphic evolution of Lake Melville terrane, Labrador and implications for basement reworking in the northeastern Grenville Province. *Precambrian Research*, 99, 65–90

Corrigan, D. (1995). Mesoproterozoic evolution of the south-central Grenville orogen; structural, metamorphic, and geochronologic constraints from the Mauricie transect (PhD thesis, Carleton University), 65-190

Corriveau, L., and van Breemen, O. (2000). Docking of the Central Metasedimentary Belt to Laurentia in geon 12: evidence from the 1.17–1.16 Ga Chevreuil intrusive suite and host gneisses, Quebec. *Canadian Journal of Earth Sciences*, 37(2–3), 253–269.

Culshaw, N., Van De Kerckhove, S., Slagstad, T., Marsh, J., and Easton, R. M. (2023). Crustal evolution of the Laurentian continental margin from the Paleo-through Mesoproterozoic: a zircon

U–Pb and Hf transect through the western Grenville Province, Ontario, Canada. *Precambrian Research*, 386, 106963.

Culshaw, N., Foster, J., Marsh, J., Slagstad, T., and Gerbi, C. (2016). Kiosk domain, Central Gneiss Belt, Grenville Province, Ontario: a Labradorian palimpsest preserved in the ductile deep crust. *Precambrian Research*, 280, 249-278.

Cox, R. A., Indares, A., and Dunning, G. R. (2002). Temperature–time paths in the high-P Manicouagan Imbricate zone, eastern Grenville Province: Evidence for two metamorphic events. *Precambrian Research*, 117(3-4), 225-250.

Darling, R. S., and Peck, W. H. (2016). Metamorphic conditions of Adirondack rocks. *Adirondack Journal of Environmental Studies*, 21(1), 7.

Davis, D. W., and Bartlett, J. R. (1988). Geochronology of the Belmont Lake metavolcanic complex and implications for crustal development in the Central Metasedimentary Belt, Grenville Province, Ontario. *Canadian Journal of Earth Sciences*, 25(11), 1751-1759.

Dewey, J. F. (2005). Orogeny can be very short. Proceedings of the National Academy of Sciences, 102(43), 15286-15293.

Dickin, A. P., and McNutt, R. H. (2007). The Central Metasedimentary Belt (Grenville Province) as a failed back-arc rift zone: Nd isotope evidence. *Earth and Planetary Science Letters*, 259(1–2), 97–106.

Dickin, A., Hynes, E., Landry, E., and Vautour, S. (2023). The significance of Nd isotope mapping in Precambrian orogenic belts: a case study from the Saguenay region of the Quebec Grenville Province. *Precambrian Research*, 394, 107126.

Doig, R. (1991). U-Pb zircon dates of Morin anorthosite suite rocks, Grenville Province, Quebec. *The Journal of Geology*, 99(5), 729–738.

Dragovic, B., Baxter, E. F., and Caddick, M. J. (2015). Pulsed dehydration and garnet growth during subduction revealed by zoned garnet geochronology and thermodynamic modeling, Sifnos, Greece. *Earth and Planetary Science Letters*, 413, 111-122.

Du, K. Y., Cheng, H., and Yang, R. (2024). Thermal evolution of the North China Craton revealed by microsampling garnet geochronology on single xenoliths. *Chemical Geology*, 663, 122264.

Duchêne, S., Blichert-Toft, J., Luais, B., Télouk, P., Lardeaux, J. M., and Albarede, F. (1997). The Lu–Hf dating of garnets and the ages of the Alpine high-pressure metamorphism. *Nature*, 387(6633), 586–589.

Duc-Tin, Q., and Keppler, H. (2015). Monazite and xenotime solubility in granitic melts and the origin of the lanthanide tetrad effect. *Contributions to Mineralogy and Petrology*, 169(1), 8.

Dunning, G., and Indares, A. (2010). New insights on the 1.7–1.0 Ga crustal evolution of the central Grenville Province from the Manicouagan–Baie Comeau transect. *Precambrian Research*, 180(3–4), 204–226.

Dyer, S. C., Edgeworth, I., Kendall, B., and Yakymchuk, C. (2025). Late-orogenic retrograde zircon growth. *Contributions to Mineralogy and Petrology*, 180(5), 31.

Elmore, R. D., Milavec, G. J., Imbus, S. W., and Engel, M. H. (1989). The Precambrian Nonesuch Formation of the North American mid-continent rift, sedimentology and organic geochemical aspects of lacustrine deposition. *Precambrian Research*, 43(3), 191-213.

Emslie, R. F. (1978). Elsonian magmatism in Labrador: age, characteristics and tectonic setting. *Canadian Journal of Earth Sciences*, 15(3), 438–453.

Engi, M. (2017). Petrochronology based on REE–minerals: monazite, allanite, xenotime, apatite. *Reviews in Mineralogy and Geochemistry*, 83(1), 365–418.

Foster, G., Gibson, H. D., Parrish, R., Horstwood, M., Fraser, J., and Tindle, A. (2002). Textural, chemical and isotopic insights into the nature and behaviour of metamorphic monazite. *Chemical Geology*, 191(1–3), 183–207.

Foster, G., and Parrish, R. R. (2003). Metamorphic monazite and the generation of P–T–t paths. *Geochronology, Geological Society of London*, 220, 151–181.

Friedman, R. M., and Martignole, J. (1995). Mesoproterozoic sedimentation, magmatism, and metamorphism in the southern part of the Grenville Province (western Quebec): U–Pb geochronological constraints. *Canadian Journal of Earth Sciences*, 32 (12), 2103–2114.

Gaidies, F., Mccarron, T., Simpson, A. D., Easton, R. M., Glorie, S., Putlitz, B., and Trebus, K. (2024). Polymetamorphism during the Grenvillian Orogeny in SE Ontario: Results from trace element mapping, *in situ* geochronology, and diffusion geospeedometry. *Journal of Metamorphic Geology*, 42(1), 35–61.

Gaidies, F., Morneau, Y. E., Petts, D. C., Jackson, S. E., Zagorevski, A., and Ryan, J. J. (2021). Major and trace element mapping of garnet: Unravelling the conditions, timing and rates of metamorphism of the Snowcap assemblage, west-central Yukon. *Journal of Metamorphic Geology*, 39(2), 133-164.

Gervais, F., Beaudry, A., Kavanagh-Lepage, C., Moukhsil, A., Larson, K. P., and Guilmette, C. (2023). Far from boring: a new Grenvillian perspective on Mesoproterozoic tectonics. *Earth and Planetary Science Letters*, 610, 118129.

Gervais, F., Beaudry, A., Kavanagh-Lepage, C., Moukhsil, A., Guilmette, C., and Larson, K. (2024). Reply to comment on: Far from boring: A new Grenvillian perspective on Mesoproterozoic tectonics. *Earth and Planetary Science Letters*, 641, 118804.

Gibson, H. D., Carr, S. D., Brown, R. L., and Hamilton, M. A. (2004). Correlations between chemical and age domains in monazite, and metamorphic reactions involving major pelitic phases: an integration of ID–TIMS and SHRIMP geochronology with Y–Th–U X-ray mapping. *Chemical Geology*, 211(3–4), 237–260.

Glorie, S., Simpson, A., Gilbert, S. E., Hand, M., and Müller, A. B. (2024). Testing the reproducibility of in situ Lu-Hf dating using Lu–rich garnet from the Tørdal pegmatites, southern Norway. *Chemical Geology*, 653, 122038.

Godet, A., Jouvent, M., Laureijs, C., Guilmette, C., Larson, K., Coleman, M., and Côté–Roberge, M. (2024). *In Situ* Lu–Hf Garnet Dating of Archean Deep Crust Granulites from the Polymetamorphic Grenville Front Tectonic Zone. *Journal of Petrology*, 65(11).

Godet, A., Guilmette, C., Labrousse, L., Smit, M. A., Cutts, J. A., Davis, D. W., and Vanier, M. A. (2021). Lu–Hf garnet dating and the timing of collisions: Palaeoproterozoic accretionary tectonics revealed in the Southeastern Churchill Province, Trans-Hudson Orogen, Canada. *Journal of Metamorphic Geology*, 39(8), 977-1007.

Godet, A., Guilmette, C., Labrousse, L., Davis, D. W., Smit, M. A., Cutts, J. A., and Charette, B. (2020). Complete metamorphic cycle and long-lived anatexis in the c. 2.1 Ga Mistinibi Complex, Canada. *Journal of Metamorphic Geology*, 38(3), 235-264.

Goncalves, P., Raimondo, T., Paquette, J. L., and Santos de Souza de Oliveira, J. (2021). Garnet as a monitor for melt–rock interaction: Textural, mineralogical, and compositional evidence of partial melting and melt-driven metasomatism. *Journal of Metamorphic Geology*, 39(5), 617-648.

Gower, C. F., and Krogh, T. E. (2002). A U–Pb geochronological review of the Proterozoic history of the eastern Grenville Province. *Canadian Journal of Earth Sciences*, 39(5), 795–829.

Gower, C. F., Schärer, U., and Heaman, L. M. (1992). The Labradorian orogeny in the Grenville Province, eastern Labrador, Canada. *Canadian Journal of Earth Sciences*, 29(9), 1944–1957.

Gower, C. F., Kamo, S. L., Kwok, K., and Krogh, T. E. (2008). Proterozoic southward accretion and Grenvillian orogenesis in the interior Grenville Province in eastern Labrador: Evidence from U–Pb geochronological investigations. *Precambrian Research*, 165(1–2), 61–95.

Gower, C. F. (1996). The evolution of the Grenville Province in eastern Labrador, Canada. *Geological Society, London, Special Publications*, 112(1), 197–218.

Green, J. C., Boerboom, T. J., Schmidt, S. T., and Fitz, T. J. (2011). The North Shore Volcanic Group: Mesoproterozoic plateau volcanic rocks of the Midcontinent Rift system in northeastern Minnesota, *in* Miller, J.D., Hudak, G.J., Wittkop, C., and McLaughlin, Archean to Anthropocene: Field Guides to the Geology of the Mid-Continent of North America: *Geological Society of America Field Guide* 24, 121–146.

Groulier, P. A., Indares, A., Dunning, G., and Moukhsil, A. (2020). Andean style 1.50–1.35 Ga arc dynamics in the Southeastern Laurentian margin: The rifting and reassembly of Quebecia. *Terra Nova*, 32(6), 450–457.

Groulier, P. A., Indares, A., Dunning, G., Moukhsil, A., and Wälle, M. (2018a). Peri-Laurentian, Pinwarian-age oceanic arc crust preserved in the Grenville Province: insights from the Escoumins supracrustal belt. *Precambrian Research*, 311, 37–64.

Groulier, P. A., Indares, A., Dunning, G., Moukhsil, A., and Jenner, G. (2018b). Syn-orogenic magmatism over 100 my in high crustal levels of the central Grenville Province: characteristics, age and tectonic significance. *Lithos*, 312, 128–152.

Hagen-Peter, G., Cottle, J. M., Smit, M., and Cooper, A. F. (2016). Coupled garnet Lu–Hf and monazite U–Pb geochronology constrain early convergent margin dynamics in the Ross orogen, Antarctica. *Journal of Metamorphic Geology*, 34(4), 293–319.

Hamilton, M.A., McLelland, J., and Selleck, B. (2004). SHRIMP U-Pb zircon geochronology of the anorthosite-mangerite-charnockite-granite suite, Adirondack Mountains, New York: Ages of emplacement and metamorphism, *in* Tollo, R.P., Corriveau, L., McLelland, J., and Bartholomew, M.J., eds., Proterozoic tectonic evolution of the Grenville orogen in North America: Boulder, Colorado, *Geological Society of America Memoir,* 197, 337–355.

Hanmer, S., and McEachern, S. (1992). Kinematical and rheological evolution of a crustal-scale ductile thrust zone, Central Metasedimentary Belt, Grenville orogen, Ontario. *Canadian Journal of Earth Sciences*, 29(8), 1779–1790.

Harlov, D. E., Marschall, H. R., and Hanel, M. (2007). Fluorapatite-monazite relationships in granulite-facies metapelites, Schwarzwald, southwest Germany. *Mineralogical magazine*, 71(2), 223-234.

Hébert, C., and van Breemen, O. (2004). Mesoproterozoic basement of the Lac St. Jean Anorthosite Suite and younger Grenvillian intrusions in the Saguenay region, Québec: structural relationships and U–Pb geochronology. *Geological Society of America*,197, 65–79.

Hébert, C., Cadieux, A.M., and van Breemen, O. (2005). Temporal evolution and nature of Ti Fe P mineralization in the anorthosite mangerite charnockite granite (AMCG) suites of the south-central Grenville Province, Saguenay Lac St. Jean area, Quebec, Canada. *Canadian Journal of Earth Sciences*, 42 (10), 1865–1880.

Hermann, J., and Rubatto, D. (2003). Relating zircon and monazite domains to garnet growth zones: age and duration of granulite facies metamorphism in the Val Malenco lower crust. *Journal of Metamorphic Geology*, 21(9), 833–852.

Heumann, M. J., Bickford, M. E., Hill, B. M., McLelland, J. M., Selleck, B. W., and Jercinovic, M. J. (2006). Timing of anatexis in metapelites from the Adirondack lowlands and southern highlands: A manifestation of the Shawinigan orogeny and subsequent anorthosite–mangerite–charnockite–granite magmatism. *Geological Society of America Bulletin*, 118(11–12), 1283–1298.

Higgins, M. D., Ider, M., and van Breemen, O. (2002). U–Pb ages of plutonism, wollastonite formation, and deformation in the central part of the Lac–Saint–Jean anorthosite suite. *Canadian Journal of Earth Sciences*, 39(7), 1093–1105.

Higgins, M. D., and van Breemen, O. (1992). The age of the Lac-Saint-Jean anorthosite complex and associated mafic rocks, Grenville Province, Canada. *Canadian Journal of Earth Sciences*, 29(7), 1412-1423.

Higgins, M. D., and van Breemen, O. (1996). Three generations of anorthosite-mangerite-charnockite-granite (AMCG) magmatism, contact metamorphism and tectonism in the Saguenay-Lac-Saint-Jean region of the Grenville Province, Canada. *Precambrian research*, 79(3-4), 327-346.

Hodgin, E. B., Swanson-Hysell, N. L., DeGraff, J. M., Kylander-Clark, A. R., Schmitz, M. D., Turner, A. C., and Stolper, D. A. (2022). Final inversion of the Midcontinent Rift during the Rigolet Phase of the Grenvillian Orogeny. *Geology*, 50(5), 547-551.

Holder, R. M., Horton, F., Swindle, C., and Rakotondrazafy, A. F. M. (2024). The monazite record of (ultra) high-temperature metamorphism in southern Madagascar: Gondwana terrane correlations and structural trapping of hot middle crust. *Journal of the Geological Society*, 182(2), 1-20.

Holder, R. M., Hacker, B. R., Kylander-Clark, A. R., and Cottle, J. M. (2015). Monazite trace-element and isotopic signatures of (ultra) high-pressure metamorphism: Examples from the Western Gneiss Region, Norway. *Chemical Geology*, 409, 99–111.

Holder, R. M., Yakymchuk, C., and Viete, D. R. (2020). Accessory mineral Eu anomalies in suprasolidus rocks: Beyond feldspar. *Geochemistry, Geophysics, Geosystems*, 21(8), 1-16.

Hollings, P., Fralick, P., and Cousens, B. (2007). Early history of the Midcontinent Rift inferred from geochemistry and sedimentology of the Mesoproterozoic Osler Group, northwestern Ontario. *Canadian Journal of Earth Sciences*, 44(3), 389-412.

Holness, M. B., and Sawyer, E. W. (2008). On the pseudomorphing of melt-filled pores during the crystallization of migmatites. *Journal of Petrology*, 49(7), 1343-1363.

Horstwood, M. S., Košler, J., Gehrels, G., Jackson, S. E., McLean, N. M., Paton, C., and Schoene, B. (2016). Community-derived standards for LA-ICP-MS U–Th–Pb geochronology–Uncertainty propagation, age interpretation and data reporting. *Geostandards and Geoanalytical Research*, 40(3), 311–332.

Hynes, A., and Rivers, T. (2010). Protracted continental collision—Evidence from the Grenville orogen. *Canadian Journal of Earth Sciences*, 47(5), 591–620.

Indares, A., and Martignole, J. (1990). Metamorphic constraints on the tectonic evolution of the allochthonous monocyclic belt of the Grenville Province, western Quebec. *Canadian Journal of Earth Sciences*, 27(3), 371–386.

Indares, A. and Dunning, G. (2001). Partial melting of high-P–T metapelites from the Tshenukutish Terrane (Grenville Province): petrography and U–Pb geochronology. *Journal of Petrology*, 42(8), 1547-1565.

Indares, A., and Moukhsil, A. (2013). Geon 12 crustal extension in the central Grenville Province, implications for the orogenic architecture, and potential influence on the emplacement of anorthosites. *Canadian Journal of Earth Sciences*, 50(9), 955–966.

Indares, A., Dunning, G., Cox, R., Gale, D., and Connelly, J. (1998). High-pressure, high-temperature rocks from the base of thick continental crust: Geology and age constraints from the Manicouagan Imbricate Zone, eastern Grenville Province. *Tectonics*, 17(3), 426–440.

Indares, A., Dunning, G., and Cox, R. (2000). Tectono-thermal evolution of deep crust in a Mesoproterozoic continental collision setting: the Manicouagan example. *Canadian Journal of Earth Sciences*, 37(2-3), 325–340.

Indares, A. (2020). Deciphering the metamorphic architecture and magmatic patterns of large hot orogens: Insights from the central Grenville Province. *Gondwana Research*, 80, 385–409.

Indares, A. (2025). The Grenville Province: revisiting the orogenic framework and integrating recent findings. *Canadian Journal of Earth Sciences*, 62 (2), 1–20.

Jamieson, R. A., Beaumont, C., Warren, C. J., and Nguyen, M. H. (2010). The Grenville Orogen explained? Applications and limitations of integrating numerical models with geological and geophysical data. *Canadian Journal of Earth Sciences*, 47(4), 517–539.

Jamieson, R. A., Culshaw, N. G., Wodicka, N., Corrigan, D., and Ketchum, J. W. F. (1992). Timing and tectonic setting of Grenvillian metamorphism—constraints from a transect along Georgian Bay, Ontario. *Journal of Metamorphic Geology*, 10(3), 321–332.

Jamieson, R. A., Beaumont, C., Nguyen, M. H., and Culshaw, N. G. (2007). Syn-convergent ductile flow in variable-strength continental crust: Numerical models with application to the western Grenville orogen. *Tectonics*, 26(5).

Jannin, S., Gervais, F., Moukhsil, A., and Augland, L. E. (2018). Late–Grenvillian channel flow in the central Grenville Province (Manicouagan Reservoir area): New constraints from a structural and geochronological study of the Allochthon Boundary Thrust. *Journal of Structural Geology*, 115, 132–151.

Jiang, Y., Štípská, P., Schulmann, K., Aguilar, C., Wang, S., Anczkiewicz, R., and Chopin, F. (2022). Barrovian and Buchan metamorphic series in the Chinese Altai: P–T–t–D evolution and tectonic implications. *Journal of Metamorphic Geology*, 40(4), 823-857.

Jiao, S., Guo, J., Harley, S. L., and Peng, P. (2013). Geochronology and trace element geochemistry of zircon, monazite and garnet from the garnetite and/or associated other high-grade rocks: Implications for Palaeoproterozoic tectonothermal evolution of the Khondalite Belt, North China Craton. *Precambrian Research*, 237, 78-100.

Jochum, K. P., Weis, U., Stoll, B., Kuzmin, D., Yang, Q., Raczek, I., and Enzweiler, J. (2011). Determination of reference values for NIST SRM 610–617 glasses following ISO guidelines. *Geostandards and Geoanalytical Research*, 35(4), 397–429.

Johnson, T. E., Clark, C., Taylor, R. J., Santosh, M., and Collins, A. S. (2015). Prograde and retrograde growth of monazite in migmatites: An example from the Nagercoil Block, southern India. *Geoscience Frontiers*, 6(3), 373–387.

Kelly, N. M., Clarke, G. L., and Harley, S. L. (2006). Monazite behaviour and age significance in poly–metamorphic high–grade terrains: a case study from the western Musgrave Block, central Australia. *Lithos*, 88(1–4), 100–134.

Kylander-Clark, A. R., Hacker, B. R., and Cottle, J. M. (2013). Laser-ablation split-stream ICP petrochronology. *Chemical Geology*, 345, 99-112.

Labrousse, L., Bonnet, G., François, C., Godet, A., and Gyomlai, T. (2024). Recent advances in petrochronology: from dates to ages and rates of deep orogenic processes. *Comptes Rendus. Géoscience*, 356(S2), 551-577.

Lambert, C., Gervais, F., Crowley, J. L., Moukhsil, A., and Kavanagh–Lepage, C. (2023). Protracted melt–present deformation during the Rigolet phase of the Grenvillian Orogeny. Insights from geochronology along the highway 117 transect through the Grenville Province in western Quebec, Canada. *Precambrian Research*, 384, 106939.

Larson K.P. (2024) LA-QQQ-ICP-MS Lu-Hf Data Reduction Scheme Center For Open Science doi: 10.17605/OSF.IO/AD75Z.

Larson, K. P., Shrestha, S., Cottle, J. M., Guilmette, C., Johnson, T. A., Gibson, H. D., and Gervais, F. (2022). Re-evaluating monazite as a record of metamorphic reactions. *Geoscience Frontiers*, 13(2), 101340.

Larson, K. P., Cottle, J. M., Button, M., Dyck, B., Lihter, I., and Shrestha, S. (2024). Investigating low dispersion isotope dissolution Lu–Hf garnet dates via *in situ* Lu–Hf geochronology, Kanchenjunga Himal. *Geoscience Frontiers*, 15(3), 101781.

Lasalle, S., Dunning, G., and Indares, A. (2014). In situ LA–ICP–MS dating of monazite from aluminous gneisses: insights on the tectono-metamorphic history of a granulite-facies domain in the central Grenville Province. *Canadian Journal of Earth Sciences*, 51(6), 558-572.

Lévesque, S. (1995). Zonation metamorphique et évolution thermique de la region Portneuf-Mauricie, orogène de Grenville (M.Sc. thesis). Université Laval, Québec, Canada.

Li, Y., and Vermeesch, P. (2021). Inverse isochron regression for Re–Os, K–Ca and other chronometers. *Geochronology*, 3(2), 415–420.

Lin, L., and Sawyer, E. W. (2019). Microstructure and compositional changes across biotite-rich reaction selvedges around mafic schollen in a semipelitic diatexite migmatite. *Journal of Metamorphic Geology*, 37(4), 539-566.

Loosveld, R. J. (1989). The synchronism of crustal thickening and low-pressure facies metamorphism in the Mount Isa inlier, Australia 2. Fast convective thinning of mantle lithosphere during crustal thickening. *Tectonophysics*, 165(1-4), 191-218.

Lotout, C., Indares, A., Vervoort, J., and Deloule, E. (2023). High–P metamorphism in the Mesoproterozoic: petrochronological insights from the Grenville Province. *Precambrian Research*, 399, 107208.

Markley, M. J., Dunn, S. R., Jercinovic, M. J., Peck, W. H., and Williams, M. L. (2018). Monazite U–Th–Pb geochronology of the Central Metasedimentary Belt Boundary Zone (CMBbz), Grenville Province, Ontario Canada. *Canadian Journal of Earth Sciences*, 55(9), 1063–1078.

Marsh, J. H., and Culshaw, N. G. (2014). Timing and conditions of high-pressure metamorphism in the western Grenville Province: Constraints from accessory mineral composition and phase equilibrium modeling. *Lithos*, 200, 402–417.

Martignole, J., and Schrijver, K. (1970). Tectonic setting and evolution of the Morin anorthosite, Grenville Province, Quebec. *Bulletin of the Geological Society of Finland*, 42, 165–209.

Martignole, J., Calvert, A. J., Friedman, R., and Reynolds, P. (2000). Crustal evolution along a seismic section across the Grenville Province (western Quebec). *Canadian Journal of Earth Sciences*, 37(2–3), 291–306.

McCarron, T., Gaidies, F., McFarlane, C. R., Easton, R. M., and Jones, P. (2014). Coupling thermodynamic modeling and high-resolution in situ LA-ICP-MS monazite geochronology:

evidence for Barrovian metamorphism late in the Grenvillian history of southeastern Ontario. *Mineralogy and Petrology*, 108(6), 741-758.

McCarron, T., McFarlane, C. R., and Gaidies, F. (2019). The significance of Mn-rich ilmenite and the determination of P–T paths from zoned garnet in metasedimentary rocks from the western Cape Breton Highlands, Nova Scotia. *Journal of Metamorphic Geology*, 37(9), 1171–1192.

McEachern, S. J., and van Breemen, O. (1993). Age of deformation within the Central Metasedimentary Belt boundary thrust zone, southwest Grenville Orogen: constraints on the collision of the Mid-Proterozoic Elzevir terrane. *Canadian Journal of Earth Sciences*, 30(6), 1155–1165.

McFarlane, C. R. M., Carlson, W. D., and Connelly, J. N. (2003). Prograde, peak, and retrograde P–T paths from aluminium in orthopyroxene: High-temperature contact metamorphism in the aureole of the Makhavinekh Lake Pluton, Nain Plutonic Suite, Labrador. *Journal of Metamorphic Geology*, 21(5), 405-423.

McLelland, J. M., Bickford, M. E., Hill, B. M., Clechenko, C. C., Valley, J. W., and Hamilton, M. A. (2004). Direct dating of Adirondack massif anorthosite by U-Pb SHRIMP analysis of igneous zircon: Implications for AMCG complexes. *Geological Society of America Bulletin*, 116(11–12), 1299–1317.

McLelland, J., Goldstein, A., Cunningham, B., Olson, C., and Orrell, S. (2002). Structural evolution of a quartz–sillimanite vein and nodule complex in a late-to post-tectonic leucogranite, Western Adirondack Highlands, New York. *Journal of structural geology*, 24(6-7), 1157-1170.

McLelland, J., Hamilton, M., Selleck, B., McLelland, J., Walker, D., and Orrell, S. (2001). Zircon U-Pb geochronology of the Ottawan orogeny, Adirondack highlands, New York: regional and tectonic implications. *Precambrian Research*, 109(1-2), 39-72.

McLelland, J. M., Selleck, B. W., Hamilton, M. A., and Bickford, M. E. (2010). Late-to post-tectonic setting of some major Proterozoic anorthosite–mangerite–charnockite–granite (AMCG) suites. *The Canadian Mineralogist*, 48(4), 729–750.

McLelland, J. M., Selleck, B. W., and Bickford, M. E. (2013). Tectonic evolution of the Adirondack Mountains and Grenville orogen inliers within the USA. *Geoscience Canada*, 40(4), 318–352.

Miyashiro, A. (2012). Metamorphism and metamorphic belts. *Springer Science and Business Media*.19-34.

Miller, J. D., Nicholson, S. W., Easton, R. M., Ripley, E. M., and Feinberg, J. M. (2013). Geology and mineral deposits of the 1.1 Ga Midcontinent Rift in the Lake Superior region—An overview. Field guide to the copper-nickel-platinum group element deposits of the Lake Superior Region. Edited by Miller, J. *Precambrian Research Center Guidebook*, 13, 1-49.

Miller, J.D., and Vervoort, J.D. (1996). The latent magmatic stage of the Midcontinent Rift: A period of magmatic underplating and melting of the lower crust: Institute on Lake Superior Geology Proceedings, 42, 33–35.

Moore, S. J., Carlson, W. D., and Hesse, M. A. (2013). Origins of yttrium and rare earth element distributions in metamorphic garnet. *Journal of Metamorphic Geology*, 31(6), 663–689.

Mottram, C. M., Warren, C. J., Regis, D., Roberts, N. M., Harris, N. B., Argles, T. W., and Parrish, R. R. (2014). Developing an inverted Barrovian sequence; insights from monazite petrochronology. *Earth and Planetary Science Letters*, 403, 418–431.

Nadeau, L., and Brouillette, P. (1994). Structural map of the La Tuque area (NTS 31P), Grenville Province, Quebec. Geological Survey of Canada, Open File 2938, echelle 1:250 000.

Nadeau, L., and Brouillette, P. (1995). Structural map of the Shawinigan area (NTS 31I), Grenville Province, Quebec. Geological Survey of Canada, Open File 3012, echelle 1:250 000.

Nadeau, L., Brouillette, P., and Hébert, C. (2008). Arc magmatism, continental collision and exhumation: the mesoproterozoic evolution of the south-central Grenville Province, Portneuf–Mauricie region, Quebec, *Geological Association of Canada Field Trip B3*.

Nadeau, L., Brouillette, P., and Hébert, C. (2009). Geological compilation map of the Portneuf-St. Maurice region, Grenville Province, Quebec. Ministère des Ressources Naturelles et de la Faune, Québec, (GM 63830), scale 1/125000.

Nebel, O., Morel, M. L., and Vroon, P. Z. (2009). Isotope dilution determinations of Lu, Hf, Zr, Ta and W, and Hf isotope compositions of NIST SRM 610 and 612 glass wafers. *Geostandards and Geoanalytical Research*, 33(4), 487–499.

Nesheim, T. O., Vervoort, J. D., McClelland, W. C., Gilotti, J. A., and Lang, H. M. (2012). Mesoproterozoic syntectonic garnet within Belt Supergroup metamorphic tectonites: Evidence of Grenville-age metamorphism and deformation along northwest Laurentia. *Lithos*, 134, 91-107.

O'Neill, H. S. C. (2016). The smoothness and shapes of chondrite-normalized rare earth element patterns in basalts. *Journal of Petrology*, 57(8), 1463–1508.

Palin, R. M., and Dyck, B. (2021). Metamorphism of pelitic (Al–rich) rocks. *Encyclopedia of Geology*, 2, 445–456.

Paton, C., Hellstrom, J., Paul, B., Woodhead, J., and Hergt, J. (2011). Iolite: Freeware for the visualisation and processing of mass spectrometric data. *Journal of Analytical Atomic Spectrometry*, 26(12), 2508–2518.

Peck, W. H., and Lin, H. Y. (2025). Provenance and depositional age of metasedimentary rocks in the Frontenac terrane (Grenville Province, Ontario). *Canadian Journal of Earth Sciences*, 62(2).

Peck, W. H., and Quinan, M. P. (2022). New age constraints on magmatism and metamorphism in the Morin terrane (Grenville Province, Quebec). *Canadian Journal of Earth Sciences*, 59(4), 232–242.

Peck, W.H., DeAngelis, M.T., Meredith, M.T., and Morin, E. (2005). Polymetamorphism of marbles in the Morin Terrane, Grenville Province, Quebec. *Canadian Journal of Earth Sciences*, 42(10), 1949–1965.

Peck, W. H., Quinan, M. P., and Selleck, B. W. (2019). Detrital zircon constraints on Grenville sedimentation at the margin of Laurentia. *Precambrian Research*, 331, 105342.

Peck, W.H. (2012). Reconnaissance geochronology and geochemistry of the Mont–Tremblant gneiss of the Morin terrane, Grenville Province, Québec. *Geosphere*, 8, 1356–1365.

Peck, W. H., Selleck, B. W., Wong, M. S., Chiarenzelli, J. R., Harpp, K. S., Hollocher, K., and Stocker, A. (2013). Orogenic to postorogenic (1.20–1.15 Ga) magmatism in the Adirondack Lowlands and Frontenac terrane, southern Grenville Province, USA and Canada. *Geosphere*, 9(6), 1637-1663.

Pownceby, M. I., Wall, V. J., and O'Neill, H. S. C. (1987). Fe–Mn partitioning between garnet and ilmenite: experimental calibration and applications. *Contributions to Mineralogy and Petrology*, 97, 116–126.

Pullen, A., Ibáñez-Mejia, M., Gehrels, G. E., Giesler, D., and Pecha, M. (2018). Optimization of a laser ablation-single collector-inductively coupled plasma-mass spectrometer (Thermo Element 2) for accurate, precise, and efficient zircon U-Th-Pb geochronology. *Geochemistry, Geophysics, Geosystems*, 19(10), 3689–3705.

Pyle, J. M., and Spear, F. S. (1999). Yttrium zoning in garnet: coupling of major and accessory phases during metamorphic reactions. *Geological Materials Research*, 1(6), 1–49.

Pyle, J. M., and Spear, F. S. (2003). Four generations of accessory-phase growth in low-pressure migmatites from SW New Hampshire. *American Mineralogist*, 88(2–3), 338–351.

Pyle, J. M., Spear, F. S., Rudnick, R. L., and Mc Donough, W. F. (2001). Monazite–xenotime–garnet equilibrium in metapelites and a new monazite–garnet thermometer. *Journal of Petrology*, 42(11), 2083–2107.

Rapp, R. P., and Watson, E. B. (1986). Monazite solubility and dissolution kinetics: implications for the thorium and light rare earth chemistry of felsic magmas. *Contributions to Mineralogy and Petrology*, 94(3), 304-316.

Regan, S. P., Chiarenzelli, J. R., McLelland, J. M., and Cousens, B. L. (2011). Evidence for an enriched asthenospheric source for coronitic metagabbros in the Adirondack Highlands. *Geosphere*, 7(3), 694–709.

Regis, D., Warren, C. J., Mottram, C. M., and Roberts, N. M. (2016). Using monazite and zircon petrochronology to constrain the P–T–t evolution of the middle crust in the Bhutan Himalaya. *Journal of Metamorphic Geology*, 34(6), 617–639.

Ribeiro, B. V., Finch, M. A., Cawood, P. A., Faleiros, F. M., Murphy, T. D., Simpson, A., and Barrote, V. R. (2022). From microanalysis to supercontinents: insights from the Rio Apa Terrane into the Mesoproterozoic SW Amazonian Craton evolution during Rodinia assembly. *Journal of Metamorphic Geology*, 40(4), 631–663.

Ribeiro, B. V., Kirkland, C. L., Smit, M., Musiyachenko, K., Korhonen, F. J., Evans, N. J., and Makin, S. (2024). Garnet Reference Materials for *In Situ* Lu-Hf Geochronology. *Geostandards and Geoanalytical Research*, 48(4), 887–908.

Rivers, T. (2021) The Grenvillian Orogeny and Rodinia. *Encyclopedia of Geology*, 2nd edition, 4, 187-201.

Rivers, T., and Corrigan, D. (2000). Convergent margin on southeastern Laurentia during the Mesoproterozoic: tectonic implications. *Canadian Journal of Earth Sciences*, 37(2–3), 359–383.

Rivers, T., Culshaw, N., Hynes, A., Indares, A., Jamieson, R., Martignole, J., and Clowes, R. M. (2012). The Grenville orogen—A post-LITHOPROBE perspective. Tectonic styles in Canada: the LITHOPROBE perspective, 49, 97–236.

Rivers, T. (1997). Lithotectonic elements of the Grenville Province: review and tectonic implications. *Precambrian Research*, 86(3–4), 117–154.

Rivers, T., Martignole, J., Gower, C. F., and Davidson, A. (1989). New tectonic divisions of the Grenville Province, southeast Canadian Shield. *Tectonics*, 8(1), 63-84.

Rivers, T. (2008). Assembly and preservation of lower, mid, and upper orogenic crust in the Grenville Province—Implications for the evolution of large hot long-duration orogens. *Precambrian Research*, 167(3–4), 237–259.

Rivers, T. (2012). Upper-crustal orogenic lid and mid-crustal core complexes: signature of a collapsed orogenic plateau in the hinterland of the Grenville Province. *Canadian Journal of Earth Sciences*, 49(1), 1–42.

Romer, R. L., and Smeds, S. A. (1996). U-Pb columbite ages of pegmatites from Sveconorwegian terranes in southwestern Sweden. *Precambrian Research*, 76(1–2), 15–30.

Rubatto, D., Hermann, J., and Buick, I. S. (2006). Temperature and bulk composition control on the growth of monazite and zircon during low-pressure anatexis (Mount Stafford, central Australia). *Journal of Petrology*, 47(10), 1973–1996.

Rubatto, D., Chakraborty, S., and Dasgupta, S. (2013). Timescales of crustal melting in the Higher Himalayan Crystallines (Sikkim, Eastern Himalaya) inferred from trace element–constrained monazite and zircon chronology. *Contributions to Mineralogy and Petrology*, 165, 349–372.

Sappin, A. A., Constantin, M., Clark, T., and van Breemen, O. (2009). Geochemistry, geochronology, and geodynamic setting of Ni–Cu±PGE mineral prospects hosted by mafic and ultramafic intrusions in the Portneuf–Mauricie Domain, Grenville Province, Quebec. *Canadian Journal of Earth Sciences*, 46(5), 331–353.

Sappin, A. A., Constantin, M., and Clark, T. (2012). Petrology of mafic and ultramafic intrusions from the Portneuf–Mauricie Domain, Grenville Province, Canada: Implications for plutonic complexes in a Proterozoic island arc. *Lithos*, 154, 277–295.

Scherer, E. E., Cameron, K. L., and Blichert–Toft, J. (2000). Lu–Hf garnet geochronology: closure temperature relative to the Sm–Nd system and the effects of trace mineral inclusions. *Geochimica et Cosmochimica Acta*, 64(19), 3413–3432.

Shinevar, W. J., Jagoutz, O., and VanTongeren, J. A. (2021). Gore Mountain garnet amphibolite records UHT conditions: Implications for the rheology of the lower continental crust during orogenesis. *Journal of Petrology*, 62(4), egab007.

Schoene, B. (2014). U-Th–Pb geochronology. *Treatise on Geochemistry*: 2nd edition, 341–378.

Schneider, D. A., Cope, N., and Holm, D. K. (2013). Thermochronology of the Mont Laurier terrane, southern Canadian Grenville Province, and its bearing on defining orogenic architecture. *Precambrian Research*, 226, 43-58.

Simpson, A., Gilbert, S., Tamblyn, R., Hand, M., Spandler, C., Gillespie, J., and Glorie, S. (2021). In-situ LuHf geochronology of garnet, apatite and xenotime by LA ICP MS/MS. *Chemical Geology*, 577, 120299.

Simpson, A., Glorie, S., Hand, M., Spandler, C., and Gilbert, S. (2023). Garnet Lu–Hf speed dating: A novel method to rapidly resolve polymetamorphic histories. *Gondwana Research*, 121, 215–234.

Slagstad, T., Hamilton, M. A., Jamieson, R. A., and Culshaw, N. G. (2004). Timing and duration of melting in the mid orogenic crust: constraints from U–Pb (SHRIMP) data, Muskoka and Shawanaga domains, Grenville Province, Ontario. *Canadian Journal of Earth Sciences*, 41(11), 1339–1365.

Slagstad, T., Culshaw, N. G., Daly, J. S., and Jamieson, R. A. (2009). Western Grenville province holds key to midcontinental Granite-Rhyolite province enigma. *Terra Nova*, 21(3), 181–187.

Slagstad, T., Rivers, T., and Corrigan, D. (2023). Comment on "Far from boring: A new Grenvillian perspective on Mesoproterozoic tectonics" by Gervais et al., (2023). *Earth and Planetary Science Letters*, 621, 118381.

Smit, M. A., Scherer, E. E., and Mezger, K. (2013). Lu–Hf and Sm–Nd garnet geochronology: chronometric closure and implications for dating petrological processes. *Earth and Planetary Science Letters*, 381, 222–233.

Smit, C. A., Van Reenen, D. D., Gerya, T. V., and Perchuk, L. L. (2001). P–T conditions of decompression of the Limpopo high-grade terrane: record from shear zones. *Journal of Metamorphic Geology*, 19(3), 249-268.

Soret, M., Larson, K. P., Cottle, J. M., Smit, M., Johnson, A., Shrestha, S., and Faisal, S. (2019). Mesozoic to Cenozoic tectono-metamorphic history of the South Pamir–Hindu Kush (Chitral, NW Pakistan): Insights from phase equilibria modelling, and garnet–monazite petrochronology. *Journal of Metamorphic Geology*, 37(5), 633-666.

Soucy La Roche, R., Gervais, F., Tremblay, A., Crowley, J. L., and Ruffet, G. (2015). Tectono-metamorphic history of the eastern Taureau shear zone, Mauricie area, Québec: Implications for the exhumation of the mid-crust in the Grenville Province. *Precambrian Research*, 257, 22–46.

Soucy La Roche, R., Dyer, S. C., Zagorevski, A., Cottle, J. M., and Gaidies, F. (2022). 150 Myr of episodic metamorphism recorded in the Yukon–Tanana Terrane, Northern Canadian Cordillera: evidence from monazite and xenotime petrochronology. *Lithosphere*, 2022(1), 7708357.

Spear, F. S. (1991). On the interpretation of peak metamorphic temperatures in light of garnet diffusion during cooling. *Journal of Metamorphic Geology*, 9(4), 379-388.

Spear, F. S., and Pyle, J. M. (2002). Apatite, monazite, and xenotime in metamorphic rocks. *Reviews in Mineralogy and Geochemistry*, 48, 293–336.

Spencer, C. J., Mitchell, R. N., and Brown, M. (2021). Enigmatic mid-Proterozoic orogens: Hot, thin, and low. *Geophysical Research Letters*, 48(16).

Stein, C. A., Stein, S., Merino, M., Randy Keller, G., Flesch, L. M., and Jurdy, D. M. (2014). Was the Midcontinent Rift part of a successful seafloor-spreading episode?. *Geophysical Research Letters*, 41(5), 1465–1470.

Stockwell, C. H. (1964). Fourth report on structural provinces, orogenies, and time-classification of rocks of the Canadian Precambrian Shield. *Geological Survey of Canada. Pap*, 64(17), 1-21.

Swanson-Hysell, N. L., Vaughan, A. A., Mustain, M. R., and Asp, K. E. (2014). Confirmation of progressive plate motion during the Midcontinent Rift's early magmatic stage from the Osler Volcanic Group, Ontario, Canada. *Geochemistry, Geophysics, Geosystems*, 15(5), 2039-2047.

Swanson-Hysell, N. L., Ramezani, J., Fairchild, L. M., and Rose, I. R. (2019). Failed rifting and fast drifting: Midcontinent Rift development, Laurentia's rapid motion and the driver of Grenvillian orogenesis. *Bulletin*, 131(5–6), 913–940.

Swanson-Hysell, N.L., Rivers, T., and Van der Lee, S. (2023). The late Mesoproterozoic to early Neoproterozoic Grenvillian orogeny and the assembly of Rodinia. *Geological Society of America*, 220, 221–250.Tamblyn, R., Hand, M., Simpson, A., Gilbert, S., Wade, B., and Glorie, S. (2022). *In situ* laser ablation Lu–Hf geochronology of garnet across the Western Gneiss Region: campaign-style dating of metamorphism. *Journal of the Geological Society*, 179(4).

Tamblyn, R., Hand, M., Simpson, A., Gilbert, S., Wade, B., and Glorie, S. (2022). In situ laser ablation Lu–Hf geochronology of garnet across the Western Gneiss Region: campaign-style dating of metamorphism. *Journal of the Geological Society*, 179(4), jgs2021-094.

Tomascak, P. B., Krogstad, E. J., and Walker, R. J. (1996). U-Pb monazite geochronology of granitic rocks from Maine: Implications for late Paleozoic tectonics in the northern Appalachians. *The Journal of Geology*, 104(2), 185–195.

Tual, L., Smit, M. A., Kooijman, E., Kielman-Schmitt, M., and Ratschbacher, L. (2022). Garnet, zircon, and monazite age and REE signatures in (ultra) high-temperature and high-pressure rocks: Examples from the Caledonides and the Pamir. *Journal of Metamorphic Geology*, 40(8), 1321–1346.

Tucker, R. D., and Gower, C. F. (1990). Salient features of the Pinware terrane, Grenville Province, eastern Labrador. *Geological Association of Canada–Mineralogical Association of Canada*, 15, A133.

Valentino, D. W., Chiarenzelli, J. R., and Regan, S. P. (2019). Spatial and temporal links between Shawinigan accretionary orogenesis and massif anorthosite intrusion, southern Grenville Province, New York, USA. *Journal of Geodynamics*, 129, 80–97.

Van Schmus, W. R., and Hinze, W. J. (1985). The midcontinent rift system. *Annual Review of Earth and Planetary Sciences*, 13, 345–383.Vermeesch, P. (2018). IsoplotR: A free and open toolbox for geochronology. *Geoscience Frontiers*, 9(5), 1479–1493.

Vielzeuf, D., and Holloway, J. R. (1988). Experimental determination of the fluid-absent melting relations in the pelitic system: consequences for crustal differentiation. *Contributions to Mineralogy and Petrology*, 98(3), 257-276.

Volante, S., Blereau, E., Guitreau, M., Tedeschi, M., van Schijndel, V., and Cutts, K. (2024). Current applications using key mineral phases in igneous and metamorphic geology: perspectives for the future. *Geological Society, London, Special Publications*, 537, 57–121.

Wang, J.M., Wu, F.Y., Rubatto, D., Liu, S.R., Zhang, J.J., Liu, X.C. and Yang, L. (2017). Monazite behaviour during isothermal decompression in pelitic granulites: a case study from Dinggye, Tibetan Himalaya. *Contributions to Mineralogy and Petrology*, 172(10), 81.

Warren, C. J., Greenwood, L. V., Argles, T. W., Roberts, N. M., Parrish, R. R., and Harris, N. B. (2019). Garnet–monazite rare earth element relationships in sub–solidus metapelites: a case study from Bhutan. *Geological Society, London, Special Publications*, 478(1), 145–166.

Weller, O. M., Jackson, S., Miller, W. G., St-Onge, M. R., and Rayner, N. (2020). Quantitative elemental mapping of granulite-facies monazite: Textural insights and implications for petrochronology. *Journal of Metamorphic Geology*, 38(8), 853–880.

Williams, M. L., Jercinovic, M. J., and Hetherington, C. J. (2007). Microprobe monazite geochronology: understanding geologic processes by integrating composition and chronology. *Annual Review of Earth and Planetary Sciences*, 35(1), 137–175.

Williams, M. L., Grover, T., Jercinovic, M. J., Regan, S. P., Pless, C. R., and Suarez, K. A. (2019). Constraining the timing and character of crustal melting in the Adirondack Mountains using multi-scale compositional mapping and in-situ monazite geochronology. *American Mineralogist*, 104(11), 1585–1602.

Wing, B. A., Ferry, J. M., and Harrison, T. M. (2003). Prograde destruction and formation of monazite and allanite during contact and regional metamorphism of pelites: petrology and geochronology. *Contributions to Mineralogy and petrology*, 145, 228–250.

Wodicka, N., Ketchum, J. W., and Jamieson, R. A. (2000). Grenvillian metamorphism of monocyclic rocks, Georgian Bay, Ontario, Canada: Implications for convergence history. *The Canadian Mineralogist*, 38(2), 471–510.

Wodicka, N., Corriveau, L., Stern, R. A., Tollo, R., McLelland, J. and Bartholomew, M. (2004). SHRIMP U-Pb zircon geochronology of the Bondy Gneiss complex: Evidence for circa 1.39 Ga arc magmatism and polyphase Grenvillian metamorphism in the Central Metasedimentary Belt, Grenville Province, Quebec. *Memoirs-Geological Society of America*, 243-266.

Woodruff, L. G., Schulz, K. J., Nicholson, S. W., and Dicken, C. L. (2020). Mineral deposits of the Mesoproterozoic Midcontinent Rift system in the Lake Superior region–a space and time classification. *Ore Geology Reviews*, 126, 103716.

Wolf, M. B., and London, D. (1995). Incongruent dissolution of REE-and Sr-rich apatite in peraluminous granitic liquids: Differential apatite, monazite, and xenotime solubilities during anatexis. *American Mineralogist*, 80(7-8), 765-775.

Yakymchuk, C., and Brown, M. (2019). Divergent behaviour of Th and U during anatexis: Implications for the thermal evolution of orogenic crust. *Journal of Metamorphic Geology*, 37(7), 899–916.

Yakymchuk, C., Clark, C., and White, R. W. (2017). Phase relations, reaction sequences and petrochronology. *Reviews in Mineralogy and Geochemistry*, 83(1), 13-53.

Zhang, H., van der Lee, S., Wolin, E., Bollmann, T. A., Revenaugh, J., Wiens, D. A., and Jurdy, D. M. (2016). Distinct crustal structure of the North American Midcontinent Rift from P wave receiver functions. *Journal of Geophysical Research: Solid Earth*, 121(11), 8136-8153.

Zhu, X. K., and O'nions, R. K. (1999). Zonation of monazite in metamorphic rocks and its implications for high temperature thermochronology: a case study from the Lewisian terrain. *Earth and Planetary Science Letters*, 171(2), 209–220.